Mechanisms of Luminescence in α-Al_2O_3:C: Investigations using Time-Resolved Optical Stimulation and Thermoluminescence Techniques

By: Angel Newton Nyirenda

Supervisor: Professor Makaiko Chithambo

December, 2012

Submitted to the Department of Physics and Electronics, Faculty of Science, Rhodes University, in fulfilment of the requirements of the degree of Master of Science

Abstract

Carbon-doped aluminium oxide, α-Al_2O_3:C , is a ultra-sensitive dosimeter of topical research interest. The aim of this project was to investigate the dynamics of luminescence in this material. The methods of investigation consisted of thermoluminescence and time-resolved optical stimulation. Thermoluminescence measurements provide information on trap distribution and kinetic parameters of the traps involved in luminescence whereas time-resolved optical stimulation is a handy technique in investigations of luminescence lifetimes and provides an insight into the charge transitions between traps and recombination centres. Measurements were made on samples annealed at a nominal temperature of 900°C for 15 minutes. The material shows the presence of five thermoluminescence peaks at 37°C, 160°C, 300°C, 410°C, and 480°C at a heating rate of 0.03 K/s when irradiated to 6.0 Gy of beta. The main peak at 160°C, shows a linear dose response for doses between 0.1 Gy and 10 Gy and then goes sublinear above 10 Gy, the peak at 37°C shows a sublinear dose response for doses between 0.1 Gy and 10 Gy and appears to saturate thereafter, whereas the dose response of the peak at 300°C goes from linear to supralinear then apparently quadratic behaviour in the dose range of 0.1 Gy to 16.0 Gy. The trap depth of the main peak, that is, its activation energy as determined below the conduction band, has been approximated at 1.3 eV with a kinetic order of approximately 1.2. Time-resolved optical stimulation has been used to investigate luminescence lifetimes. The mean luminescence lifetime obtained for the sample at ambient temperatures is 35.0±1.0 ms. The investigations of the dependence of luminescence lifetimes on measurement temperature show that the material suffers from thermal quenching effects at measurement temperatures above 140°C with the activation energy of thermal quenching estimated at 1.045±0.002 eV. Shallow traps i.e. traps lying close to the conduction band, seem to elongate the lifetimes of optically stimulated luminescence in the material at temperatures between 30°C - 80°C due to charge retrapping. The material exhibits both fading and recuperation of the optically stimulated luminescence signal with storage time.

Acknowledgements

First and foremost, I would like to thank my supervisor, Professor Makaiko Chithambo, for giving me this rare opportunity to conduct research under his supervision. I would also like to thank him for his support, academic or otherwise during my two-year stay at Rhodes University.

Let me thank Prof Chithambo in a special way for extending to me the NRF bursary, without which I would not have been able to come to Rhodes University and carry out my research. God bless you Prof Chithambo and your family.

A lot of thanks to all the staff members in the department of Physics and Electronics at Rhodes University, so numerous to mention, and my fellow MSc students for making my stay at Rhodes University easy and memorable. I wont forget you folks.

To my Mom, my late Dad, Louisa, and the rest of my family members, I say thanks a lot guys and may the good Lord bless you abundantly.

Whatever Nature has in store for mankind, unpleasant as it may be, men must accept, for ignorance is never better than knowledge - Enrico Fermi

Contents

List of Figures

List of Tables

Chapter 1

Introduction

This study was aimed at investigating the underlying physical processes of luminescence in carbon-doped alpha-aluminium oxide (α-Al_2O_3:C) in order to gain a better understanding of the behaviour of point defects in the material. The luminescence investigations were carried out using time-resolved optically stimulated luminescence (TR-OSL) and thermoluminescence (TL) methods.

α-Al_2O_3:C is a well known ultra-sensitive thermoluminescence and optically stimulated luminescence dosimeter (TLD/OSLD) [1], due to its ability to detect and measure ultraviolet (UV) and ionizing radiation. The doping by carbon has been found to introduce a large number of oxygen vacancies, which in turn lead to the formation of F and F^+ centers that are responsible for radiation sensitivity of Al_2O_3:C [2]. The material is grown from the melt in a reducing atmosphere of graphite at high temperatures of about 2050°C [3] and then cooled rapidly to room temperature. An F-centre is formed when an oxygen vacancy is filled with two electrons, whereas an F^+ centre is formed when an oxygen vacancy is filled with one electron.

α-Al_2O_3:C has desirable dosimetric material characteristics such as high optical, chemical and thermal stability under irradiation [4]. Besides, it has a low-dose threshold, saturates at high doses, has a large band gap and good optical transparency which make it suitable for dosimetric applications [5, 6]. For example, its very low-dose threshold ($\sim 10^{-6}$ Gy) has made α-Al_2O_3:C applicable to low dose dosimetry in environmental monitoring as well as in personal, medical and accidental dosimetry [5]. By 1993, α-Al_2O_3:C was already being used for radiation monitoring in personal and environmental dosimetry in many parts of the world [4]. Its high sensitivity also makes it an appropriate material for use in space dosimetry, nuclear tracking and security applications.

In spite of the fact that α-Al_2O_3:C is being used widely in some fields of dosimetry such as personal dosimetry, the mechanisms of luminescence in the material are not fully understood. In

effect this inadequate knowledge of the physical processes underlying luminescence phenomenon in the material poses a challenge for using the material for radiation detection and measurement, as it may lead to overestimation or underestimation of the material's exposure to irradiation dose. Up to date, the kinetic order of the main peak which is used in dosimetry applications is not known with certainty because different values of kinetic order have been reported by different authors e.g. the work of Kitis et al [7], Kortov et al [8], and Kortov and Milman [9] respectively report kinetic orders of 1.45, 2 and 1.6 for the main peak. The effects of storing the sample after exposure to irradiation, and the processes therein involved have not been clearly understood. The presence of other electron traps, apart from that responsible for the main dosimetric peak in the material, affects the dose response of the dosimetric trap to irradiation dose because the other traps act as charge competitors during irradiation. Since it is not clear as to how many traps are active in the material during irradiation, there have been dissenting reports concerning the dose response of the dosimetric trap. In addition, the role of shallow traps in α-Al_2O_3:C has not been fully investigated.

Knowing that to realise the full potential of the applicability of α-Al_2O_3:C in radiation dosimetry requires a better understanding of the underlying mechanisms of the luminescence process in the material, it behoved us to carry out an experimental study of the material. Our aim is to ensure that the high-sensitivity of α-Al_2O_3:C is put to optimal use.

The thesis is organized as follows: Chapter 2 gives a general account of the luminescence process in solids; Chapter 3 provides the theoretical considerations of the two techniques of investigation used in this project namely: time-resolved optical stimulation luminescence (TR-OSL) and thermoluminescence (TL); Chapter 4 provides a brief description of the luminescence model of α-Al_2O_3:C that was used as a guide in this study; Chapter 5 gives an account of the instrumentation used during the experimental investigations. In addition, chapter 5 describes the samples and methodology employed in the investigations. Chapter 6 presents results and the discussion of the results. Chapter 7 summarizes the most important findings of this study.

We are hopeful that the work presented here will help to enhance the understanding of luminescence processes in α-Al_2O_3:C and in some instances, refine the existing knowledge about the material. Most importantly, the findings presented in this work may help to improve the applicability of α-Al_2O_3:C in radiation dosimetry beyond its current use.

Chapter 2

Theoretical background

This chapter is aimed at introducing the fundamental concepts related to luminescence phenomenon in solids. The luminescence process will be defined and the various kinds of luminescence will be briefly described. The band theory of solids is essential for the understanding of the process underlying luminescence in materials, hence a discussion of this theory has been provided. A brief account of defects in solids has been included due to the crucial role they play in the stimulated luminescence phenomena.

2.1 Luminescence

Luminescence is a process whereby matter generates non-thermal radiation that occurs after a material absorbs energy from an external source. The absorbed energy could be ultraviolet light or ionization energy such as X-rays, gamma rays or beta radiation. Luminescence occurs due to the relaxation of electronic charges from excited (or metastable states), to ground state configurations. The luminescence process usually takes place at low temperatures (i.e. it is cold body radiation) in contrast with incandescence which occurs at very high temperatures only.

2.1.1 Types of Luminescence

Luminescence can be classified as either being spontaneous or stimulated depending on whether an external energy source is required for the luminescence process to occur. Spontaneous luminescence occurs immediately after exposing the material to an irradiation source e.g. fluorescence. On the other hand, stimulated luminescence e.g. phosphorescence, takes a few seconds or more to occur.

2.1.1.1 Fluorescence

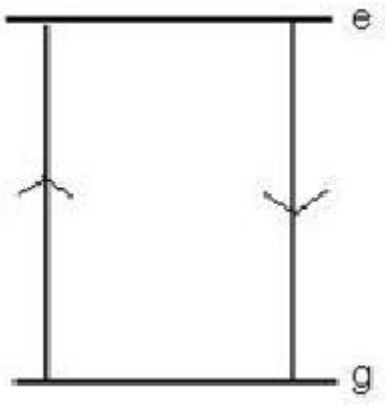

Figure 2.1: Electron transitions, $g \rightarrow e \rightarrow g$, that account for the occurence of fluorescence in materials. g is the ground state, e is the excited state. Diagram reproduced from McKeever [10]

Fluorescence is luminescence that occurs during irradiation and lasts as long as the irradiation period. Fluorescence usually takes less than 10^{-8} s. It involves band-to-band electron transitions i.e. excitation energy generates electron-hole pairs in the valence band and conduction band respectively which subsequently recombine to produce luminescence (g→e, then e→g in Figure 2.1). The process of fluorescence is temperature independent [10].

2.1.1.2 Phosphorescence

Phosphorescence can be discussed with reference to Figure 2.2. Phosphorescence is a kind of delayed luminescence because it involves the transition into and out of the metastable state, m, leading to much longer delays between excitation and emission. The time delay between stimulation and emission of phosphorescence is usually longer than 10^{-8} s. The lifetime, τ, of a trapped electron in state m at a temperature T is given by the Arrhenius equation:

$$\tau = s^{-1} \exp(\frac{E}{kT}), \tag{2.1}$$

where s in units of s^{-1}, is a constant called the tendency-to-escape frequency, E is the trap depth measured in electron volts (eV), T is the absolute temperature and k (eV K^{-1}) is Boltzmann's constant. Lifetime as defined by equation 2.1 represents the time delay between trapping of the electron in state m and the ultimate release of the electron from state m for recombination and

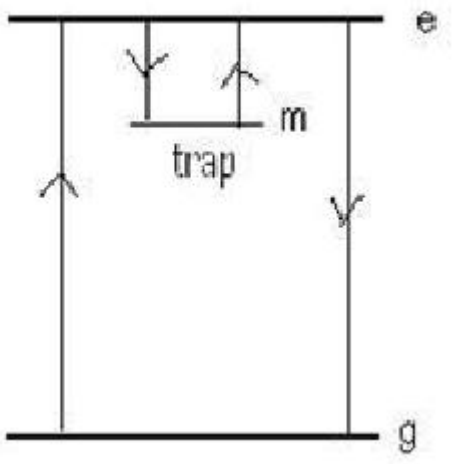

Figure 2.2: Electron transitions resulting into the occurence of phosphorescence. g is the ground state, e is the excited state, and m is the metastable state. Diagram reproduced from McKeever [10].

should not be mistaken for luminescence lifetime (to be described later), which is the time delay between stimulation and emission of luminescence.

The attempt-to-escape frequency also known as the frequency factor, s, represents the number of times per second, ν, that an electron interacts with the crystal lattice of a solid, multiplied by a transition probability κ, multiplied by a term which accounts for the change in entropy ΔS, associated with the transition from a trap to the delocalized band [11]. Thus,

$$s = \nu\kappa \exp(\frac{\Delta S}{k}). \tag{2.2}$$

The expected maximum value of s should be similar to the lattice vibrational frequency (Debye frequency), i.e. 10^{12} - 10^{14} s^{-1} [11]. The parameter E in equation 2.1 is the energy required to free an electron from state m, into the conduction band and is similar to ionization energy of an atomic electron. The reciprocal of equation 2.1 gives the probability per unit time, p, for the escape of an electron from the trap,

$$p = \tau^{-1} = s \exp(-\frac{E}{kT}). \tag{2.3}$$

Under the assumptions of no retrapping and radiative recombinations only, the intensity of phosphorescence emission at any instant $I(t)$ is proportional to the rate of recombination (i.e. rate of $m \rightarrow e$ transitions) [10]. Hence,

$$I(t) = -C\frac{dn}{dt} = C\frac{n}{\tau}, \tag{2.4}$$

where n is the number of trapped electrons in state m and C is a constant of proportionality. The negative sign signifies reduction in electron concentration in state m. The solution to equation 2.4 is:

$$I(t) = I_0 \exp(-\frac{t}{\tau}). \tag{2.5}$$

Equation 2.5 shows that phosphorescence decays exponentially at constant temperature, T.

At room temperatures, phosphorescence results from the detrapping of charges from shallow traps. The energy depth of shallow traps is small enough such that thermal lattice vibrations at room temperature are sufficient to stimulate trapped electrons into delocalized bands from which subsequent decay into ground state can occur without involving external influences. The difference between fluorescence and phosphorescence lies in their luminescence lifetimes, with phosphorescence having considerably longer lifetimes than fluorescence.

2.1.2 Band theory of solids

The occupancy of atomic orbitals by electrons is determined by the Pauli Exclusion principle which limits the maximum number of electrons occupying a given atomic orbital. The Pauli exclusion principle allows electrons having different sets of quantum numbers to occupy a given atomic orbital in an individual atom, thus limiting the orbital occupancy to two electrons only. The solutions that satisfy the Schroedinger equation on the other hand, determine the energy states in the electron cloud about the nucleus that are allowed to be occupied by electrons. These solutions to the Schroedinger equation introduce discreteness in atomic energy levels. No electron is allowed to occupy an energy level other than those corresponding to solutions to Schroedinger equation i.e. some energy levels are forbidden. When a large number of atoms come together to form a crystal lattice, discrete energy levels of individual atoms split into closely spaced energy levels in accordance with the Pauli exclusion principle. The splitting of energy levels into closely spaced energy levels, leads to the formation of energy bands in the crystal. For example, if N atoms are allowed to come together to form a crystal lattice, the energy levels of the N atoms in a crystal divide into $(2\ell + 1)$N closely spaced levels, where ℓ is the orbital angular momentum quantum number and $(2\ell + 1)$ is therefore the orbital degeneracy of each level, forming a quasi-continuous distribution of energy levels [12]. Since the allowed bands are shared by all the atoms throughout the crystal, the bands are referred to as delocalized bands. Figure 2.3 illustrates how delocalized bands are formed when a large number of atoms come together to form a crystal.

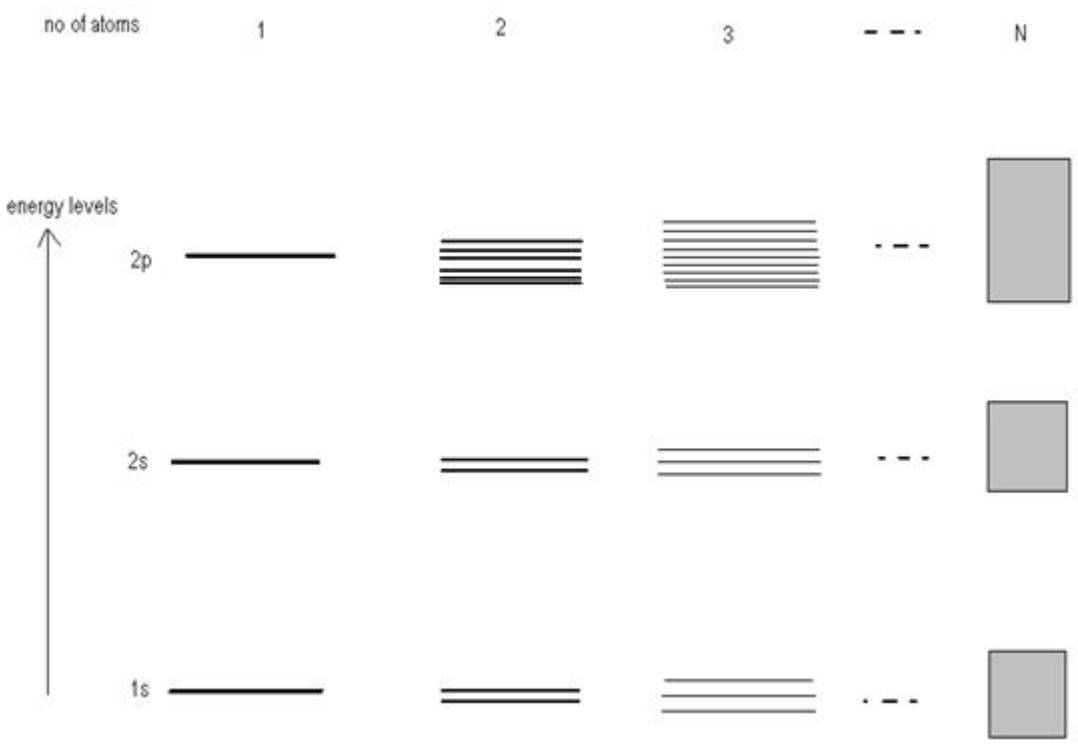

Figure 2.3: The diagram shows how energy levels split when N atoms come together to form a crystal. For large values of N, the energy bands emerge in the crystal as shown in the N^{th}column. Diagram adapted from Yukihara and McKeever [12].

In luminescence studies, the focus is shifted towards the two uppermost bands called the valence band and the conduction band. The valence band lies below the conduction band and the two bands are separated by a forbidden gap also known as the energy gap whose magnitude depends on the material under consideration. The energy gap denoted as E_g is defined as the energy difference between the minimum energy level of the conduction band and the topmost level of the valence band. The magnitude of the energy gap determines some of the properties of solids e.g. their thermal and electrical conductivity. An electron can only be promoted from the valence band into the conduction band if it acquires sufficient energy, $E \geq E_g$. Once an electron is in the conduction band, it behaves as a free particle. An electron that moves into the conduction band leaves a free hole in the valence band. As a result, stimulation of electrons into the conduction band generates free electron-hole pairs.

The magnitude of the energy gap distinguishes between metals, insulators, and semiconductors. The size of the band gap limits the concentration of free electrons and holes in the conduction band

and valence band respectively. Insulators generally have a large band gap (E_g >5 eV) such that at room temperature there are neither free electrons in the conduction band nor free holes in the valence band, rendering them poor electrical conductors. Semiconductors have a relatively smaller band gap allowing them to have few free charges in the delocalised bands at room temperature. Metals on the other hand, are good electrical conductors because metals consist of band-overlapping valence band and conduction band and the overlapping enables them to have a large concentration of free electrons in the conduction band at room temperature. Luminescent materials e.g. α-Al_2O_3:C, belong to the category of insulators. α-Al_2O_3:C has a band gap energy of approximately 9 eV [1]. Due to large band gaps in insulators, electrons can only be promoted to the conduction band owing to an external mechanism such as absorption of energy from ionizing radiation, hence the choice of insulators in radiation dosimetry.

2.1.3 Defects

In an ideal crystalline structure, there are no allowed energy levels lying in the forbidden gap as demanded by solutions satisfying Schroedinger's equation. However, ideal crystalline structures do not exist. Instead real crystals contain certain concentrations of impurities or defects. The presence of these impurities and defects in the crystal structure introduces allowed energy levels in the otherwise forbidden gap. The energy levels introduced by defects and impurities in the forbidden gap are localized and are referred to as metastable states. Delayed luminescence such as phosphorescence, thermoluminescence and optically stimulated luminescence, occur because of the existence of localized energy levels introduced in the forbidden gap by defects or imperfections in the crystal structure. These defects act as traps for electrons and holes when the crystal is excited through irradiation. Hole traps generally lie close to the valence band whereas electron traps lie close to the conduction band. The charges trapped in the defects during excitation stage, store energy which upon stimulation can be released as optically stimulated luminescence, thermoluminescence or other related phenomena. In perfect crystals, optically stimulated luminescence or thermoluminescence would not be possible because there would be no defects to trap excited charges during the irradiation stage. Kittel and Stoneham [12] define defects as violations of the periodicity of the crystal lattice. Defects can be categorized as being intrinsic (native) or extrinsic depending on the nature of their existence within the crystal. Defects formed by displacements of atoms that form the crystal are called intrinsic defects, while defects formed by foreign atoms are called extrinsic or impurity defects [12]. Point defects are where an atom is missing or is in an irregular place in the lattice

structure. Some examples of point defects include lattice vacancies such as a missing atom at a lattice point called a Schottky defect, an atom transferred from a lattice site to an interstitial position called a Frenkel defect, impurities in which foreign atoms replace atoms in the crystal lattice (as in doping) known as substitutional defects, and atomic dislocations in the lattice structure. Defects can be introduced as a result of doping the material during crystal growth, post-growth annealing or irradiation with heavy particles or photons [12].

An F-center is a defect of interest in the study of most luminescent materials and α-Al_2O_3:C is no exception. An F-center can be defined as an intrinsic point defect consisting of a negative ion (anionic) vacancy with one excess electron bound at the vacancy site. The concentration of anions (negative ions) and cations (positive ions) in a neutral material is the same. Mott and Gurney [12] noted that when a crystal is heated in vapour of its cation metal, an excess of anion vacancies is produced and the only way to achieve crystal neutrality is through electron capture at the anionic vacancy . In this regard, oxides are expected to contain F-centres comprising oxygen vacancies with two captured electrons.

Chapter 3

Stimulated luminescence phenomena

This chapter aims at describing the two kinds of stimulated luminescence phenomena namely, thermoluminescence and optically stimulated luminescence.

It has already been pointed out in the previous chapter that stimulated luminescence phenomena require external energy sources to release charges from the traps into the delocalized bands for recombination at the recombination site, in order to produce luminescence. There are several kinds of stimulated luminescence phenomena. However, for the purpose of this study, only two kinds of stimulated luminescence phenomena are of interest. The two kinds of stimulated luminescence of interest in this study are thermoluminescence (TL) and optically stimulated luminescence (OSL). In thermoluminescence, charges from the traps are stimulated by heat whereas light is the stimulation agent in optically stimulated luminescence. Figure 3.1 represents a simple illustration of the processes involved in stimulated luminescence phenomena.

Luminescence studies involve collecting and analysing photons that are emitted at the stimulation stage in order to get an understanding of the physical processes underlying luminescence in the material. The emitted photons also contain latent information about the radiation field, hence by analysing these photons you can extract some information about the radiation field.

3.1 Thermoluminescence

Pagonis et al [13], define thermoluminescence as the emission of light from a semiconductor or an insulator when it is heated, due to the previous absorption of energy from irradiation. Thus, typically thermoluminescence requires that a material must be an insulator or a semiconductor and must have been previously exposed to an irradiation source such as beta or gamma irradiation before being

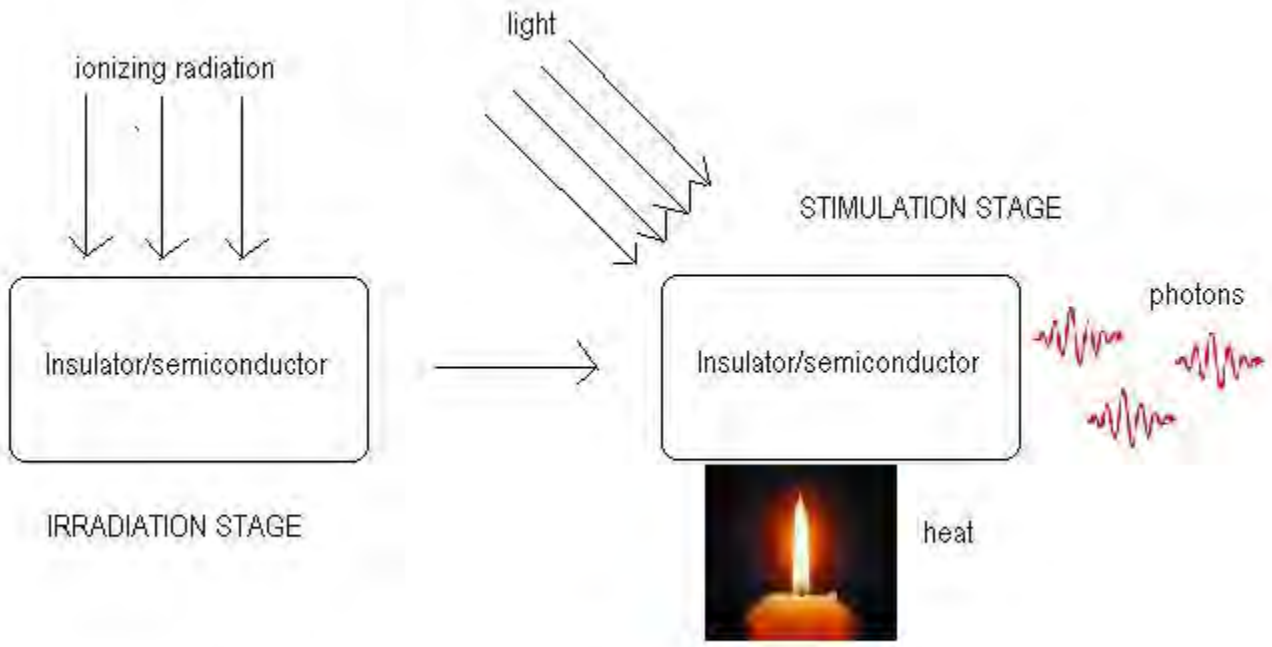

Figure 3.1: Schematic diagram illustrating sample irradiation stage, and thermal and optical stimulation of luminescence. At irradiation stage, the material is exposed to ionizing radiation which excites charges into traps. At stimulation stage, the captured charges are released thermally (by heating) or optically (by light) from the traps into the recombination sites where luminescence (shown as photons) occurs.

heated at a controlled rate to produce luminescence. Heating a sample that has been previously irradiated, releases electrons from the traps into the conduction band from where the electrons then have some probability to recombine with a hole at a recombination centre and emit light at certain wavelengths. The graph obtained after heating the sample at a controlled heating rate is called a glow curve and is a plot of TL intensity against temperature. The TL glow curve generally has peaks with each peak reflecting a trap type with a unique activation energy [11]. The TL glow curves are analyzed in order to extract parameters that can be used to describe the TL process in the material. Some of the parameters that can be extracted from TL glow curves include the trap depth E, tendency-to-escape frequency, s, kinetic order, b, the capture cross-sections of traps and recombination centers, as well as the concentrations of traps and recombination centers. TL has proved useful for the study of lattice defects which act as charge traps for electrons and holes, besides its application in radiation dosimetry and in archaeological and geological dating [14].

A simple model of thermoluminescence (TL) is shown in Figure 3.2 and consists of one trap and

one recombination centre (OTOR) and represents the simplest model for explaining TL processes in luminescent materials. The trap is responsible for capturing electrons whereas the recombination center captures holes during the irradiation stage. During heating, electrons are evicted from the trap of concentration N, into the conduction band and then recombine with holes that have been previously captured at the recombination centre of concentration M. It should be pointed out that the inverted scenario is also possible i.e. holes may be thermally released from the hole trapping state, M, into the valence band and then recombine with electrons at the electron trapping state, N, in which case the the hole trapping state is termed as the trap, and the electron trapping state is the recombination centre [15].

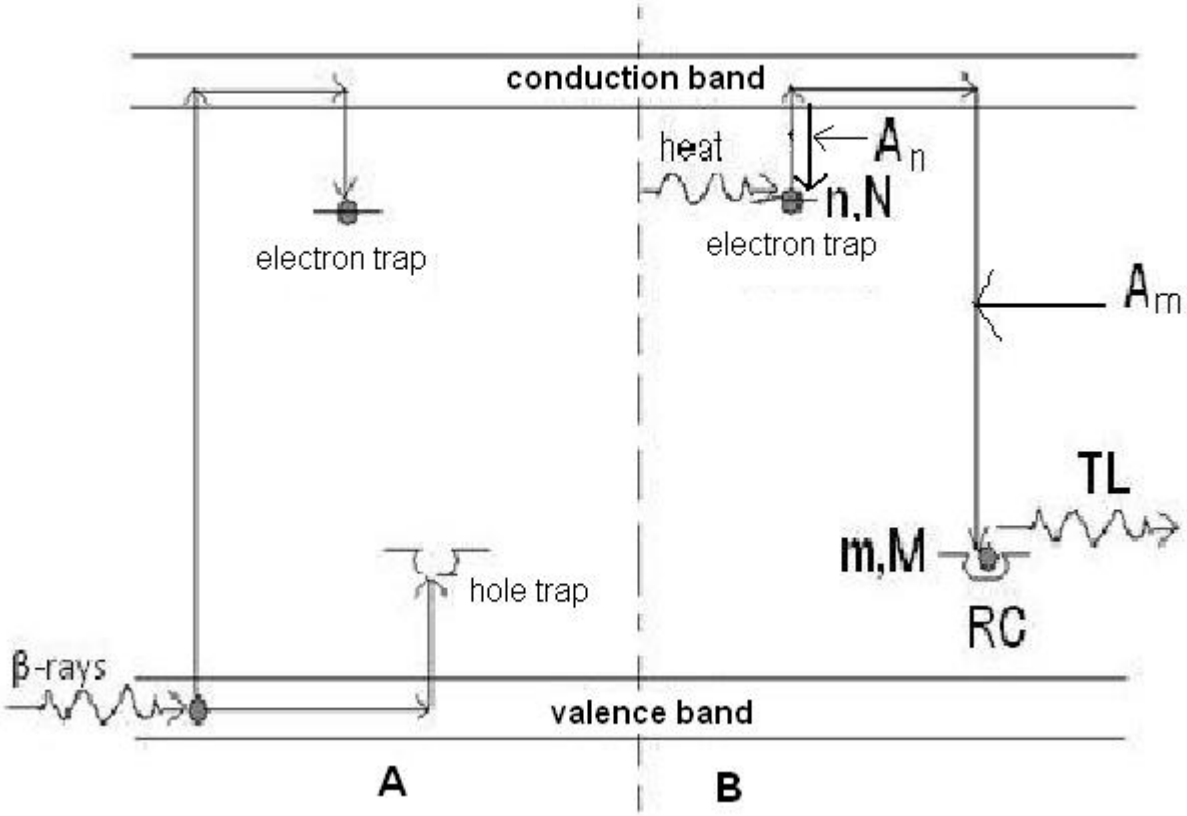

Figure 3.2: A simple TL band model. Part A represents the irradiation stage during which ionization takes place and part B is the stimulation stage during which trapped charges are thermally stimulated. All parameters shown have been defined in the text.

3.2 Kinetic Equations governing the OTOR model

The kinetic equations describe quantitatively the transitions of the charges taking place during the irradiation and stimulation stages. In Figure 3.2, n (cm^{-3}) is the instantaneous electron concentration in traps, m (cm^{-3}) is the instantaneous hole concentration in recombination centers, N (cm^{-3}) is the concentration of electron traps, M (cm^{-3}) is the concentration of recombination centers, A_n ($\mathrm{cm}^{-3}\mathrm{s}^{-1}$) is the retrapping probability coefficient of electrons, A_m ($\mathrm{cm}^{-3}\mathrm{s}^{-1}$) is the recombination probability coefficient of electrons. Other parameters not shown in 3.2 include the trap depth, E (eV), s (s^{-1}), the tendency-to-escape frequency, n_c (cm^{-3}), the instantaneous concentration of free electrons in the conduction band, n_v (cm^{-3}), the instantaneous concentration of free holes in the valence band,, B ($\mathrm{cm}^{-3}\mathrm{s}^{-1}$), the trapping probability coefficient of holes in centers, and X ($\mathrm{cm}^{-3}\mathrm{s}^{-1}$), the rate at which electron-holes pairs are being generated during the irradiation stage. The kinetic equations governing the process during the irradiation stage form a set of simultaneous equations and are summarized as follows:

$$\frac{dn}{dt} = A_n(N-n)n_c - np \tag{3.1}$$

where p is given by equation 2.3. Equation 3.1 represents the rate of change of concentration of electrons in trap N. The first term in the equation represents retrapping whereas the second term represents thermal detrapping from N to the conduction band. For example equation 3.1 may describe phosphorescence from shallow traps during irradiation. A general case of 3.1 is discussed later under stimulation stage.

$$\frac{dm}{dt} = B(M-m)n_v - A_m m n_c \tag{3.2}$$

Equation 3.2 means that the rate of change of concentration of holes in the recombination center is equal to the rate of hole trapping at M (first term) minus the rate of recombination (second term).

$$\frac{dn_c}{dt} = X - A_n(N-n)n_c - A_m m n_c \tag{3.3}$$

Equation 3.3 represents the rate of change of concentration of free electrons in the conduction band and X increases n_c.

$$\frac{dn_v}{dt} = \frac{dn}{dt} + \frac{dn_c}{dt} - \frac{dm}{dt} \tag{3.4}$$

Equation 3.4 is the charge neutrality equation.

At low temperatures, the second term in equation 3.1 can be ignored because it becomes negligible, but as temperature increases the thermal detrapping term becomes significant enough not to

be ignored. The set of simultaneous equations describing the mechanics of charges during irradiation stage, can be solved analytically by making simplifying assumptions in order to approximate the behaviour of the sample in response to irradiation. The final values of n, m, n_c and n_v at the irradiation stage become the initial values of the heating (stimulation) stage. If we take a heating function that varies linearly with time i.e. $T = T_0 + \beta t$, where β is the constant heating rate, and taking into consideration the fact the irradiation has ended ($X = 0$) and the assumption that all holes have been captured ($n_v \approx 0$), then the equations governing the TL process during heating will still be:

$$\frac{dn}{dt} = A_n(N - n)n_c - np \tag{3.5}$$

where the first term is the retrapping term and the second term represents thermal stimulation of electrons from the trap into conduction band as previously defined. The recombination rate 3.6, hence the TL intensity, $I(T)$, is therefore proportional the rate of change of free electron concentration in the conduction band and the concentration of active recombination centres and is given by:

$$I(T) = -\frac{dm}{dt} = A_m m n_c \tag{3.6}$$

Taking into account $n_v \approx 0$, the charge neutrality equation becomes

$$\frac{dm}{dt} = \frac{dn}{dt} + \frac{dn_c}{dt} \tag{3.7}$$

Halperin and Braner[15] made the following simplifying assumptions which later became known as quasi-equilibrium or quasi-steady assumptions:

$$|\frac{dn_c}{dt}| << |\frac{dn}{dt}|, |\frac{dm}{dt}|; n_c << n \tag{3.8}$$

Equation 3.8 implies that the rate of change of the concentration of free electrons in the conduction band is much less than the rate of change of the concentration of trapped carriers. For the case where the electrons evicted from the trap during stimulation go through the conduction band to the recombination site, the TL intensity is given by:

$$I = -\frac{dm}{dt} = \frac{A_m m}{A_m m + A_n(N - n)} sn \exp\left(-\frac{E}{kT}\right) \tag{3.9}$$

Equation 3.9 has been arrived at by solving equation 3.3 for n_c using $\frac{dn_c}{dt} = 0$ and $X = 0$ and inserting this value of n_c in equation 3.6.

3.2.1 First order kinetics

First order kinetics make use of the following simplifying assumptions: $n \cong m$, $\frac{dn}{dt} \cong \frac{dm}{dt}$ and $A_m m >> A_n(N-n)$ (i.e. slow retrapping). Applying these assumptions to equation 3.9, generates the equation of first order kinetics:

$$I = -\frac{dn}{dt} \equiv np = sn\exp(-\frac{E}{kT}) \tag{3.10}$$

The solution to equation 3.10 is:

$$I(T) = sn_0\exp(-\frac{E}{kT})\exp[-(s/\beta)\int_{T_0}^{T}\exp(-\frac{E}{kT'})dT'] \tag{3.11}$$

where n_0 is the initial concentration of trapped electrons prior to heating, T_0 is the initial temperature, and T' is the dummy integration variable representing temperature.

3.2.2 Second order kinetics

Garlick and Gibson [15] made different simplifying equations to equation 3.9. Besides the assertion that $m = n$, Garlick and Gibson [15] made the assumptions that $A_n(N-n) >> A_m m$ i.e. retrapping dominates, and $N << n$ i.e. the trap is far from saturation and they arrived at the following equation, called the equation of second order kinetics:

$$I = -\frac{dn}{dt} = \frac{sA_m}{A_n N}n^2\exp(-\frac{E}{kT}). \tag{3.12}$$

By making a further assumption that the retrapping and recombination probability coefficients are equal, $A_m = A_n$, as suggested by Wrezesinska [11], equation 3.12 reduces to

$$I = -\frac{dn}{dt} = \frac{s}{N}n^2\exp(-\frac{E}{kT}) = s'n^2\exp(-\frac{E}{kT}). \tag{3.13}$$

where $s' = s/N$ is a constant with units of $\mathrm{cm^3 s^{-1}}$. The solution to equation 3.13 is

$$I(T) = \frac{n_0 s''\exp(-\frac{E}{kT})}{[1+(s''/\beta)\int_{T_0}^{T}\exp(-\frac{E}{kT'}dT']^2}. \tag{3.14}$$

where $s'' = s'n_0$, and other parameters are as previously defined.

3.2.3 General order kinetics

May and Partridge [15] considered a general case in which the kinetics are neither first order nor second order, and arrived at the following equation known as the equation of general order kinetics:

$$I = -\frac{dn}{dt} = s'n^b\exp(-\frac{E}{kT}). \tag{3.15}$$

where b is the order of kinetics. For $b = 1$ and $b = 2$, equation 3.15 reduces to first order and second order kinetics, respectively. The solution to equation 3.15 is

$$I(T) = s'' n_0 \exp(-\frac{E}{kT})[1 + (b-1)(s''/\beta) \int_{T_0}^{T} \exp(-\frac{E}{kT'})dT']^{-\frac{b}{b-1}}. \tag{3.16}$$

where $s'' = s' n_0^{b-1}$ and other parameters as previously defined.

In addition to first, second and general order kinetics, there is another order of kinetics called the mixed order kinetics which uses a different assertion from $n = m$ [15]. In our work, mixed order kinetics was not used, hence has not been discussed in the thesis.

3.3 Kinetic analysis

Kinetic analysis is the analysis of a thermoluminescence glow curve in order to determine physical parameters of the traps and establish the kinetics of the charge-carrier transfer between them [14]. There are several methods that can be used in order to extract relevant information from the TL glow curve. This section describes some methods of kinetic analysis that were particularly useful in this study.

3.3.1 Initial rise method

The initial rise (IR) method can be used to analyse any glow peak irrespective of the order of kinetics and is based on the analysis of the low temperature region of the TL glow peak. The IR method makes use of the assumption that the amount of trapped electrons in the low temperature region of the glow peak is approximately constant, $n \approx n_0$. Thus in the low temperature region of the peak, the intensity, $I(T)$, becomes proportional to the Boltzmann factor i.e. $I(T) \propto \exp(-E/kT)$. The equation showing the temperature dependence of the emitted TL signal in the lower temperature region of the glow peak can be written as

$$I(T) = C \exp(-\frac{E}{kT}), \tag{3.17}$$

where E is the activation energy in eV, k is Boltzmann's constant in eV/K, T is the absolute temperature and C is the constant of proportionality. As a rule of thumb, region of analysis must not go beyond 15% of maximum intensity, I_M [13]. However, other literature [15] talk of 5% of maximum intensity as being the rule of thumb. Taking natural logarithm of equation 3.17 gives us

$$\ln(I) = \ln C - E/kT. \tag{3.18}$$

A plot of $\ln(I)$ against $1/T$ is expected to yield a straight line with a slope of $-E/k$. Hence the initial rise method helps in evaluation of the activation energy, E, for a trap responsible for a given peak.

3.3.2 Peak shape methods

The methods in this category use geometrical properties for the evaluation of E, s, and b. Unlike methods which are based on portions of peaks e.g. the initial rise method, peak shape methods are based on use of a few points on the peak, usually two or three points [10]. Unlike the initial rise method, peak shape methods are also dependent on the order of kinetics. The points of interest on a peak used in peak shape method described by Chen [10] are the temperature for the maximum of the peak, T_M and the temperatures at half-maximum intensities on the rising (T_1) and descending (T_2) parts of the peak. The parameters τ, δ and ω are defined as: $\tau = T_M - T_1$, $\delta = T_2 - T_M$, and $\omega = T_2 - T_1$. Figure 3.3 illustrates these points. The symmetry of the peak is established by the

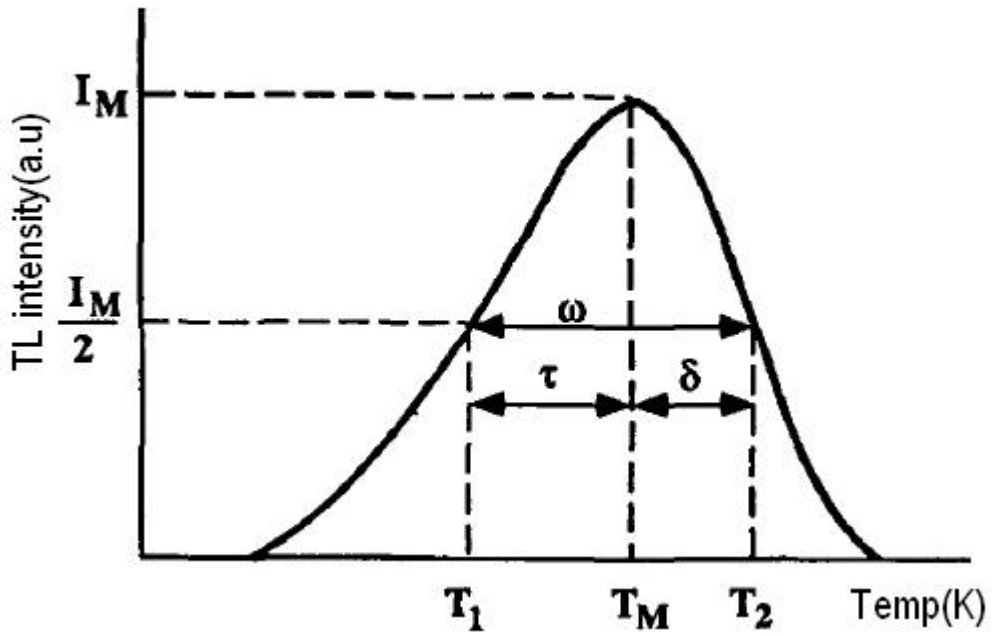

Figure 3.3: A TL peak showing T_M, T_1, T_2 and the parameters $\tau = T_M - T_1$, $\delta = T_2 - T_M$, and $\omega = T_2 - T_1$. T_M is the peak intensity, T_1 and T_2 are the temperatures at half-maximum intensities on the rising and descending parts of the peak.

value of the geometrical factor, μ_g, which is defined as:

$$\mu_g = \frac{\delta}{\omega}. \tag{3.19}$$

Chen's method [10] is one popular method of kinetic analysis based on the shape of the glow curve. Using the various geometrical parameters at half-maximum intensity of the curve, Chen's method [10] can be used to evaluate the order of kinetics b, and the activation energy, E. Chen [11] showed that for first-order peaks, $\mu_g \approx 0.42$, and for second-order peaks, $\mu_g \approx 0.52$ [15]. Thus, the geometrical factor can help in determining the kinetic order, b, of a given TL peak. Chen [10] also derived a general order equation for the evaluation of the activation energy of the trap responsible for a given peak. Chen's equation, as is popularly known, is given by:

$$E_\alpha = c_\alpha(kT_M^2/\alpha) - b_\alpha(2kT_M), \tag{3.20}$$

where α stands for δ, τ, or ω. The coefficients c_α are

$$c_\tau = 1.51 + 3(\mu_g - 0.42); \qquad b_\tau = 1.58 + (4.2(\mu_g - 0.42) \tag{3.21}$$

$$c_\delta = 0.976 + 7.3(\mu_g - 0.42); \qquad b_\delta = 0, \tag{3.22}$$

$$c_\omega = 2.52 + 10.2(\mu_g - 0.42); \qquad b_\omega = 1. \tag{3.23}$$

The formulas for first order and second order kinetics can be derived from the equations 3.22 and 3.23 by inserting μ_g=0.42 and μ_g=0.52, respectively.

The value of μ_g can also be used to obtain the order of kinetics, b, using the graph plotted by Chen [16]. Chen's graph (Figure 3.4) gives a relationship between the geometrical factor calculated from a given peak and the order of kinetics. Once the geometrical factor, has been calculated, the corresponding order of kinetics can be determined from Chen's graph.

3.3.3 Curve fitting methods

Developed by Mohan and Chen [15] for first and second order kinetics, and then extended to handle general order kinetics by Shenker and Chen [15], curve fitting methods have become more popular with the progress of computerized data recording methods. Curve fitting is a computerized method in which a function involving kinetic parameters is defined and fitted to the experimental glow curve. The curve fitting exercise starts by making intelligent guesses of the number of glow peaks in a given glow curve. The second step is to assign an appropriate mathematical function, $y(T)$,

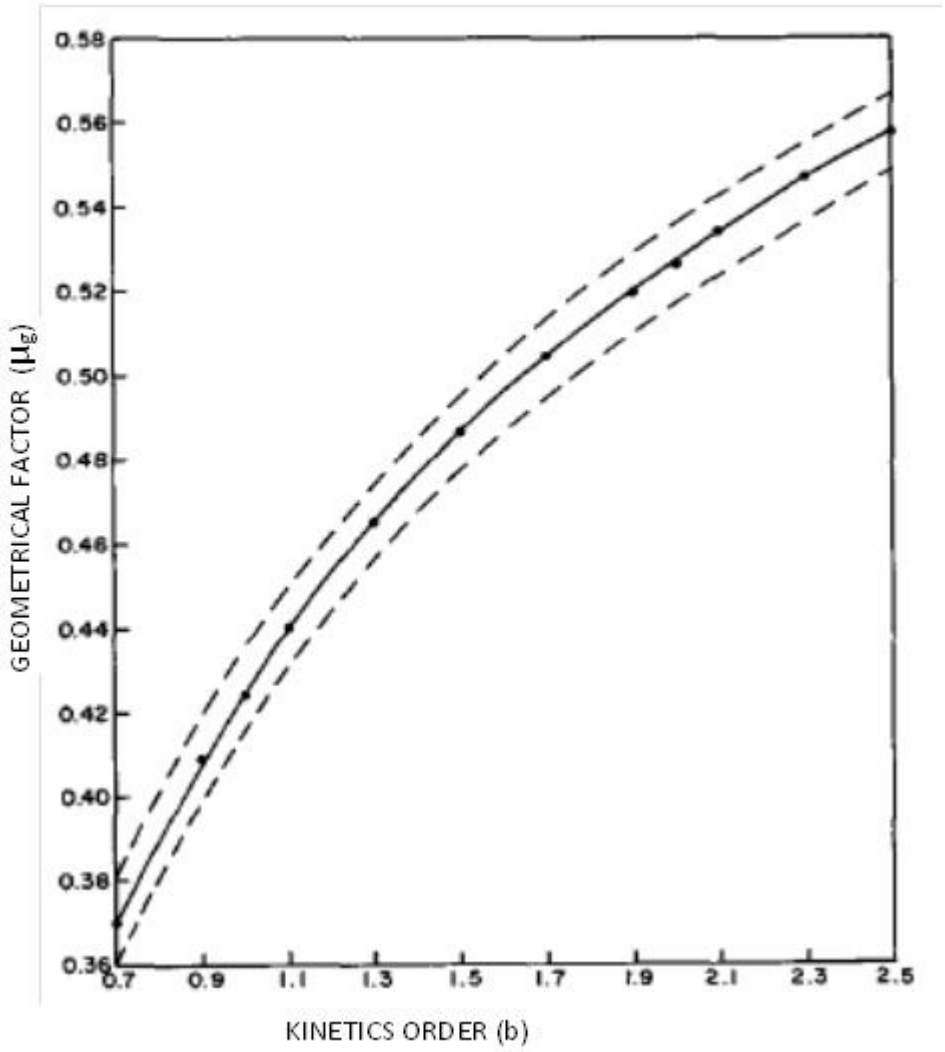

Figure 3.4: The calculated values of the factor, μ_g, as a function of the kinetic order, b. The solid middle curve represents the average values, while as the upper and lower dashed curves represent the most possible variations. Diagram reproduced from Chen [16].

to the identified peaks. Kitis et al [13], derived the mathematical equations for the first, second and general order equations using the series approximation of the TL integrals (i.e using successive integration by parts, in a second order approximation). The approximate equations for first, second and general order respectively as obtained by Kitis et al [13] are

$$I(T) = I_M \exp\left[1 + \frac{E}{kT}\frac{T - T_M}{T_M} - \frac{T^2}{T_M^2}(1 - \frac{2kT_M}{E})\exp(\frac{E}{kT}\frac{T - T_M}{T_M}) - \frac{2kT_M}{E}\right] \tag{3.24}$$

$$I(T) = 4I_M \exp(\frac{E}{kT}\frac{T - T_M}{T_M})\left[\frac{T^2}{T_M^2}(1 - \frac{2kT}{E})\exp(\frac{E}{kT}\frac{T - T_M}{T_M}) + 1 + \frac{2kT_M}{E}\right]^{-2} \tag{3.25}$$

$$I(T) = I_M b^{\frac{b}{b-1}} \exp(\frac{E}{kT}\frac{T-T_M}{T_M}) \left[1 + (b-1)\frac{2kT_M}{E} + (b-1)(1 - \frac{2kT}{E})(\frac{T^2}{T_M^2}\exp(\frac{E}{kT}\frac{T-T_M}{T_M}))\right]^{-\frac{b}{b-1}} \tag{3.26}$$

where I_M is the maximum intensity of the peak in arbitrary units, T_M is the temperature at maximum intensity in K, and the rest of the parameters are as previously defined. Normally E and b are treated as variable parameters while I_M and T_M are usually known from experimental data. The objective of the curve fitting exercise is to find values of E and b which give the optimal fit in terms of least-squares criterion [14]. The popular way of minimizing the difference between the experimental and predicted data (i.e. the residuals) is the Marquardt nonlinear least-squares fitting [15]. A good fit when using Marquadt algorithm gives a high percentage value of regression squared, R^2. Besides R^2, the goodness of fit and hence the reliability of the parameter values, can be determined by using the figure of merit (FOM). The use of FOM as a measure of goodness of fit in fitting TL data was first suggested by Horowitz and Yossian [15]. FOM is calculated as follows:

$$FOM = \sum_i \frac{100 \times |y_{experimental} - y_{fit}|}{\sum_i y_{fit}} \tag{3.27}$$

where $y_{experimental}$ and y_{fit} represent the experimental TL data and the values predicted by the fitting equation, respectively. The summation extends over all region of interest, i, where i denotes experimental data points. The frequency factor, s, is calculated from the values of E, T_M and b obtained from the fitting. The equations for s can be derived by taking the first derivatives of equations 3.11, 3.14, and 3.16 at $T = T_M$ where $dI/dT = 0$. For first order kinetics:

$$s = \frac{\beta E}{kT_M^2}\exp(\frac{E}{kT_M}) \tag{3.28}$$

For second order kinetics:

$$s = \frac{\beta E}{kT_M^2(1 + \frac{2kT_M}{E})}\exp(\frac{E}{kT_M}) \tag{3.29}$$

For general order kinetics:

$$s = \frac{\beta E}{kT_M^2(1 + \frac{2kT_M(b-1)}{E})}\exp(\frac{E}{kT_M}) \tag{3.30}$$

where β is the heating rate in K/s and the rest of the parameters as previously defined.

3.4 Optically stimulated luminescence

Optically stimulated luminescence (OSL) is the luminescence emitted from a previously irradiated insulator or semiconductor during exposure to light [17]. The intensity of OSL is a function of dose

of radiation absorbed by a given material, thus it can be used as a radiation dosimetry method. The OSL process is very similar to the thermoluminescence process and involves the following stages:

Sample irradiation During irradiation, the OSL material is exposed to ionizing radiation (e.g. β-rays, X-rays, gamma rays) which deposits energy that is responsible for ionizing and thus exciting atoms in the crystal lattice and subsequent generation of electron-and-hole pairs. The electrons and holes that have been generated move into delocalized bands i.e. electrons into the conduction band and holes into the valence band, where they become free charges. The irradiation stage which is also known as the excitation stage represents the effect to be measured in the dosimetry applications.

There is a probability that the free electrons in the conduction band and free holes in the valence band may become trapped at the defects in the crystal lattice. For shallow traps i.e. electron traps close to the bottom of the conduction band and hole traps just above the valence band, the trapped charges are subsequently released due to thermal stimulation at ambient temperatures into delocalized bands. In cases where the potential wells (also called trap depth or energy depth) associated with trapping centres are deep enough, thermal energy at ambient temperatures becomes negligible and can no longer release trapped charges. The concentration of trapped charges in metastable states is related to absorbed radiation dose during excitation.

Illumination of an irradiated sample The light incident on the sample may release trapped charge carriers from localized energy states. The released charge carriers may either take part in recombination at a recombination centre to produce light or may get recaptured by the trapping centres. A recombination that results into photon emission is termed as radiative recombination as opposed to non-radiative recombination in which phonons are produced.

The OSL simple model describes the OSL process by considering the case of a one trap centre and one recombination centre model (OTOR), as was the case with the TL simple model described in section 3.1. Charge transport is through the conduction band and assumes that every electron-hole recombination process is radiative. The OSL OTOR model is shown in Figure 3.5. Note that the only difference between the TL model and the OSL model is the stimulating agent: heat in TL model and light in OSL model. Part A of Figure 3.5 shows an electron being excited by ionizing radiation i.e. beta particles. The excited electron moves into the conduction band and then immediately gets captured at the electron trap. The corresponding hole is again captured at the hole trap. Part B of Figure 3.5 represents the simple model of OSL process (OTOR model) in which the captured

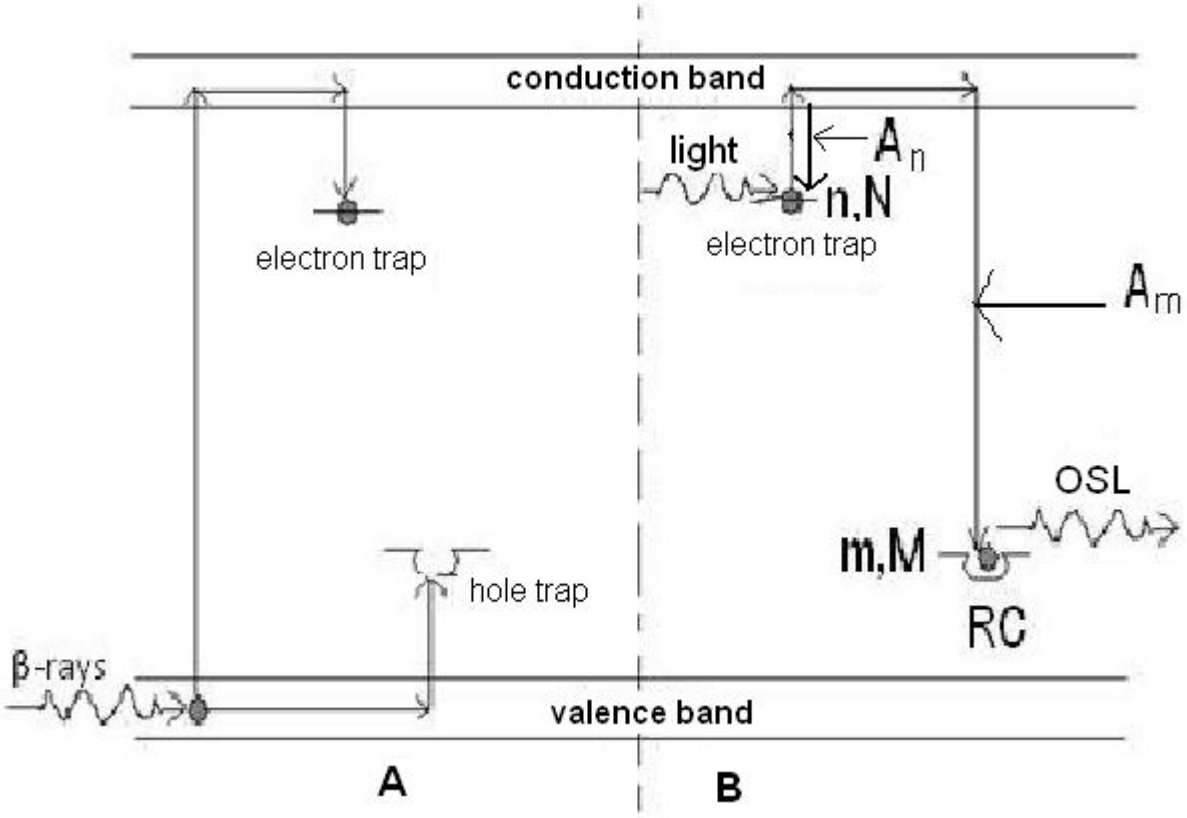

Figure 3.5: A simple OSL model. Part A represents the irradiation stage during which ionization occurs and part B is the stimulation stage during which trapped charges are optically stimulated. All parameters shown have been defined in the text.

electron is released from the trap by stimulation light of de Broglie wavelength λ_{stim} and moves via the conduction band to recombine with the trapped hole at the recombination centre, emitting a photon of wavelength λ_{OSL}. The probability per unit time, p, of electron release from trapping states into the conduction band is directly proportional to the stimulation intensity and the photoionization cross-section,

$$p = \sigma\phi(\lambda) \tag{3.31}$$

where ϕ in photons·m^{-2} s^{-1} is the stimulation intensity or the rate of photon flux and σ in m^2 is the photoionization cross-section. The rate equations of the motion of the trapped carriers between the traps and recombination centers during stimulation by light are similar to the rate equations obtained in the TL simple model and can be summarized as follows:

$$\frac{dn}{dt} = A_n(N-n)n_c - np \tag{3.32}$$

where np is the OSL detrapping rate i.e. the rate at which light stimulates trapped electrons from

trap N, into the conduction band (refer to Figure 3.5).

$$\frac{dn_c}{dt} = np - A_n(N-n)n_c - n_c m A_m \tag{3.33}$$

$$\frac{dm}{dt} = -n_c m A_m \tag{3.34}$$

$$\frac{dn_c}{dt} = -\frac{dn}{dt} + \frac{dm}{dt} \tag{3.35}$$

where A_n ($\mathrm{cm^{-3}s^{-1}}$) is the retrapping probability coefficient of electrons and A_m ($\mathrm{cm^{-3}s^{-1}}$) is the recombination probability coefficient of electrons. Rearranging equation 3.35 we get:

$$\frac{dm}{dt} = \frac{dn_c}{dt} + \frac{dn}{dt} \tag{3.36}$$

Integrating equation 3.36 generates the equation of charge conservation:

$$m = n_c + n \tag{3.37}$$

Equations 3.32, 3.33, and 3.34 form a set of three simultaneous differential equations that is used to describe the dynamics of charge carriers during emptying of traps. The intensity of the optically stimulated luminescence, $I_{OSL}(t)$ must be equal to the rate at which recombination occurs:

$$I_{OSL}(t) = -\frac{dm}{dt} = -(\frac{dn_c}{dt} + \frac{dn}{dt}) \tag{3.38}$$

Assuming quasi-equilibrium state conditions i.e. $n_c << n$ and $|dn_c/dt| << |dn/dt|$:

$$I_{OSL} = -\frac{dm}{dt} = -\frac{dn}{dt} \tag{3.39}$$

Using an approximation that $dn_c/dt \approx 0$ and substituting the expression for n_c from equation 3.33 into equation 3.32 we get:

$$-\frac{dn}{dt} = np\left[1 - \frac{A_n(N-n)}{A_m m + A_n(N-n)}\right] \tag{3.40}$$

Combining equations 3.39 and 3.40 gives:

$$I_{OSL} \approx np\left[1 - \frac{A_n(N-n)}{A_m m + A_n(N-n)}\right]. \tag{3.41}$$

Equation 3.41 is what is referred to as the general OTOR equation for OSL.

3.4.1 First order kinetics

First order kinetics assumes that retrapping is negligible during stimulation and essentially all electrons stimulated from the trap recombine with holes at the recombination centre i.e. $mA_m \gg A_n(N-n)$. Making this assumption reduces equation 3.41 to:

$$I_{OSL} = np \equiv -\frac{dn}{dt} \tag{3.42}$$

The solution to equation 3.42 is:

$$I_{OSL} = n_0 p \exp(-pt) = I_0 \exp(-\frac{t}{\tau}) \tag{3.43}$$

where $\tau = \mathrm{p}^{-1} = [\sigma\phi]^{-1}$ is the decay time constant in seconds, and $I_0 = n_0 p$ is the initial intensity at $t = 0$. Equation 3.43 represents the OSL decay curve of first order and its graph is that of a general exponential decay curve.

3.4.2 Second order kinetics

If we consider the conditions of strong retrapping i.e. $A_n/A_m = 1$, implying $n = m$ then equation 3.40 becomes:

$$-\frac{dn}{dt} = \frac{n^2 p}{N} \tag{3.44}$$

Integrating equation 3.44 and substituting in equation 3.39 gives:

$$I_{OSL} = \frac{n_0^2 p}{N\left[1 + \frac{n_0 pt}{N}\right]^2} \tag{3.45}$$

Equation 3.45 is the normalized second order equation for OSL i.e. $I_{OSL} \propto n_0^2$.

3.4.3 General Order Kinetics

Chen and McKeever [12] proposed the following equations for general order kinetics which are similar to TL general order kinetics equations:

$$-\frac{dn}{dt} = \frac{n^b p}{N^{b-1}} \tag{3.46}$$

where b is a dimensionless kinetic parameter. Thus, the general order kinetics equation for OSL intensity becomes:

$$I_{OSL} = \frac{n_0^b p}{N^{(b-1)}}\left[1 + (b-1)(\frac{n_0}{N})^{(b-1)} pt\right]^{-\frac{b}{b-1}} \tag{3.47}$$

Note that equation 3.47 reduces to first order and second order kinetics when $b \rightarrow 1$ and $b = 2$ respectively.

Optically stimulated luminescence (OSL) has various experimental approaches by which luminescence can be stimulated. The OSL methods are continuous-wave optically stimulated luminescence (CW-OSL), linear modulation optically stimulated luminescence (LM-OSL) and time-resolved optically stimulated luminescence (TR-OSL). These OSL methods are described next.

3.4.4 Continuous wave optically stimulated luminescence

Continuous wave optically stimulated luminescence (CW-OSL) is a technique for measuring OSL in which the stimulation light intensity is kept constant throughout the simulation period while continuously monitoring the OSL signal. CW-OSL makes use of a bandpass filter placed between the stimulation source and the material sample to discriminate between the luminescence and the stimulation signal. A transmission filter placed between the sample and the luminescence detector helps in shielding the detector from scattered stimulation light. The observed luminescence decays in time due to depletion of captured charges and their subsequent radiative recombinations at luminescence centres. The expression for CW-OSL intensity in case of first-order kinetics is given by equation 3.43:

$$I = I_0 \exp(-t/\tau),$$

where τ is the lifetime of the luminescence. For a CW-OSL signal containing multiple components, equation 3.43 becomes

$$I = \sum_{i=1}^{m} I_{0i} \exp(-t/\tau_i) \tag{3.48}$$

where m is the number of components in the CW-OSL signal and I_{0i} is the initial luminescence of signal component i. Figure 3.6 shows a CW-OSL signal obtained from quartz at ambient temperatures following irradiation to 14.3 Gy of beta and stimulated by blue LEDs. The inset in Figure 3.6 shows that the CW-OSL signal for quartz is comprised of three components termed as fast component, medium component and slow component [18].

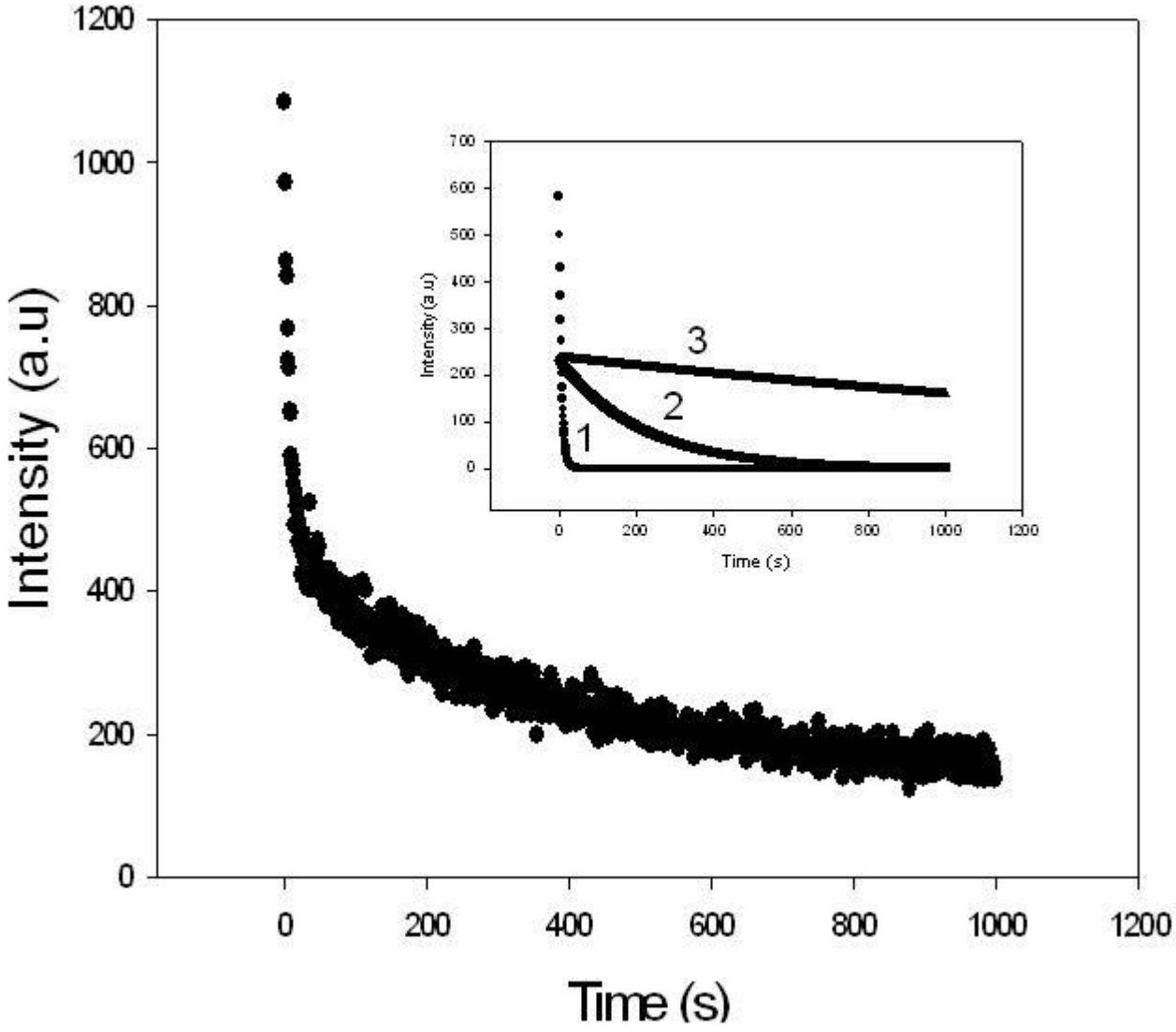

Figure 3.6: CW-OSL signal obtained from quartz at ambient temperatures after being irradiated to 14.3 Gy of beta. Blue LEDs were used for stimulation. The inset shows the fast component (1), the medium component (2) and the slow component (3) of the CW-OSL signal after deconvolution [19].

3.4.5 Linear modulation optically stimulated luminesence

Linear modulation optically stimulated luminescence (LM-OSL) is a method that involves linear ramping of the stimulating light while the OSL signal is being measured. The LM-OSL signal increases proportionally with the constant increase in the stimulation power until a maximum is achieved after which the signal decreases. This produces a peak shape on the curve when the intensity of the linearly modulated OSL signal is plotted against time. In cases where the OSL

signal contains more than one component, the linear increase in power of the stimulation light may result in a curve containing several overlapping peaks, where the most easily stimulated component occurs at a shorter time [20], hence linear modulation can be used to separate overlapping OSL components, which are assumed to originate from different traps. Figure 3.7 shows a LM-OSL spectrum obtained from α-Al_2O_3 :C at ambient temperatures after a beta irradiation dose of 0.1 Gy.

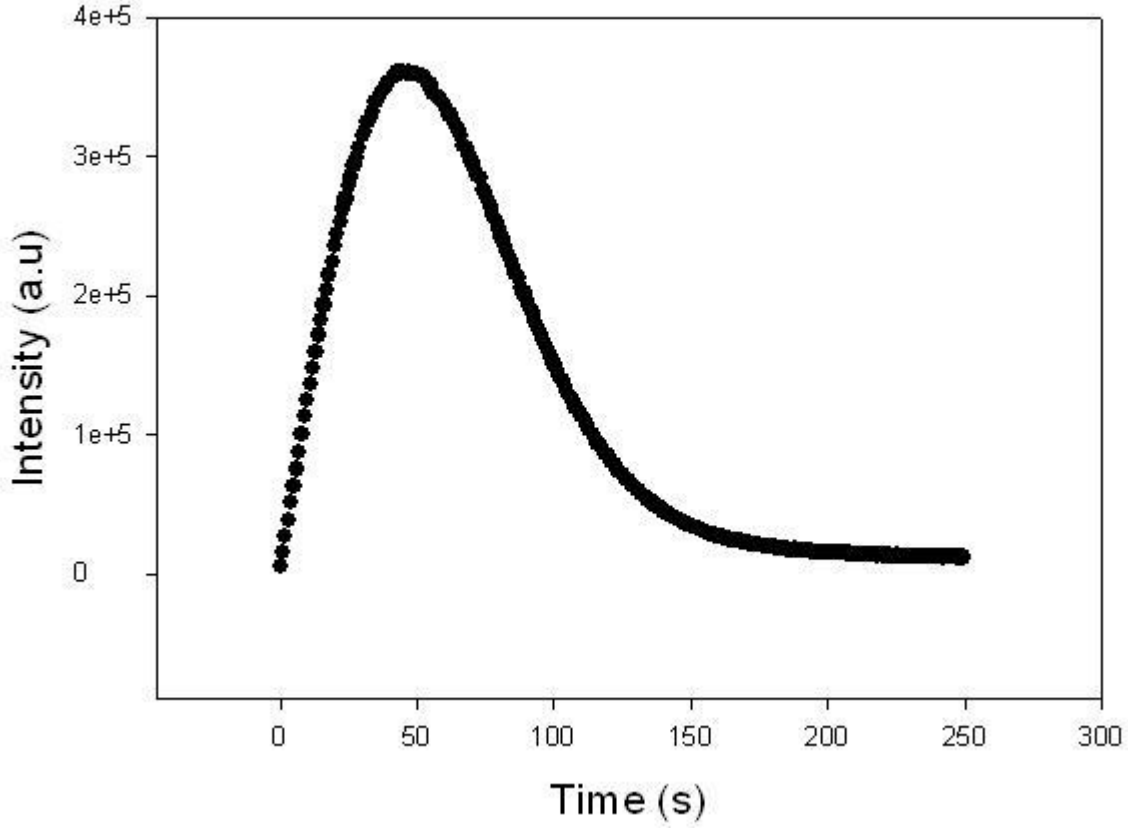

Figure 3.7: LM-OSL spectrum obtained from α-Al_2O_3 :C at ambient temperatures after a beta irradiation dose of 0.1 Gy. The stimulating power of the blue LEDs was ramped from 0 W to 100 W.

For a first-order LM-OSL process in which stimulation photon fluence rate ϕ is increased linearly from zero to a maximum value ϕ_{max} within a period of time, T, the rate of change of electron concentration in the OSL trap is given by

$$\frac{dn}{dt} = -\frac{n\sigma\phi_{max}}{T}t \tag{3.49}$$

Combining equation 3.42 and equation 3.49 provides the expression for the intensity of LM-OSL signal i.e.

$$I_{LM-OSL}(t) \propto \frac{n_0\sigma\phi_{max}}{T}t\exp(-\frac{\sigma\phi_{max}t^2}{2T}) \tag{3.50}$$

The time, t_{max}, at which the peak of the OSL curve occurs, is given by

$$t_{max} = \sqrt{\frac{T}{\sigma\phi_{max}}}. \tag{3.51}$$

The maximum intensity, I_{max} of the peak is given by

$$I_{max} \propto n_0\sqrt{\frac{\sigma\phi_{max}}{T}}\exp(-\frac{1}{2}) = \frac{n_0}{t_{max}}\exp(-\frac{1}{2}). \tag{3.52}$$

3.4.6 Time-resolved optically stimulated luminescence

In time-resolved optically stimulated luminescence (TR-OSL), the stimulation light and the emission light are separated in time. The stimulation source sends out pulses of light and the OSL signal is measured during and after the pulse (i.e. when the stimulation signal is off). A time-resolved spectrum therefore consists of two portions: the luminescence signal during the pulse and the luminescence signal after the pulse [17]. Analysis of time-resolved spectra provides information on the luminescence lifetimes and thus helps to improve our understanding of the dynamics that underlie the emission of the luminescence [21]. TR-OSL is advantageous over CW-OSL in that it allows study of recombination and/or relaxation pathways in the material, and therefore provides important information on the underlying luminescence mechanisms [22].

3.4.6.1 Kinetic analysis of time-resolved optically stimulated luminescence

Kinetic analysis of time-resolved optically stimulated luminescence is aimed at quantitatively analysing the motion of charges from traps to recombination centres both during and after the stimulating pulse. The pulse width of the stimulating signal defines the length of time that a single pulse lasts. Figure 3.8 illustrates the stimulation signal in TR-OSL whereas figure 3.9 is an illustration of a TR-OSL output obtained from high purity synthetic quartz [23]. The kinetic analysis described here has been adapted from Chithambo's work [21, 24].

Let us consider a simple case in which the electron trap, N, as shown in figure 3.5, has an initial electron concentration of A (cm^{-3}). Let the probability of stimulation per unit time from the trap be denoted by p ($cm^{-3}s^{-1}$). And let the probability per unit time that a stimulated electron will recombine radiatively at the recombination centre be denoted by λ ($cm^{-3}s^{-1}$). If n (cm^{-3}) is the number of stimulated electrons at time t during stimulation, then

$$dn(t) = pAdt - \lambda n(t)dt = [pA - \lambda n(t)]\,dt \tag{3.53}$$

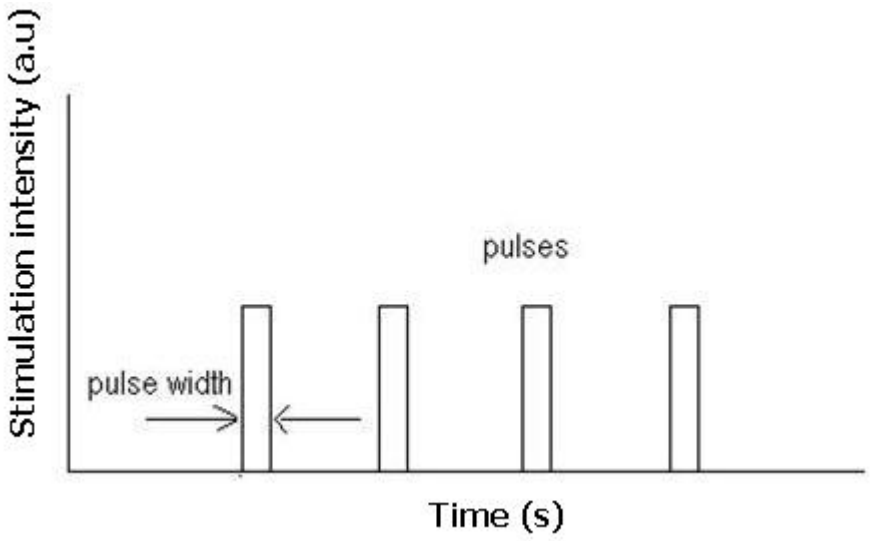

Figure 3.8: The schematic of time-resolved optical stimulation pulses. The pulse width defines the duration of the pulse. The dynamic range is less than or equal to the period of the stimulating signal.

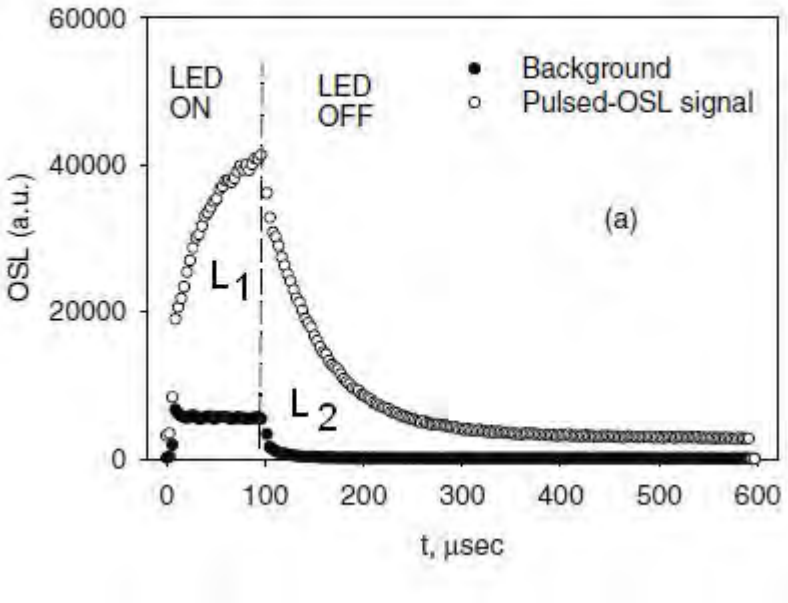

Figure 3.9: TR-OSL spectrum for high purity synthetic quartz. L_1 is the luminescence signal during the pulse and L_2 is the luminescence signal after the pulse. Drawing taken from Pagonis et al [23], modified in this work by including L_1 and L_2.

Equation 3.53 means that the number of stimulated electrons decreases with the rate of electron

recombination. Equation 3.53 is a separable differential equation whose solution is given by

$$n(t) = \frac{pA}{\lambda}\left[1 - \exp(-\lambda t)\right]. \tag{3.54}$$

Equation 3.54 shows the time dependence of stimulated electrons during stimulation at any time t. The rate of emission of luminescence during the pulse duration is given by

$$l_1(t) = pA\left[1 - \exp(-\lambda t)\right]. \tag{3.55}$$

Equation 3.55 is a saturating exponential which shows that the optical detrapping rate and hence recombination increases approximately exponentially towards a limiting maximum value during pulsing [24]. The rate of emission of luminescence after a stimulating pulse of duration t_1 is

$$l_2(t) = \lambda n(t_1)\exp[-\lambda(t - t_1)] \tag{3.56}$$

where $n(t_1)$ represents the number of stimulated electrons after t_1. Equation 3.56 shows that luminescence decays exponentially after the stimulating pulse. Since luminescence is due to decay of stimulated electrons, $n(t)$, it follows therefore that,

$$\frac{dL(t)}{dt} = \lambda n(t) \tag{3.57}$$

where $L(t)$ represents the instantaneous luminescence at any given time t in arbitrary units. Combining equations 3.54 and 3.57 we get,

$$\frac{dL(t)}{dt} = \frac{pA}{\lambda}\left[1 - \exp(-\lambda t)\right] \tag{3.58}$$

Integrating equation 3.58 with respect to time from $t = t_0$ to $t = t_1$, where $t_w = t_1 - t_0$ is the pulse width of the stimulating pulse, and taking $t_0 = 0$, we get:

$$L_1 = pAt_1 + \frac{pA}{\lambda}\left[\exp(-\lambda t_1) - 1\right] \tag{3.59}$$

where L_1 is the total integrated luminescence during stimulating pulse of width t_w. For $t \geq t_1$ i.e. the time after the stimulating pulse, the number of stimulated electrons decays exponentially hence, equation 3.54 becomes

$$n(t) = n(t_1)\exp\left[-\lambda(t - t_1)\right] \tag{3.60}$$

The time dependence of luminescence after the stimulating pulse is therefore given by

$$\frac{dL(t)}{dt} = \lambda n(t_1)\exp(-\lambda(t - t_1)) \tag{3.61}$$

where,

$$n(t_1) = \frac{pA}{\lambda}(1 - \exp(-\lambda t_1).$$

Integrating equation 3.61 from $t = t_1$ to $t = t_2$, we get

$$L_2 = \frac{pA}{\lambda}(\exp(\lambda t_1) - 1)\left[-\exp(-\lambda t_2) + \exp(-\lambda t_1)\right] \tag{3.62}$$

where L_2 is the integrated luminescence after the stimulating pulse. For $t_2 >> t_1$, equation 3.62 becomes

$$L_2 = \frac{pA}{\lambda}\left[1 - \exp(-\lambda t_1)\right]. \tag{3.63}$$

Therefore, the total integrated luminescence, L_T, between $t = t_0 = 0$ to $t = t_2$ is given by:

$$L_T = L_1 + L_2 = pAt_1 \tag{3.64}$$

The fraction of the total integrated luminescence detected after the end of the pulse is termed as the dynamic throughput, f. The term dynamic throughput was coined by Chithambo [24] and is given by

$$DT = \frac{L_2}{L_T} = \frac{L_2}{L_1 + L_2} \tag{3.65}$$

Pagonis et al [22] obtained the following analytical expressions for the luminescence intensity $I(t)$ for a time-resolved pulse,

$$I(t) = A_R \frac{f}{A_R + A_{NR}\exp(-W/kT)}(1 - e^{-[A_R + A_{NR}\exp(-W/kT)]t}) \tag{3.66}$$

$$I(t) = A_R n_2(t_0) e^{-[A_R + A_{NR}\exp(-W/kT)]} \tag{3.67}$$

where A_R and A_{NR} measured in s^{-1} are radiative and non-radiative transition probabilities respectively, W is the activation energy for the non-radiative process, n_2 in cm^{-3} is the concentration of stimulated electrons after the stimulating pulse of width t_0, f is a constant and the rest of the parameters are as previously defined. Equation 3.66 represents the luminescence intensity during the pulse whereas equation 3.67 represents the luminescence intensity after the pulse. Yukihara and McKeever [12] derived the following expressions for the TR-OSL signal during the pulse and after the pulse respectively,

$$I(t) \propto m_0^* e^{-t/\tau} + \frac{n_0 p}{-p + \tau^{-1}}(e^{-pt} - e^{-t/\tau}) \tag{3.68}$$

$$I(t) \propto m^*(\Delta t) e^{-t/\tau}/\tau, \tag{3.69}$$

where n_0 is the concentration of trapped electrons at the beginning of each pulse, m_0^* is the concentration of excited recombination centres at the beginning of each pulse, p is the probability of

photoionization of the trapping centres as defined by equation 3.31, τ is the luminescence lifetime and Δt is the pulse width. The product $m^*(\Delta t)$ in equation 3.69 represents the concentration of excited centres at the end of the stimulating pulse.

Chapter 4

Dynamics of luminescence in α-Al_2O_3 :C

This chapter briefly describes α-Al_2O_3 :C and also presents the model representing the luminescence process in the material. The focus has been placed on the model proposed by Pagonis et al [25] because it has been used to explain results presented in this work.

α-Al_2O_3 :C also known as corundum, is an important, ultrasensitive dosimetric material. α-Al_2O_3 :C samples are grown from a melt at temperatures of about $2050°C$ in a highly reducing atmosphere in the presence of graphite [3]. These growth conditions induce into the material large concentrations of oxygen vacancies i.e. F and F^+ centres which play a significant part in the luminescence process. The material has been known to exhibit strong thermal quenching for temperatures above $150°C$ owing to the fact that its luminescence efficiency is temperature dependent [3].

4.1 Luminescence model

The original model representing the luminescence process in α-Al_2O_3 :C was proposed by Nikiforov et al [26] and was later amended by Pagonis et al [25]. Figure 4.1 represents the model that was amended by Pagonis et al [25]. In this model irradiation of the material excites F-centres from ground state, ^1S, to an excited state, ^1P, (transition f) just below the conduction band (CB) where they become ionized by losing an electron into CB to become F^+-centres i.e. $F^* - e \rightarrow F^+$, where F^* is an excited F-centre and e represents an electron. Once in the conduction band, the electron can be trapped at the defect levels N, M_1 or M_2. During stimulation, the trapped electrons are released usually from trap N into the conduction band. While in the conduction band, the electrons can either be retrapped at trapping sites N, M_1 , M_2 or recombine with the F^+ to produce an excited F centre i.e. $F^+ + e \rightarrow F^*$. An excited F-centre, F^*, relaxes to the ground state ^1S through either a

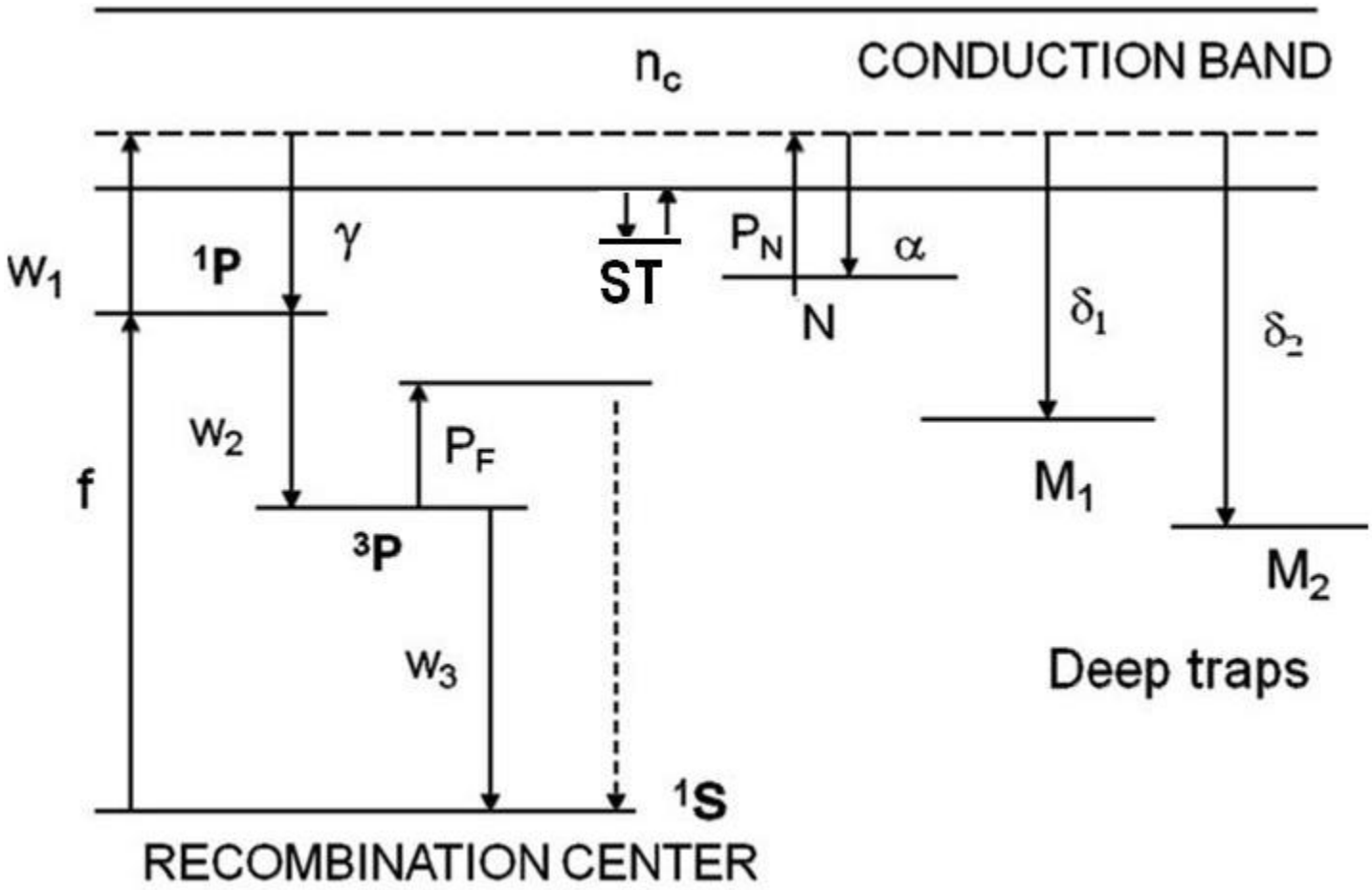

Figure 4.1: Schematic diagram of the model representing the luminescence process in α-Al_2O_3 :C proposed by Pagonis et al [25] showing the recombination centre (F-centre), the main dosimetric trap, N and the deep electron traps (M_1 and M_2), and shallow traps, ST. The diagram has been modified to include shallow traps, ST. Diagram taken from Pagonis et al [25].

radiative path w_3 or a non-radiative path P_F. Luminescence in α-Al_2O_3 :C is due to the transition ^3P to ^1S and is emitted at a 420 nm. The non-radiative path, P_F, is the one responsible for thermal quenching in the material [25], where thermal quenching is the loss in luminescence efficiency with increasing temperature. The set of equations that describe the dynamics of charges in the material during stimulation as described by Pagonis et al [25], is as follows:

$$\frac{dn}{dt} = -P_N n + \alpha(N-n)n_c \tag{4.1}$$

$$\frac{dm_1}{dt} = \sigma_1(M_1 - m_1)n_c \tag{4.2}$$

$$\frac{dm_2}{dt} = \sigma_2(M_2 - m_2)n_c \tag{4.3}$$

$$\frac{dn_{F+}}{dt} = -\gamma n_{F+} n_c + w_1 n_{1_P} \tag{4.4}$$

$$\frac{dn_c}{dt} = P_N n - \alpha(N-n)n_c - \sigma_1(M_1 - m_1)n_c - \sigma_2(M_2 - m_2)n_c - \gamma n_{F+} n_c + w_1 n_{1_P} \tag{4.5}$$

$$\frac{dn_{3_P}}{dt} = w_2 n_{1_P} - P_F n_{3_P} - w_3 n_{3_P} \tag{4.6}$$

$$\frac{dn_{1_P}}{dt} = f + \gamma n_{F+} n_c - w_{1_P} - w_2 n_{1_P} \tag{4.7}$$

$$n + m_1 + m_2 + n_c = n_{F+} \tag{4.8}$$

$$I_L = w_3 n_{3_P} \tag{4.9}$$

where N, M_1, and M_2, (cm^{-3}) denote the total concentration of dosimetric and deep traps; n, m_1, m_2, n_{1_P} and n_{3_P} (cm^3) stand for instantaneous concentration of occupied levels in N, M_1, and M_2, ^{1}P and ^{3}P, respectively; n_{F+} (cm^{-3}) is the concentration of F^+-centers; n_c (cm^{-3}) is the concentration of electrons in the conduction band; $\alpha, \sigma_1, \sigma_2$ and γ ($\mathrm{cm}^{-3}\ \mathrm{s}^{-1}$) are the capture coefficients of charges at the levels indicated in Figure 2.11; w_1, w_2 and w_3 (s^{-1}) denote the transition probabilities; f ($\mathrm{cm}^{-3}\ \mathrm{s}^{-1}$) is the excitation intensity ($f = 0$ during stimulation); $P_N = s\exp(-E/kT)$ is the detrapping probability of the dosimetric trap (s, E, k and T as previously defined); $P_N = C\exp(-W/kT)$ is the probability of thermal ionization of ^3P state where W is the thermal quenching activation energy in eV and C is a constant.

Equation 4.1 means the rate of change of the concentration of trapped electrons at N is equal to the thermal detrapping rate (first term) and retrapping rate (second term). The filling of traps M_1 and M_2 with charges, is summarized by equations 4.2 and 4.3 respectively. Equation 4.4 means that the ionization of excited F-centres increases the concentration of F^+-centres whereas the recombination of F^+- centres with conduction electrons decreases the concentration of F^+-centres. The change in the concentration of electrons in the conduction band is therefore due to change in the concentration of electrons in traps N, M_1, and M_2 as well as due to change in the concentration of F^+-centres as summarized by equation 4.5. Equation 4.6 represents the change in the concentration of excited F-centres at energy state ^3P whereas equation 4.7 represents the change in the concentration of F^+-centres at energy state ^1P. Equation 4.8 ensures that charge is conserved at all times. Equation 4.9 is the expression for the instantaneous luminescence intensity.

Chapter 5

Experimental Methods

This chapter gives a full account of the TR-OSL and TL instrumentation used for the investigations reported in this thesis. Furthermore, it describes the samples and the methodology used during the investigations. The apparatus used for the present work consisted of a luminescence pulsing system for measuring TR-OSL and the Risø TL/OSL Luminescence Reader Model TL/OSL-DA-20 for measuring TL.

5.1 TR-OSL read-out system

The TR-OSL system used in this project is the LED based pulsing system designed and described by Chithambo and Galloway [27], the modified version of which was described by Chithambo [28]. The system is comprised of a stimulation unit, detection unit, data acquisition and processing unit, and the sample stage and temperature control units. Figure 5.1 represents the schematic diagram of the pulsing system that was reported by Chithambo [28] showing the stimulation unit (LEDs), the detection unit (EMI 9635QA photomultiplier), the data acquisition and processing unit (Multichannel scaler ORTEC MCS-plus) and the multivibrator circuit (2N74221).

5.1.1 Stimulation unit

The stimulation unit consists of a set of 16 blue LEDs (Nichia NSPB-500) driven by pulses generated from a multivibrator using an integrated circuit (IC) 2N74221 at some pulse width determined by the resistor-capacitor (RC) timing components connected externally to the IC. The Multichannel Scaler (EG and G ORTEC MCS-plus^{TM}) generates the trigger signal for the initiation of the stimulation

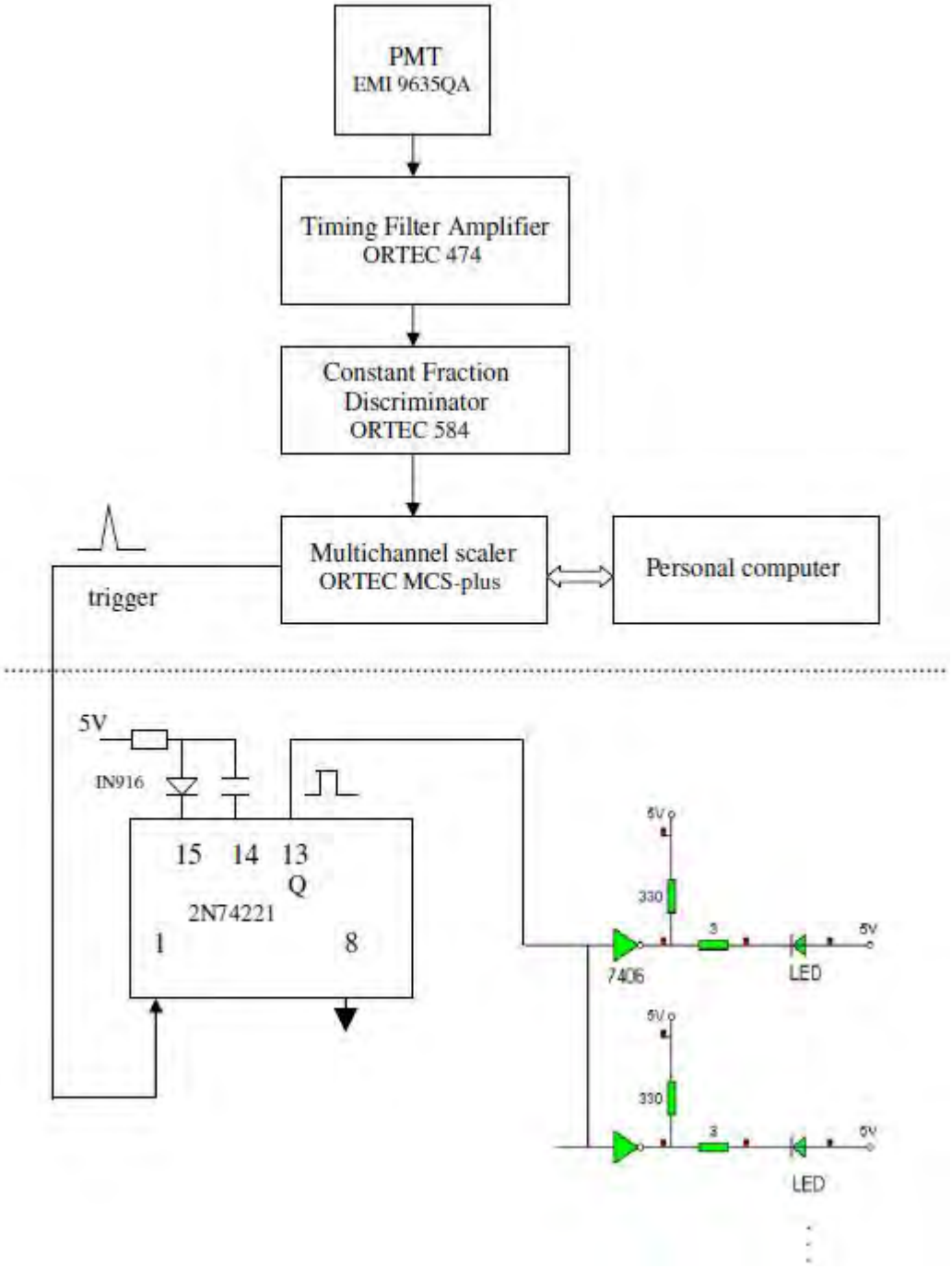

Figure 5.1: A schematic diagram of the pulsing system for stimulation, detection and processing of a time-resolved luminescence spectrum. Drawing taken from Chithambo [28].

process. The dynamic range and the number of sweeps are both set in the Multichannel Scaler (MCS).

5.1.2 Detection unit

Luminescence detection is done by the photomultiplier tube (EMI 9235). The detected luminescence signal is amplified by the timing filter amplifier (Ortec 474) and then counted by the constant fraction discriminator (Ortec 584) [28]. Detection filters used in this study were Schott BG39 and UG11 with transmission windows of 340-620 nm FWHM and 270-380 nm FWHM, respectively.

5.1.3 Data acquisition and processing unit

Besides triggering a set of LEDs, the MCS also initiates the data-recording process. Once the scan is initiated, the MCS begins to acquire photon counts, sequentially recording data in its memory one channel after another, with no dead time between channels. The time-resolved luminescence spectrum is a plot of cumulative photon counts against time for the selected dynamic range [28].

5.1.4 Sample stage and temperature control unit

Figure 5.2: The Annealing Oven Model AO500 (a) where 1 is the the sample holder, and 2 is the touch screen user panel for controlling and programming the unit, (b) top view of the sample stage.

The Annealing Oven Model AO500 (MBE-Komponenten) shown in Figure 5.2 provides both the sample stage where samples are placed, and the temperature control unit that controls the heating of the sample. The oven provides heat treatment from 30°C up to 500°C to a sample placed in air, in a well controlled gas atmosphere or vacuum with pressures set between 5 mbar to 1000 mbar. Optical access to the sample is provided by an opening on the top of the heater where LEDs are placed (see Figure 5.2). At the centre of the oven, there is a direct current driven ceramic thin film

heater with adapted PT100 temperature sensor, an arrangement that ensures rapid heating up of the heater due to minimized thermal inertia, precise temperature control and provides a low thermal load to the sample.

5.2 Thermoluminescence system

Thermoluminescence was measured using a Risø TL/OSL Luminescence Reader Model TL/OSL-DA-20, that measures both TL and OSL. The TL/OSL Reader consists of the light detection unit, thermal stimulation unit, optical stimulation unit, and irradiation unit. The Reader can hold up to 48 samples on its carousel. The heating temperature ranges from room temperature up to 700°C. Figure 5.3 represents the schematic diagram of the Risø Reader showing the irradiation unit (irradiator), the detection unit (photomultiplier tube and detection filter), the stimulation unit (heater plate, LEDs and emission filter) and the sample holder (sample carousel). The system has a controller that controls the performance of its hardware components.

5.2.1 Light detection unit

The light detection unit is comprised of the photomultiplier tube and detection filters. A photomultiplier tube (EMI 9235) is a device that detects luminescence. Detection filters prevent stimulation light that has scattered off the sample from reaching the photomultiplier tube. Thus, detection filters help in reducing the amount of unwanted signal i.e. noise in the luminescence signal. They also define the spectral window and ensure that the spectral stimulation region is well separated from the detection window. The detection filter used in this project was a 7.5 mm thick Hoya U-340 filter, with a detection window of 270 - 380 nm FWHM.

5.2.2 Thermal stimulation unit

The thermal stimulation unit is made up of the heating element that heats the sample, and the lift mechanism that places the sample into measurement position. Heating of the sample is achieved by feeding controlled direct current through the heating element. The heating system is able to heat samples at temperatures ranging from room temperature up to 700°C at various heating rates from 0.01°Cs^{-1} to 10 °Cs^{-1}. Nitrogen flow into the chamber protects the heating system from oxidation at higher temperatures. The nitrogen atmosphere also prevents spurious luminescence from any air

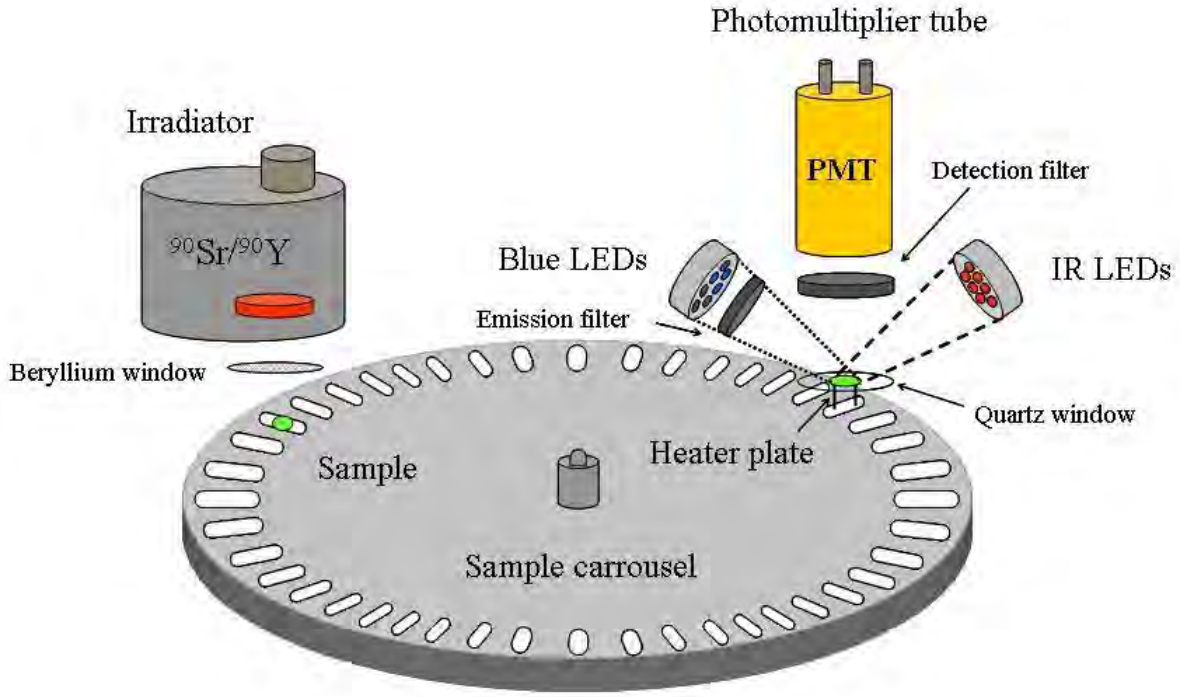

Figure 5.3: A schematic diagram of the TL/OSL Risø Reader showing the irradiation unit ($^{90}Sr/^{90}Y$ beta source), the sample carousel, the detection unit (PMT) and the stimulation units (blue LEDs for OSL, heater plate for TL, and IR LEDs for IRSL) [29].

in the chamber.

5.2.3 Irradiation source

The TL/OSL Reader uses a beta source for irradiation although alpha and X-irradiation sources are optional. A beta irradiator is located above the sample carousel and in the model used for our study, accommodates a 1.48 GBq (40 mCi) $^{90}Sr/^{90}Y$ beta source, which emits beta particles with a maximum energy of 2.27 MeV. Irradiation is software controlled allowing minimum single irradiation times of 1 s. The beta irradiation source used in the study was calibrated at 0.1028 Gy/s.

5.3 Samples and Procedures

All samples used in this project were α-Al_2O_3:C disks measuring 5 mm in diameter and 1 mm thick, obtained from Rexon TLD Systems, Ohio, USA. Samples were annealed in a furnace (LABOFURN LEF014, Kiln contracts Ltd) at 900°C for 15 minutes, followed by rapid cooling in air. Annealing is a thermal treatment procedure that involves heating the TL samples to a predetermined temperature, keeping them at that temperature for a defined period of time and then cooling the samples to room temperature. The major purpose of annealing is to erase any previous irradiation memory from the luminescent material under study before a new measurement can be made, hence annealing ensures that deep traps are empty.

TR-OSL was then measured from irradiated samples. The generated data was analysed using commercial data analysis packages namely, Sigma Plot 8.0 (Systat Software Inc.,California) and Mathematica 8.0 (Wolfram Research). Unless otherwise stated, the blue LEDs were pulsed at a pulse width of 18 ms and the signal measured with a dwell time of 1 ms, the total number of scans was 100 and the dynamic range was set to 500 ms. Thus the total illumination time was 1.8 s (number of scans× pulse width), and the stimulation source was off for about 48.2 s (number of scans ×(dynamic range - pulse width)). Aluminium oxide disks were mounted on stainless steel disks and placed on the sample holders as described in section 5.1.4. A dural holder with 16 blue LEDs lit was placed on top of the holder directly above the sample. The photomultiplier was placed on top of the dural holder to detect the TR-OSL signal. The trigger-signal was synchronized to the start of the sweep from the multichannel scaler. Once the sweep was initiated, the multichannel scaler started acquiring photon counts in the first channel of its memory. The dwell time defined time spent on a single channel after which the multichannel scaler proceeded to the next channels. This process was repeated for all the selected channels with no dead time between channels and at the end of each scan. The measurement temperature of the sample above room temperature was set on the temperature controller.

In TL measurements, samples were mounted on stainless steel disks and loaded onto a sample carousel placed in the sample chamber. Measurements were made in a nitrogen atmosphere to minimise the occurrence of spurious signals and to ensure uniform heating of the samples. The instructions governing the TL process were written in Sequence Editor software (Risø DTU) which was also responsible for the initiation of the process. The recorded TL data was extracted using Analyst software (written by Prof. G. Duller, University of Wales, UK) for analysis in Sigma Plot

8.0 imported via Windows Microsoft Excel. Unless otherwise stated, all measurements of TR-OSL were done at ambient temperatures.

Chapter 6

Results and Discussions

This chapter presents the results and discussions of the results obtained from the various TL and TR-OSL experiments carried out during the investigations.

6.1 Thermoluminescence

The number of peaks and the position of these peaks in a thermoluminescence glow curve provide important information on the distribution of traps (or defects) in the forbidden band of the luminescent material. In order to determine the number of available peaks in the TL glow curve of α-Al_2O_3:C, two sets of TL measurements were taken at a very low heating rate of 0.03°C/s, one corresponding to low dose (0.1 Gy) and the other to a relatively high dose (6.0 Gy). The low heating rate was chosen as a matter of expediency, since thermal quenching (i.e. incidences of non-radiative emission) effects are minimal at low heating rates [3]. Figure 6.1 shows the resulting TL glow curve at the irradiation dose of 0.1 Gy whereas Figure 6.2 is the TL glow curve obtained at the irradiation dose of 6.0 Gy. In the inset of both Figure 6.1 and Figure 6.2 is the corresponding plot with the intensity plotted on a log scale.

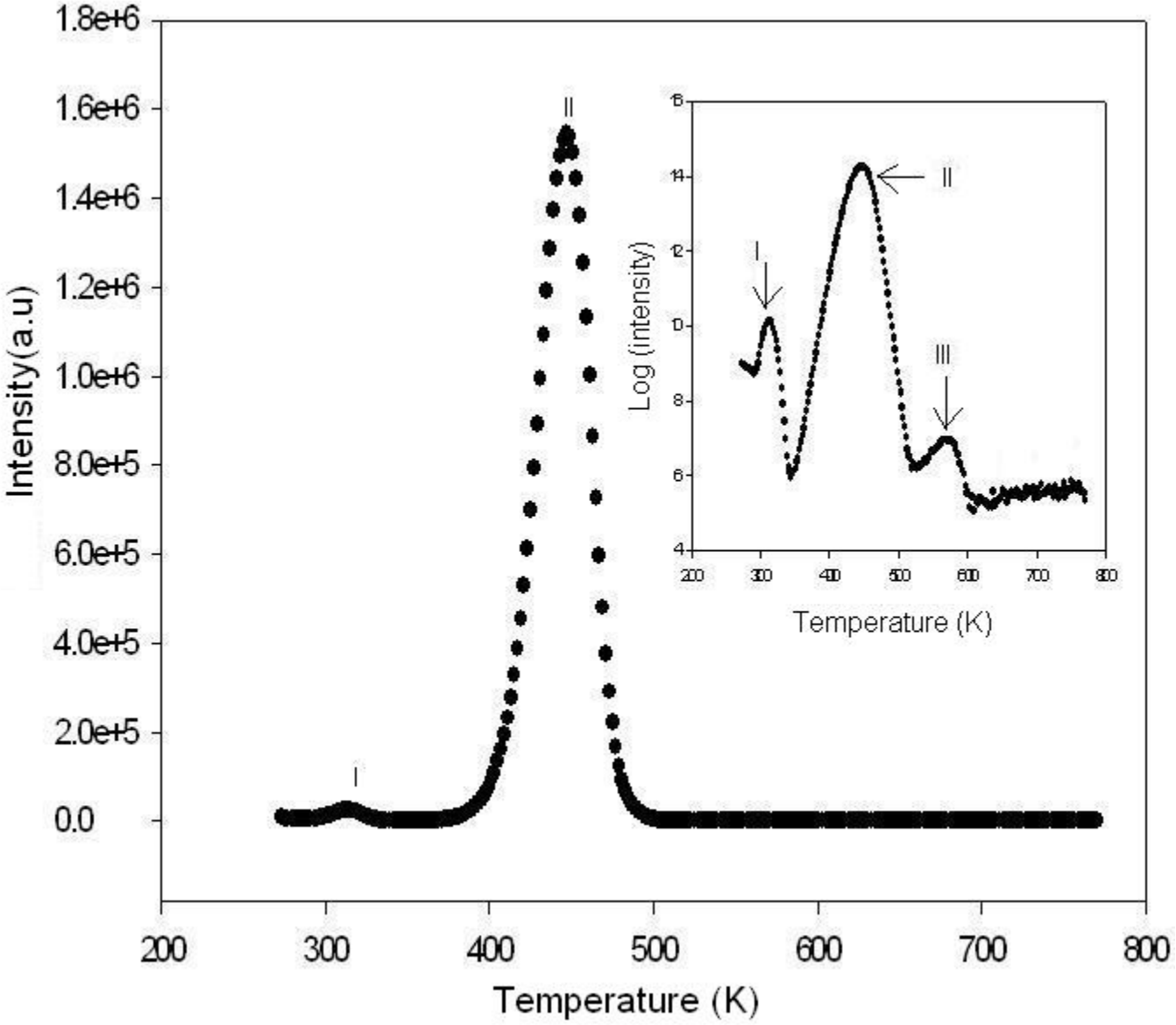

Figure 6.1: A TL glow curve obtained at a heating rate of 0.03°C/s after beta irradiation of 0.1 Gy. Two peaks, I and II are apparent in normal scale whereas the inset shows three apparent peaks. The intensity in the inset is in log scale.

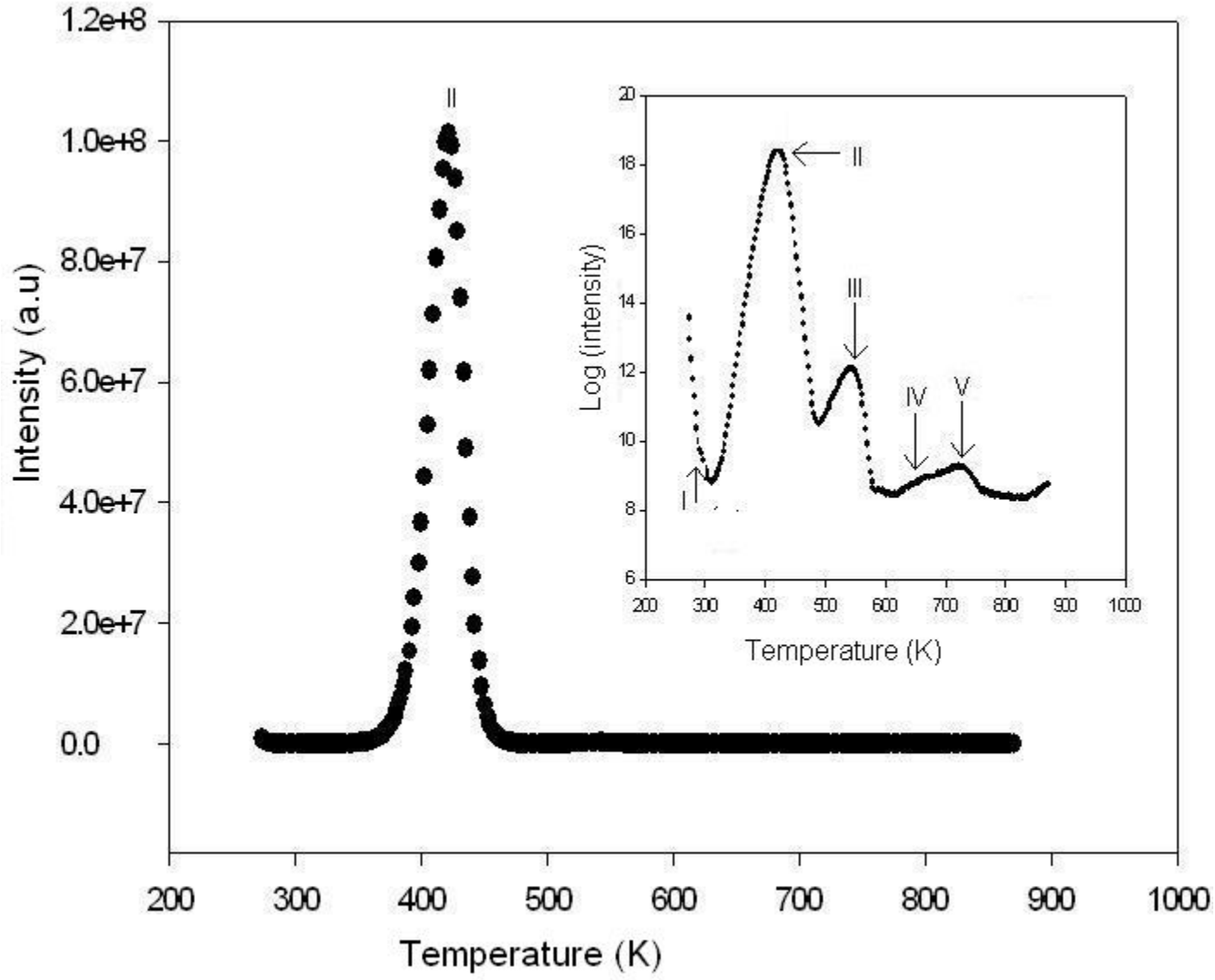

Figure 6.2: A TL glow curve obtained at a heating rate of 0.03°C/s after irradiating the sample to 6.0 Gy. The inset shows the presence of five peaks namely, I, II, III, IV and V. The intensity in the inset is in log scale.

In Figure 6.1, the main graph shows a TL glow curve with the main peak (peak II) at 160°C (433 K) and a lower temperature peak (peak I) at 37°C (310 K). Peak II is referred to as the main peak because of its very high intensity relative to the other peaks in the sample. Peak II is the peak that is used for dosimetric applications. The other peaks, such as peak I, are referred to as subsidiary or auxiliary peaks. The inset shows the presence of a third peak (peak III) at 300°C (570 K) which is not visible in the normal scale plot. The much higher intensity of peak II overshadows the presence of the low intensity peaks I and II. The three peaks (I, II, and III) have been previously

observed and studied by several researchers e.g. Chithambo [30] reported on the dose response to beta irradiaton of the three peaks at a heating rate of 5°C/s; Kulkarin et al [31] observed peaks I and II at a heating rate of 4°C/s after exposing the sample to 0.33 Gy of beta irradiation; Kortov and Milman [9] observed all three peaks and an additional peak between peaks I and II at a heating rate of 2°C/s in measurements in which their samples were initially bombarded with high energy electrons (16 MeV), annealed at 327 °C then X-ray irradiated at 120 Gy . The major focus, however, has been on peak II [7, 32, 33], because of its application in radiation dosimetry. As a result, little has been reported about the subsidiary satellite peaks.

Figure 6.2 represents the glow curve obtained from the same sample irradiated to 6.0 Gy and shows the presence of the main peak (II) only on a normal scale. The inset of Figure 6.2 however, shows the presence of five peaks namely, peaks I, II, III, IV and V. Peak I is obscure in Figure 6.2 because of increased amount of phosphorescence (shown as the decay at the initial part of the glow curve) as a result of increase in dose. Peak III shows increased intensity when the sample is irradiated to 6.0 Gy and strongly overlaps with peak II as compared to when the sample is irradiated to 0.1 Gy. Besides the three peaks (I, II,and III), two more high temperature peaks (IV and V) with strong overlapping appear at around 410°C (683 K) and 480°C (753 K). Milman et al [34] observed peaks from α-Al_2O_3:C at 180°C, 300°C, 460°C, and 610°C following ultraviolet irradiation and at a heating rate of 2°C/s . Molnar [34] also observed similar peaks reported by Milman et al when the TL measurement was done at a heating rate of 2°C/s after X-ray exposure. Lo et al [34] studied the dose dependence of the high temperature peaks in α-Al_2O_3:C at a heating rate of 5°C/s using powdered samples and observed peaks at 200°C, 330°C, 505°C, and 630°C after beta irradiation of up to about 100 Gy. The peaks at 200°C and 330°C reported by Lo et al [34] are peaks II and III shown in Figure 6.2. It is however not certain whether peaks IV and V shown in Figure 6.2 are the same peaks observed by Lo et al [34] at 505°C and 630°C. At doses above 15 Gy peaks IV and V merge (to be discussed later) hence cannot be separated, whereas the peaks at 505°C and 630°C as reported by Lo et al [34] are well separated at doses as high as 100 Gy. All the observed peaks can be attributed to the presence of different species of traps in the energy gap which are emptied at the respective temperatures at which they appear in the glow curve, and this is consistent with the TL model of α-Al_2O_3:C (Figure 4.1). Peak I is therefore as a result of emptying of the less stable shallow traps (ST); the main peak (II) is due to the detrapping of electrons from relatively stable traps (N); and peak III is attributed to charge emptying of more stable deep traps (e.g. M_1). Peaks IV and V occurring at even higher temperatures can be attributed to much deeper electron traps in

the band gap.

Figure 6.2 corresponding to a dose of 6.0 Gy shows relatively higher intensities for all the peaks than for irradiation dose of 0.1 Gy, Figure 6.1. The higher intensities at higher dose is expected because high dose increases the concentration of captured charges in the traps, and this in turn increases the number of charges involved in recombination to produce luminescence, hence increased intensities.

6.1.1 Kinetic Analysis

Kinetic analysis is the analysis of a thermoluminescence glow curve in order to determine physical parameters of the traps and establish the kinetics of the charge-carrier transfer between them [14]. Knowledge of the physical parameters of traps and the kinetics of charges, helps to enhance our understanding of the luminescence process in the material. A thorough understanding of the luminescence process in the material may improve or widen the applicability of the material. In this section, various methods of kinetic analysis are used to analyse the TL glow curve with the aim of extracting some parameters of the traps involved in the TL process, particularly the dosimetric trap which is responsible for peak II.

6.1.1.1 Curve fitting of the main peak

The aim of fitting the main peak (peak II) was to obtain kinetic parameters such as trap depth, E, kinetic order, b and the frequency factor s associated with the dosimetric trap. The sample was irradiated to 1.0 Gy followed by a TL measurement at a heating rate of 0.03°C/s. The low heating rate was chosen to ensure uniform heating of the sample and minimise thermal quenching effects on the peak height. The main peak was isolated from the rest of the TL glow curve and then fitted with a modified version of equation 3.26 for general order kinetics. Equation 3.26 was modified in this work by multiplying the whole equation with a scaling factor of 3 in order to reproduce the peak intensity obtained from the experimental data:

$$I(T) = 3I_M b^{b-1} \exp\left(\frac{E(T-T_M)}{kTT_M}\right)\left[(b-1)\frac{T^2}{T_M^2}\left(1-\frac{2kT}{E}\right)\exp\left(\frac{E(T-T_M)}{kTT_M}\right)+1+(b-1)\frac{2kT_M}{E}\right]^{-\frac{b}{b-1}}, \tag{6.1}$$

where all parameters are as previously defined. Figure 6.3 is the graph of the main peak fitted with equation 6.1 and the solid line through the data points is the best fit of equation 6.1. In the inset of Figure 6.3 is the residuals plot. Residuals are simply the differences between the experimental

values and the values predicted by the regression model. In this particular case the regression model is equation 6.1. The appropriateness of a regression model for the experimental data is shown when the points in a residual plot are randomly scattered around zero on the horizontal axis. Regression-squared, R^2, and the figure of merit, FOM, were the two parameters used to show the goodness-of-fit and hence the reliability of the fitting parameters. Table 6.1 provides a summary of values for the fitting parameters extracted using equation 6.1 from TL curves of the main peak obtained at various heating rates. The values of s presented in Table 6.1 were calculated using equation 3.30 which is valid for general-order kinetics :

$$s = \frac{\beta E}{kT_M^2(1 + \frac{2kT_M(b-1)}{E})} \exp\left(\frac{E}{kT_M}\right).$$

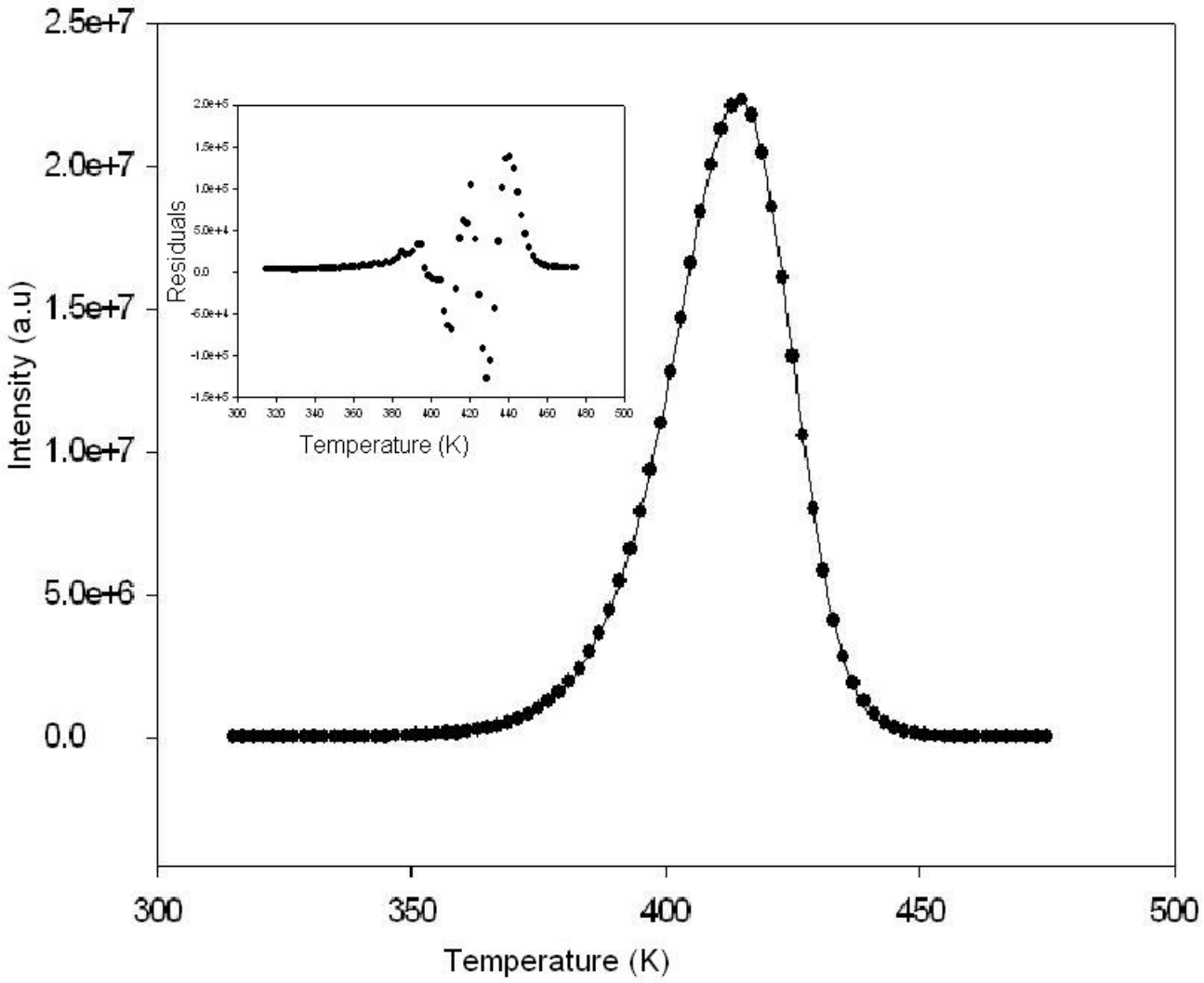

Figure 6.3: The TL main glow peak of α-Al_2O_3:C obtained at a heating rate of 0.03 K/s and fitted with equation 6.1. The sample was irradiated to 1.0 Gy at ambient temperatures. The values of the parameters showing the goodness of fit are: R^2= 0.9999 and FOM =2.8%. In the inset is the residuals plot showing the appropriateness of the regression model.

It can be seen from Table 6.1 that E and consequently s decreases slowly with increasing heating rate. This decrease in E and s with increasing heating rate can be attributed to thermal quenching effects. Kitis et al [7] and also Pagonis et al [13] explained this decrease of E with increasing heating rate on the basis of thermal quenching. The value of the kinetic order, b, on the other hand increases from 1.19 at 0.05 K/s to about 1.29 at 0.8 K/s then starts decreasing to about 1.16 at 8.0 K/s. This behaviour of b appears not to be influenced by E suggesting that there could be a different reason

Table 6.1: Kinetic parameters for the main peak: HR is the heating rate in K/s, T_M is the peak temperature in K, E is the trap depth in eV, b is the kinetic order, and s is frequency factor in s^{-1}.

HR	T_M	E	b	s(x10^{11})
0.003	414.4± 0.1	1.41±0.01	1.23±0.01	4210
0.05	421.8±0.1	1.38±0.01	1.19±0.01	1324
0.10	428.4±0.1	1.35±0.01	1.22±0.01	1050
0.30	440.4±0.1	1.32±0.01	1.27±0.01	249
0.50	450.2±0.1	1.28±0.01	1.28±0.01	65
0.80	457.2±0.1	1.24±0.01	1.28±0.01	29
1.00	459.2±0.1	1.22±0.01	1.28±0.01	16
3.00	477.7±0.1	1.14±0.01	1.23±0.02	1.5
5.00	501.4±0.1	1.14±0.01	1.12±0.01	0.77
8.00	524.3±0.1	1.16±0.01	1.16±0.01	0.54

behind such behaviour.

Figure 6.4 shows how peak height of the main peak, peak II, varies with the heating rate. Figure 6.5 shows how peak height of peak III varies with heating rate and Figure 6.6 shows how the peak height of peak I varies with heating rate. All peak heights were quoted in arbitrary units. As shown in Figure 6.4, peak height for the main peak, peak II, decreases with increasing heating rate due to thermal quenching of F-centres. Similarly for peak III as shown in Figure 6.5, peak height decreases with increasing heating rate. We can only speculate that the cause of the decrease in peak height in peak III, may be due to thermal quenching because to our knowledge, the effects of thermal quenching on peak III have not yet been investigated and it is still not clear as to whether the F-centres are also responsible for luminescence of peak III. On the other hand, peak height of peak I initially increases at low heating rates up to 3.0 K/s when it starts decreasing (see Figure 6.6). The behaviour of peak height with heating rate in peak I also needs further investigations. The change of peak intensity with heating rate as reported here was also observed by Kitis et al [7].

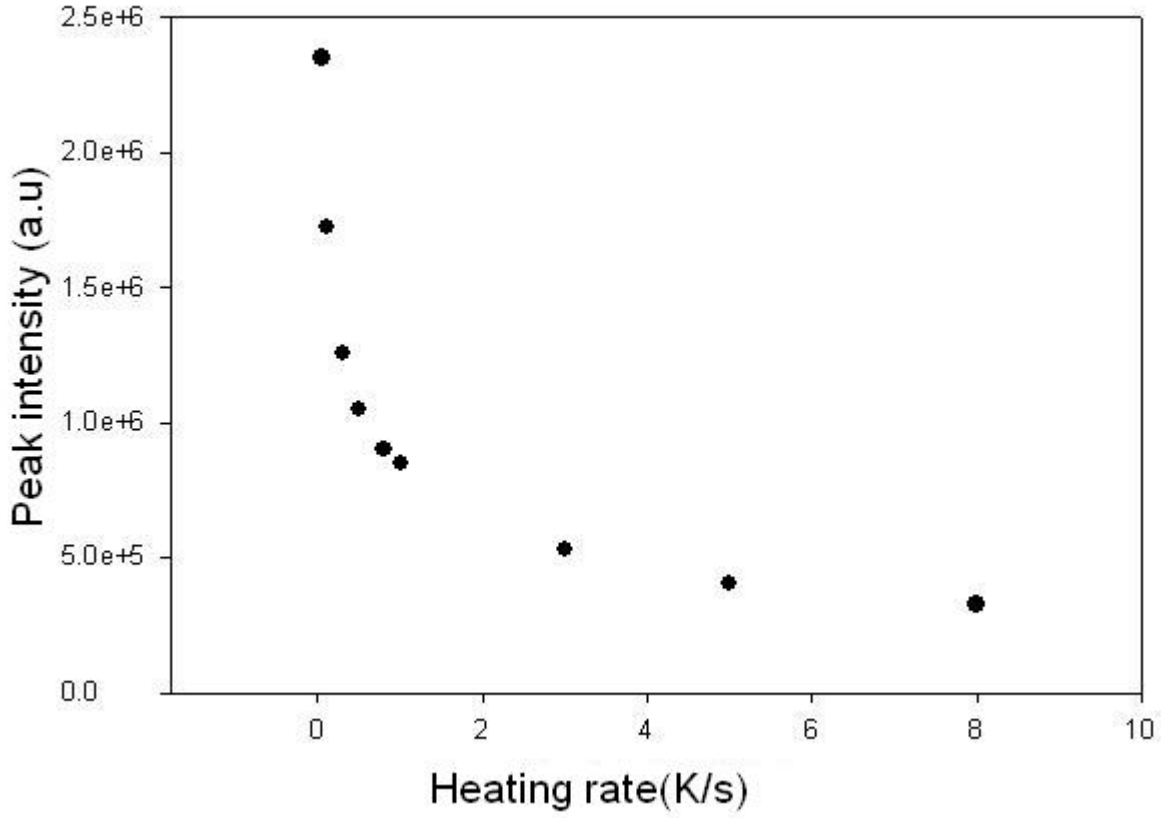

Figure 6.4: Peak height as a function of the heating rate for the main peak, peak II. The sample was irradiated to 1.0 Gy at ambient temperatures.

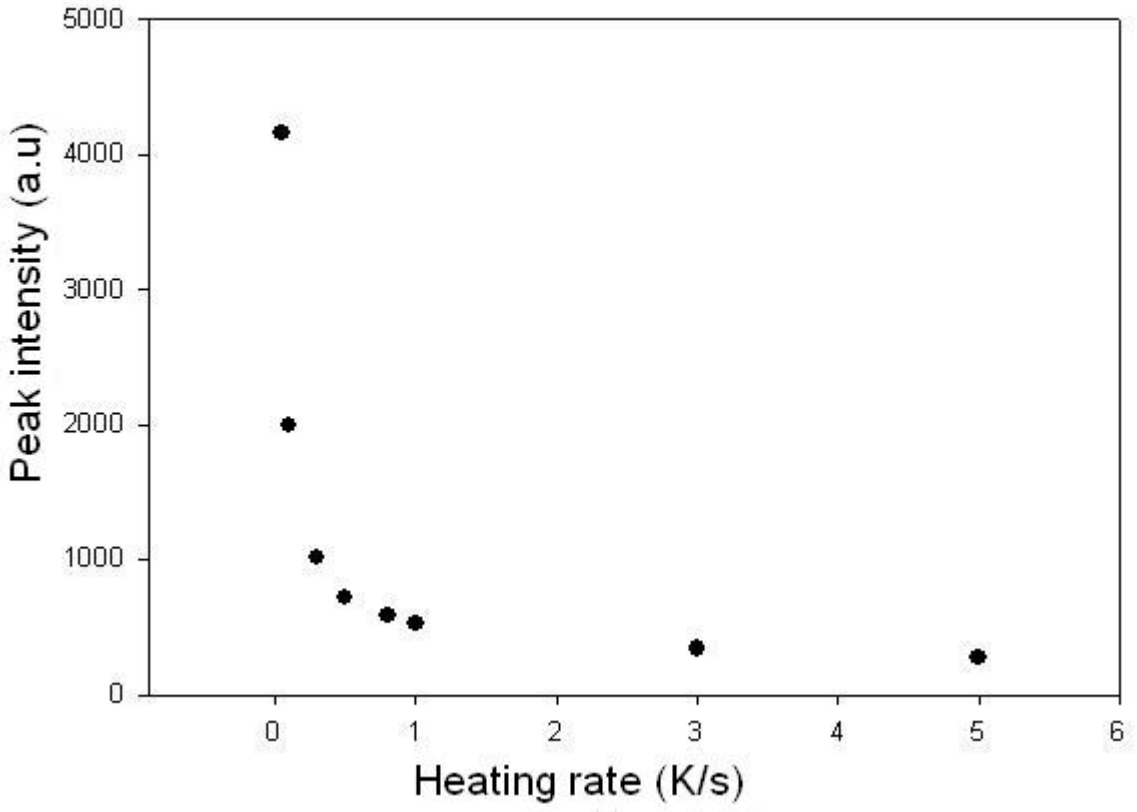

Figure 6.5: Peak height as a function of heating rate for peak III. The sample was irradiated to 1.0 Gy at ambient temperatures.

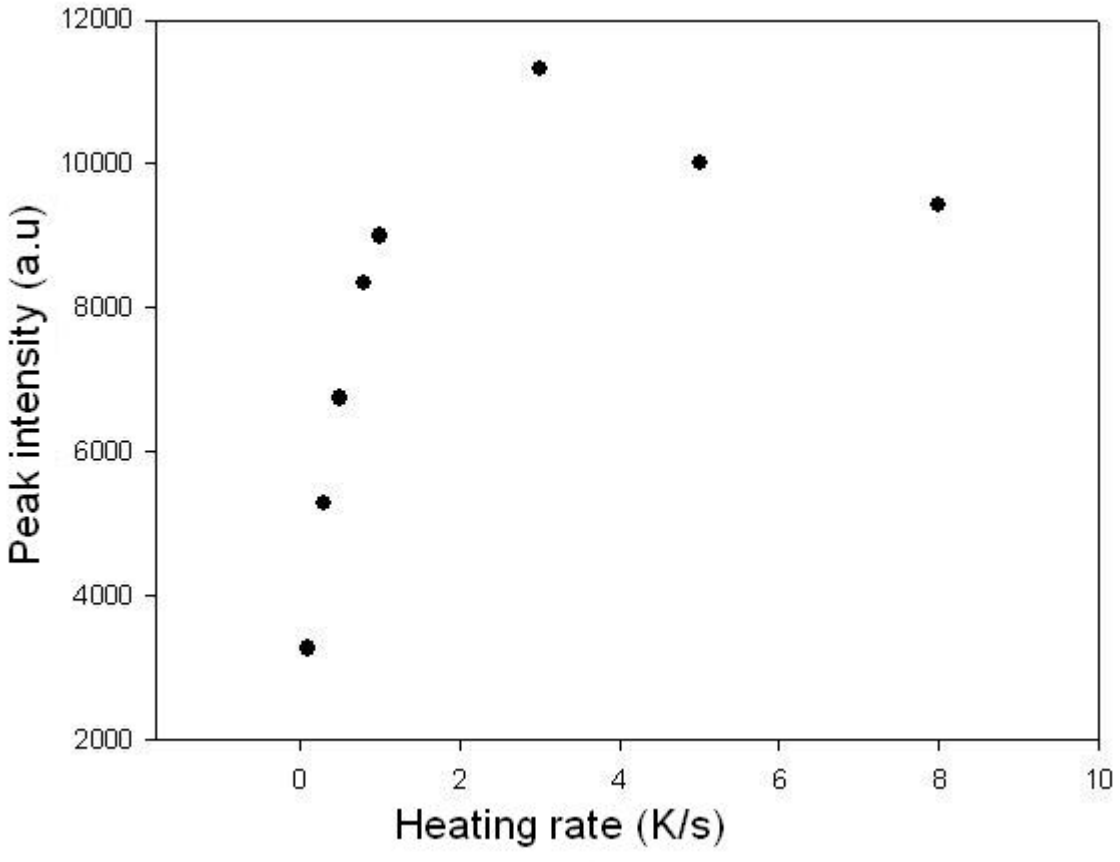

Figure 6.6: Peak height as a function of heating rate for peak I. The sample was irradiated to 1.0 Gy at ambient temperatures.

Figure 6.7 shows the dependence of peak position on the heating rate for the main peak, peak II. The peak position of the main peak shifts to higher temperatures with increasing heating rate. The shifting of the peak position to higher temperature is a mathematical consequence due to the dependence of peak position on heating rate as expressed in equation 3.30 for general-order kinetics i.e. transposing equation 3.30 to make β the subject of the formula, we get:

$$\beta = \frac{skT_M^2(1 + \frac{2kT_M(b-1)}{E})}{E\exp(E/kT_M)},$$

which shows that β is an increasing function of T_M assuming that E and s are constant. This means that as heating rate increases, the peak must shift to higher temperatures. The same behaviour is also observed in both peak I and peak III.

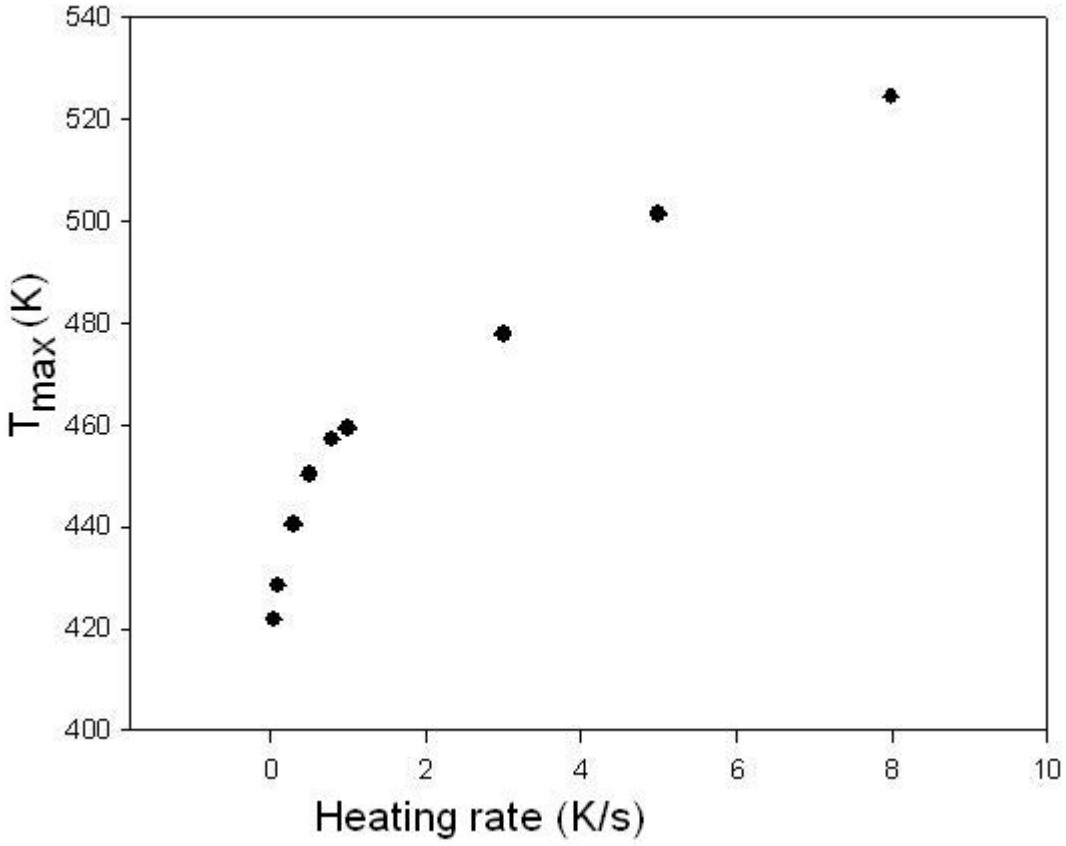

Figure 6.7: Peak position as a function of heating rate for the main peak, peak II. The sample was irradiated to 1.0 Gy at ambient temperatures.

It has been reported in the literature [30, 35] that the main peak may consist of closely overlapping peaks . However, fitting with more than one term of equation 6.1 did not yield any better goodness of fit than that for one term. Hence, for the purposes of curve fitting, it was assumed for the heating rates and doses used in this study that the main peak may be a single peak and not a composite of multiple peaks.

6.1.1.2 Peak shape method

The peak shape method was used to evaluate the trap depth, E, of the dosimetric trap responsible for the main peak (peak II) and the kinetic order, b of this peak. The geometrical parameters for the main peak for use in the peak shape method were extracted from TL glow curves obtained at various heating rates. The geometrical factor, μ_g, and the energy values corresponding to δ, τ, and ω as explained in Chapter 3, were calculated using Chen's general order equation (equation 3.20)

i.e.

$$E_\alpha = c_\alpha(kT_M^2/\alpha) - b_\alpha(2kT_M).$$

Table 6.2 is a list of the results obtained using the peak shape method.

Table 6.2: Geometrical parameters for the main peak where τ = T_M-T_1, δ =T_2- T_M, ω =T_2- T_1, $\mu_g = \delta/\omega$. T_M is the peak intensity, T_1 and T_2 are the temperatures at half-maximum intensities on the rising and descending parts of the peak. HR is the heating rate in K/s, and E_x where x represents τ, δ and ω is the apparent trap depth in eV. All samples were irradiated to 1.0 Gy.

HR	τ	δ	ω	μ_g	E_τ	E_δ	E_ω
0.03	15.68	12.58	28.25	0.45	1.38	1.36	1.38
0.05	16.50	12.98	29.47	0.44	1.34	1.33	1.35
0.10	17.20	13.81	31.01	0.45	1.33	1.33	1.34
0.30	19.00	15.68	34.68	0.45	1.28	1.29	1.26
0.50	20.43	17.04	37.48	0.46	1.25	1.26	1.26
0.80	21.68	18.17	39.85	0.46	1.21	1.23	1.23
1.00	22.12	18.56	40.68	0.46	1.19	1.22	1.21
3.00	25.23	20.80	46.02	0.45	1.11	1.14	1.13
5.00	27.37	22.31	49.68	0.45	1.12	1.16	1.14
8.00	29.29	23.46	52.74	0.44	1.13	1.16	1.16

From table 4.2, the following observations can be made:

Increasing the heating rate increases the peak width as is evident from the increasing full width at half-maximum (FWHM), ω.

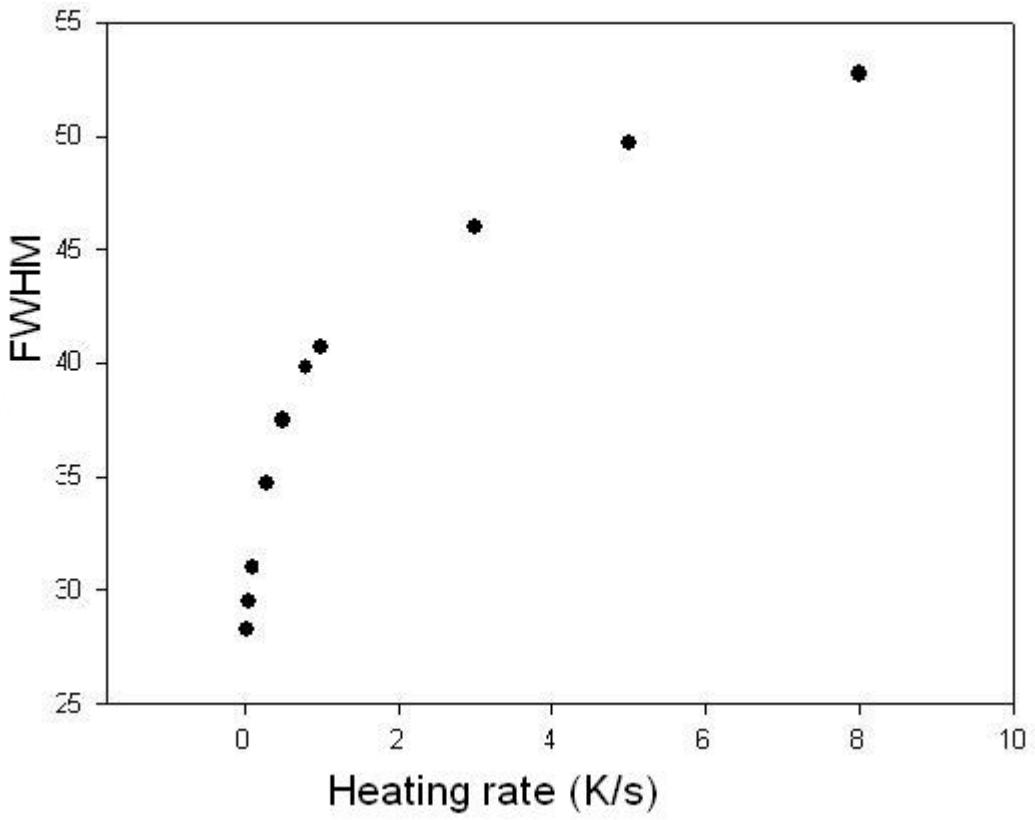

Figure 6.8: Full width at half maximum (FWHM) plotted against heating rate for the main peak, peak II. The sample was irradiated to 1.0 Gy at ambient temperatures.

The value of μ_g strongly suggests that the main peak follows general order kinetics, an indication that a certain degree of retrapping occurs during TL readout process. This conclusion that the main peak may be of general order kinetics, does not rule out the possibility that the main peak could be a composite peak consisting of closely overlapping peaks as reported by other researchers e.g. Kitis et al [35].

The values of μ_g were used to obtain the order of kinetics b, from Chen's graph (Figure 3.4). For μ_g given in table 6.2, b lies between 1.2 and 1.4 as evaluated from Chen's graph.

6.1.1.3 Initial Rise method

The initial rise (IR) method was used for the evaluation of the activation energy, E, for the trap responsible for the main peak, peak II. The lower temperature region up to fifteen percent of the

maximum intensity on the rising part of the main peak i.e. $0.15I_{max}$, was used for the evaluation of E. Samples used were those that did not show any presence of the lower temperature peak (peak I) in order to have a 'clean' initial rising part of the main glow curve to ensure minimal errors in the calculated results. Samples were irradiated to 1.0 Gy and TL was taken at various heating rates. The measurements were repeated using a constant heating rate of 0.5 K/s at various doses. Figure 6.9 shows a plot of $\ln(I)$ against $1/T$. The solid line through the data points represents the best linear fit of the data points. Table 6.3 summarises the values of the activation energy E obtained at various heating rates for the same amount of dose (0.1 Gy), whereas table 6.4 summarises the values of E obtained for various doses using the same heating rate of 0.5 K/s.

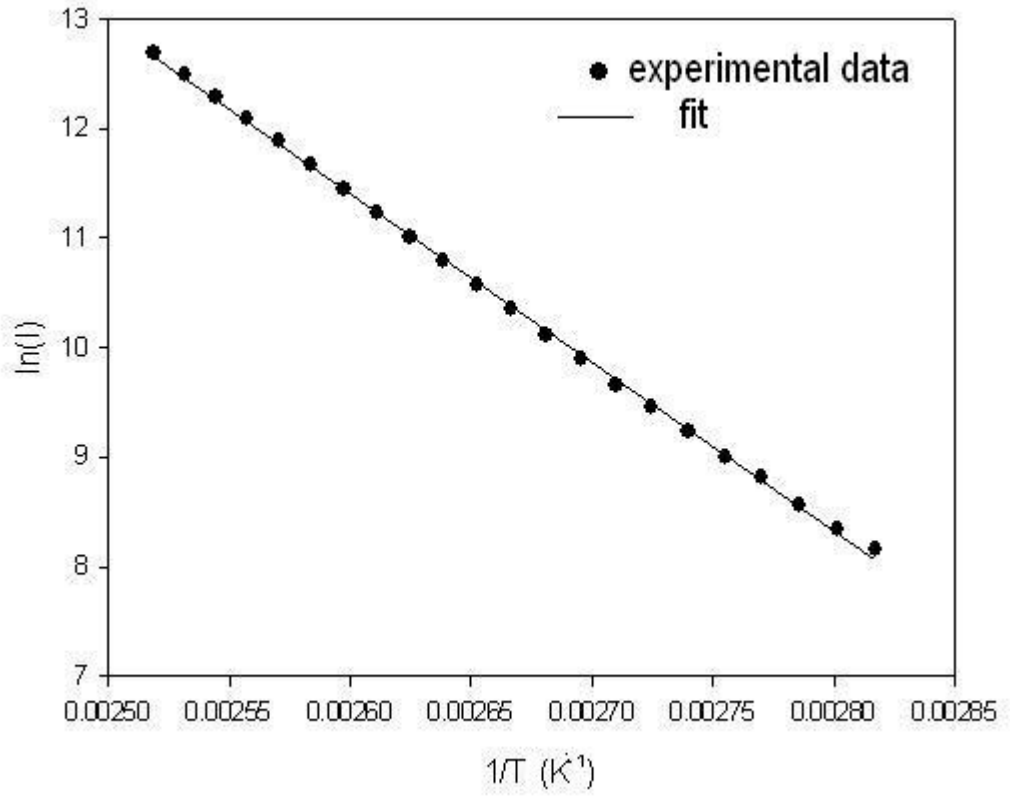

Figure 6.9: A plot of $\ln(I)$ against $1/T$ for a sample irradiated to 1.0 Gy. The TL measurement was taken at a heating rate of 0.1 K/s. The solid line represents the linear fit whose slope is numerically equal to the value of activation energy, E. In this case, $E = 1.33$ eV.

The value of the activation energy, E obtained from the slope of the fit in Figure 6.9 was 1.33±0.01 eV. The activation energy values obtained by the IR method as listed in Table 6.3 and Table 6.4 are similar except for the value $E = 1.50 \pm 0.01$ eV that was obtained at a heating rate of 5.00 K/s

Table 6.3: Activation energy values obtained using the IR method at various heating rates, at a constant dose. HR is standing for heating rate.

HR(Ks^{-1})	Dose(Gy)	E(eV)
0.03	1.00	1.38±0.01
0.10	1.00	1.33±0.01
0.50	1.00	1.36±0.01
1.00	1.00	1.39±0.01
5.00	1.00	1.50±0.01

Table 6.4: Activation energy values obtained using the IR method at various doses, at constant heating rate. HR is standing for heating rate.

Dose(Gy)	HR(Ks^{-1})	E(eV)
0.10	0.50	1.35±0.01
3.00	0.50	1.39±0.01
10.0	0.50	1.37±0.01

and at a dose of 1.00 Gy which is considerably larger than the rest of the E values.

6.1.2 A comparison of the kinetic parameters obtained using the various methods of analysis

This section aims at comparing the values of kinetic parameters E and b obtained from using curve fitting, initial rise and peak shape methods of TL glow curve analysis. The kinetic parameters have been compared at the heating rates of of 0.03 K/s, 0.1 K/s and 1 K/s. Table 6.5 is a summary of values of the activation energy, E whereas Table 6.6 summarizes the values of the kinetic order b.

For a given heating rate, all the three methods used for kinetic analysis give the values of E that are consistent as shown in Table 6.5. It is worth noting from Table 6.5 that the activation energy obtained from initial rise method seems not to be dependent on the heating rate. The values of b obtained by the whole curve and peak shape methods as displayed in Table 6.6, are also consistent. We must point out that the values of E for the main peak reported in this work agree with the values reported by other researchers. For example Kitis et al [7] reported values of 1.339 eV and

Table 6.5: Comparison of values of $E(eV)$ using whole curve, IR and peak shape methods. HR is standing for heating rate.

HR(Ks^{-1})	E (whole curve method)	E (IR method)	E_τ(eV)	$E\delta$(eV)	E_ω(eV)
0.03	1.41	1.38	1.38	1.364	1.38
0.10	1.37	1.33	1.33	1.33	1.34
1.00	1.22	1.39	1.19	1.22	1.21

Table 6.6: Comparison of values of b using whole curve and peak shape methods. HR is standing for heating rate.

HR(Ks^{-1})	b (whole curve method)	b (peak shape method)
0.03	1.23	1.25
0.10	1.22	1.25
1.00	1.29	1.32

1.435 eV for E obtained from curve fitting method and peak shape method respectively, at a heating rate of 0.6 K/s. Furthermore, various work on simulations of luminescence processes in α-Al_2O_3:C has used E=1.3 eV e.g. Nikiforov et al [26], Pagonis et al [25], a value which is consistent with the values obtained in this work.

6.1.3 Dose Response of the observed peaks

In order to investigate the dose response of peaks, samples were exposed to different amounts of irradiation doses in the range of 0.1 to 16.0 Gy. The procedure involved taking an initial TL measurement to empty the traps (for the peaks observed in this work) of any residual dose from previous exposure. The initial TL measurement was followed by a 2-minute pause to allow for the sample to cool down to room temperature before irradiating it to a beta dose for a defined period of time. After irradiation, there was another pause for 30 s, to allow for relaxation stage to last. The final TL measurement meant for analysis was taken at a heating rate of 0.5 K/s. The behaviour of peaks I, II, III and V was analysed with respect to irradiation dose. The peak heights were extracted from the experimental data and plotted against dose. We adopted the method of Lo et al [34] of analysing dose response of peaks in which a slope of the graph of log (peak intensity) against log (dose) is used to determine the dose response of a trap responsible for a particular peak. For

example in Lo's [34] method, a slope of less than 1, shows sublinear response; a slope of greater than 1 shows supralinear response whereas a slope equal to 1 denotes linear response. In the case of supralinearity, a slope of equal to 2 would be termed as quadratic response. The investigation was aimed at refining and expounding on the previous published work done on the same sample by Chithambo [30], and other researchers such as Lo et al [34].

Behaviour of peak height with irradiation dose

Figure 6.10 shows the plot of peak height of the main peak as a function of dose and the corresponding log-log plot is shown in the inset. Similarly, Figure 6.11 shows the plot of peak height of peak I as a function of dose and the corresponding log-log plot in the inset. The dose response curve of peak III is shown in Figure 6.12 whereas Figure 6.13 shows the dose response curve for peak V. Peak V was chosen and not peak IV because of the relative easiness in identifying the peak height of peak V.

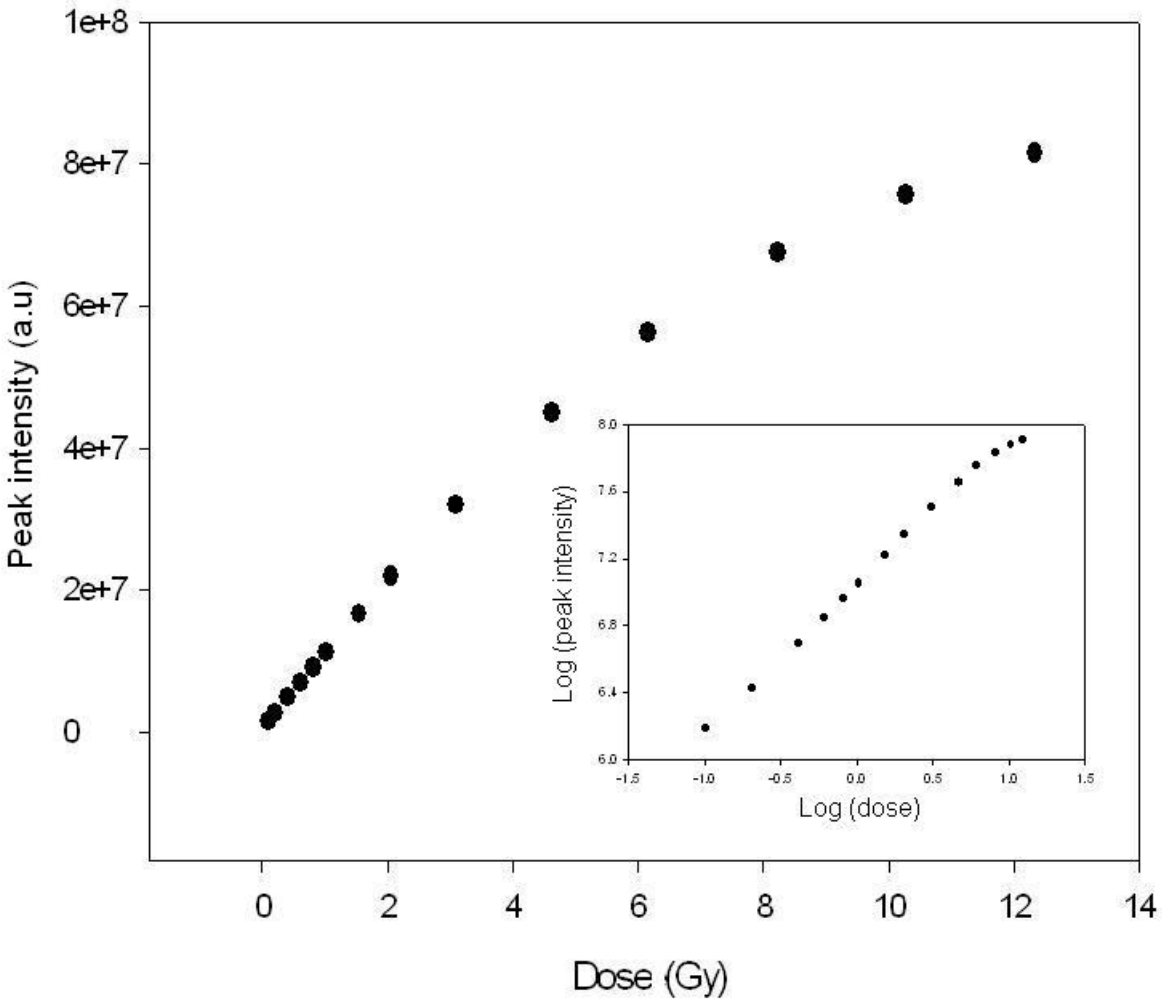

Figure 6.10: A dose response curve for the main peak, peak II, at a heating rate of 0.5 K/s. In the inset is the corresponding plot in log-log scale.

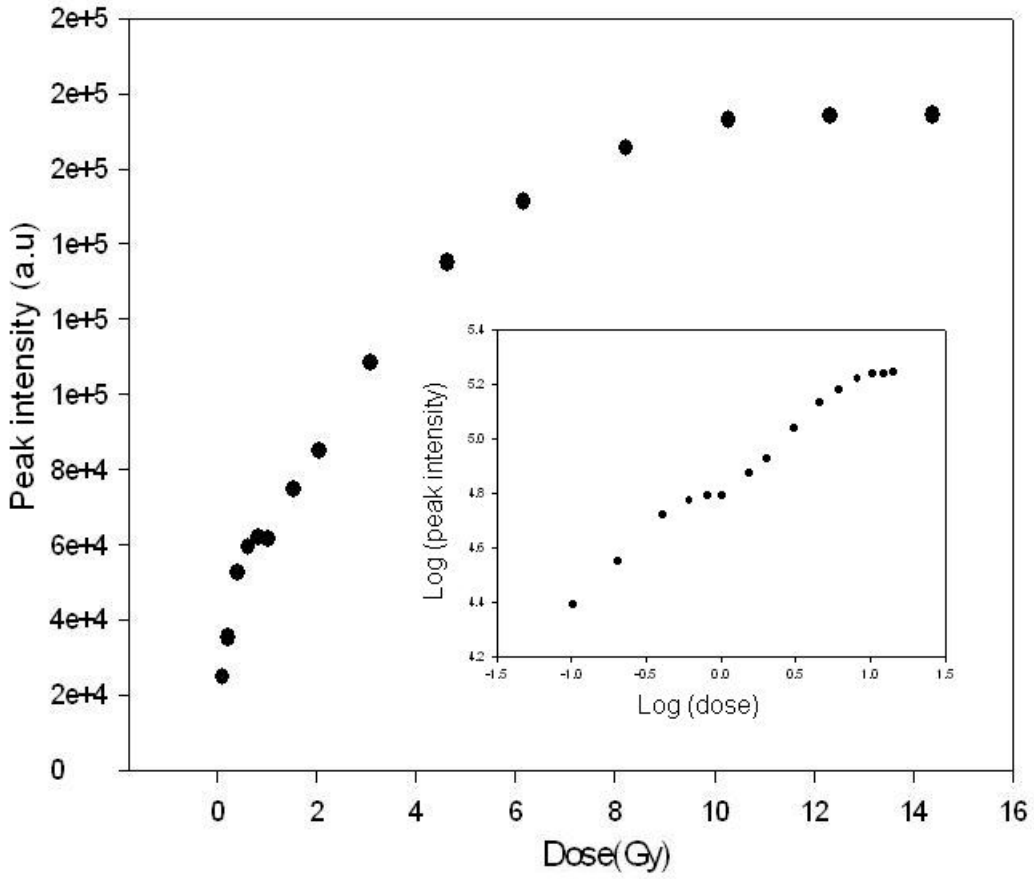

Figure 6.11: A dose response curve for peak I at a heating rate of 0.5 K/s. In the inset is the corresponding plot in log-log scale.

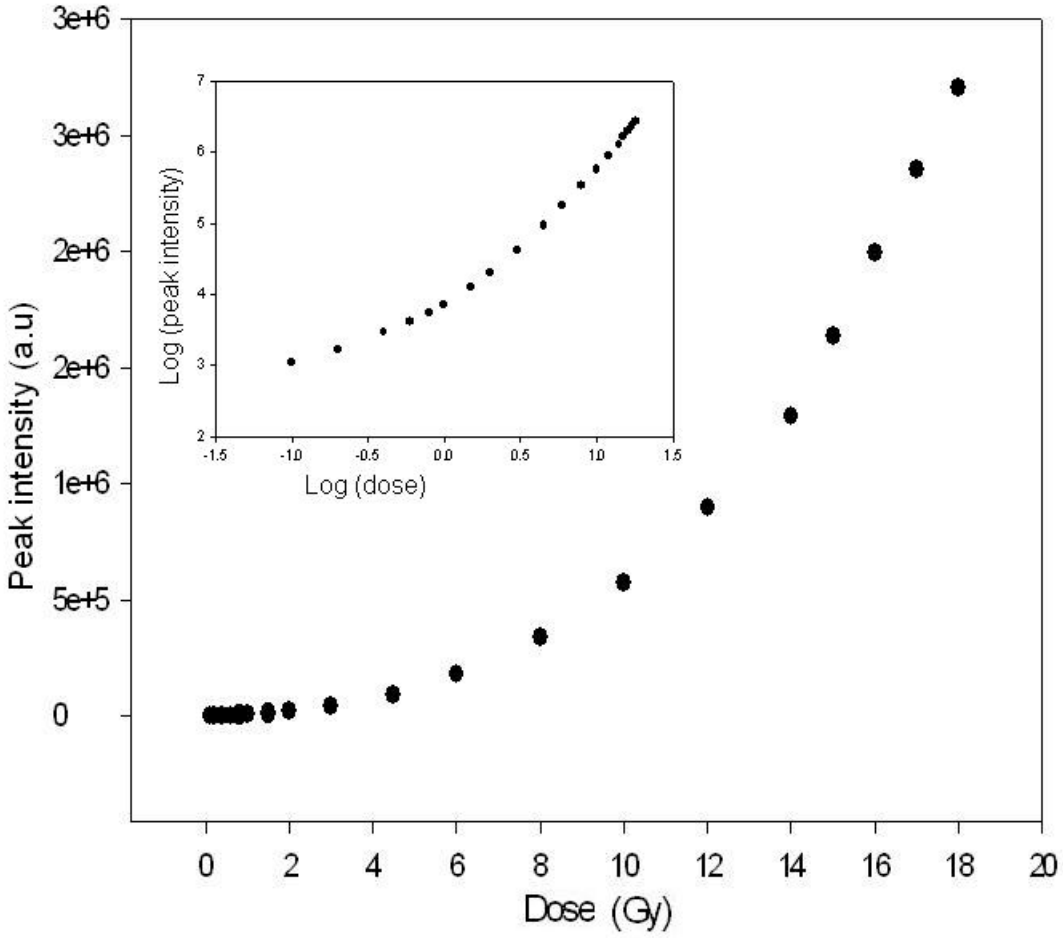

Figure 6.12: A dose response curve for peak III at a heating rate of 0.5 K/s. In the inset is the corresponding plot in log-log scale.

Figure 6.10 shows that the dose response of the main peak (peak II) is mostly linear ($slope \approx 1.0$) until about 10 Gy when it goes sublinear. As shown in figure 6.11, the dose response of peak I is mostly sublinear ($slope \approx 0.5$) then saturates completely above 10 Gy. Peak III goes from approximately linear ($slope \approx 0.8$) up to about 0.6 Gy, to supralinear ($slope \approx 1.4$) up to about 2.0 Gy, then quadratic ($slope \approx 2.0$) thereafter as shown in figure 6.12. Peak V goes from supralinear or weakly quadratic ($slope \approx 1.7$) to strongly supralinear ($slope \approx 5.0$).

From the dose responses of the peaks, it appears that the trap responsible for peak I has very little effect on the dose response of dosimetric trap apart from acting as a charge competitor during irradiation time. This is evident from the fact that even after peak I saturates, the response of the main peak still remains linear. The trap responsible for peak III on the other hand seems to be a strong charge competitor as dose increases. At low doses (up to about 2.0 Gy),the trap responsible for peak III seems to be less effective as a charge competitor and that explains why dose response for peak III is almost linear at such low doses. As dose increases (above 2.0 Gy), the trap responsible for peak III seems to compete strongly with the other traps and this explains why the slopes of the dose response curves (log-log plots) of peak I and peak II do not change with increasing dose. The strong competition for charge by the trap responsible for peak III can also be deduced from the fact that even after peak I has saturated, there seems to be no change in the response of peak II, the main peak. The growth of peak III from almost linear to supralinear then quadratic, with increasing dose, strongly suggests that the trap responsible for peak III becomes a better charge competitor with increasing dose. Comparison of the responses of peak III and peak V, gives the impression that the deeper traps fill up quickly at higher doses which suggests that the deeper the trap, the larger its capture cross-section at higher doses.

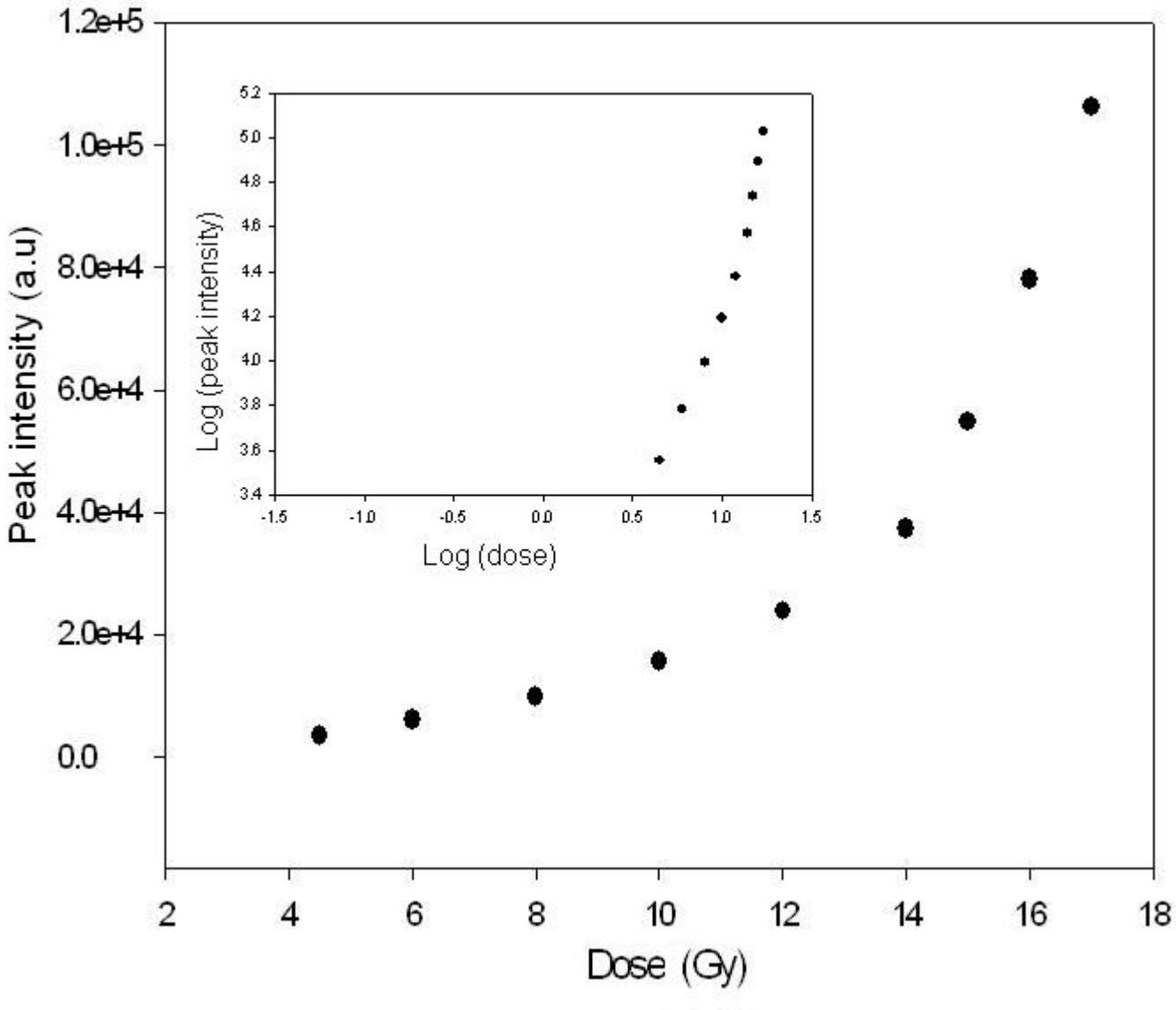

Figure 6.13: A dose response curve for peak V at a heating rate of 0.5 K/s. In the inset is the corresponding plot in log-log scale.

Dependence of peak position on irradiation dose

The dependence of the peak position on the amount of dose provides further information on the order of kinetics of the sample. Figure 6.14 shows how the peak position of the main peak, peak II, varies with irradiation dose. As shown in Figure 6.14, the peak position seems to shift to lower temperature values at low doses (0.1 Gy to 0.6 Gy). Above 0.6 Gy, the position starts to shift towards high temperature values. Since this was a rather unusual behaviour, the experiment was repeated using another sample and the behaviour was replicated as is evident in Figure 6.14. This behaviour suggests general-order kinetics for the main peak in agreement with the value of b ($\approx$1.2), for peak II, calculated using the curve fitting method as well as peak shape method. The dependence of peak position for peak I on irradiation dose is shown in Figure 6.15. The peak position of peak I as shown in Figure 6.15 appears to remain constant at 311 ± 2 K which suggests first order behaviour. Similarly, Figure 6.16 which depicts the dependence of peak III on irradiation dose, shows that the peak position of peak III remains steady at 569 ± 2 K, a behaviour that suggests first order kinetics of the peak. The peak position of peak V on the other hand as shown in Figure 6.17 shows a complex behaviour i.e. the peak position initially decreases then increases to a constant value for a few doses and starts increasing again at higher doses. This complex behaviour can be attributed to the overlapping nature with peak IV. It should be mentioned here that the extent of overlapping increases with dose such that at higher doses, it appears as one peak, making it difficult to study (see Figure 6.18).

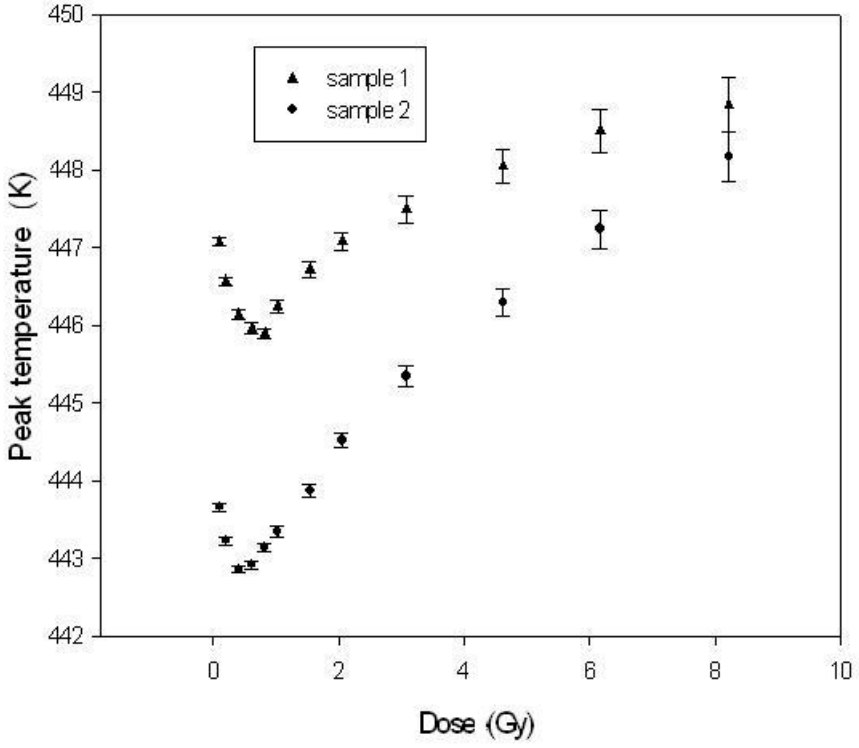

Figure 6.14: Peak position plotted againts dose for the main peak,peak II, in the range of 0.1 - 16 Gy. The heating rate used was 0.5 K/s.

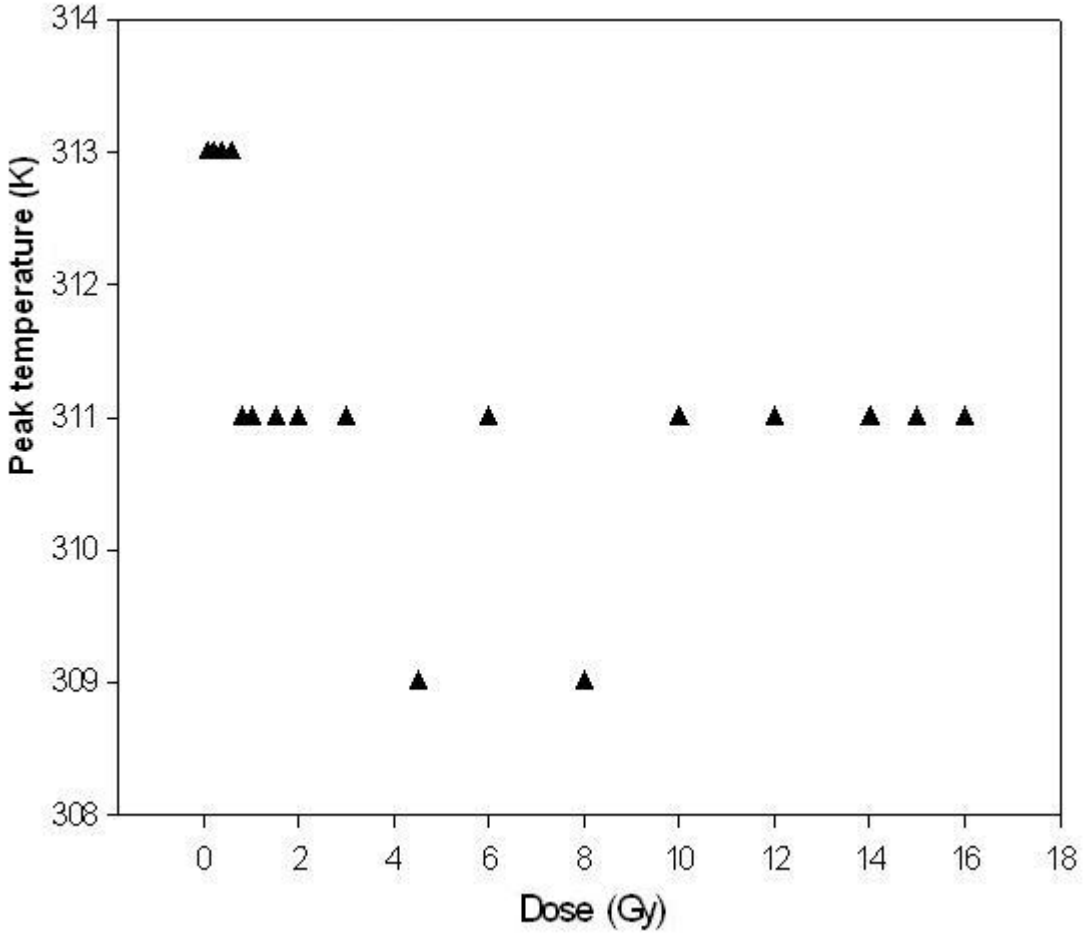

Figure 6.15: Peak position plotted againts dose for peak I in the range of 0.1 - 16 Gy. The heating rate used was 0.5 K/s.

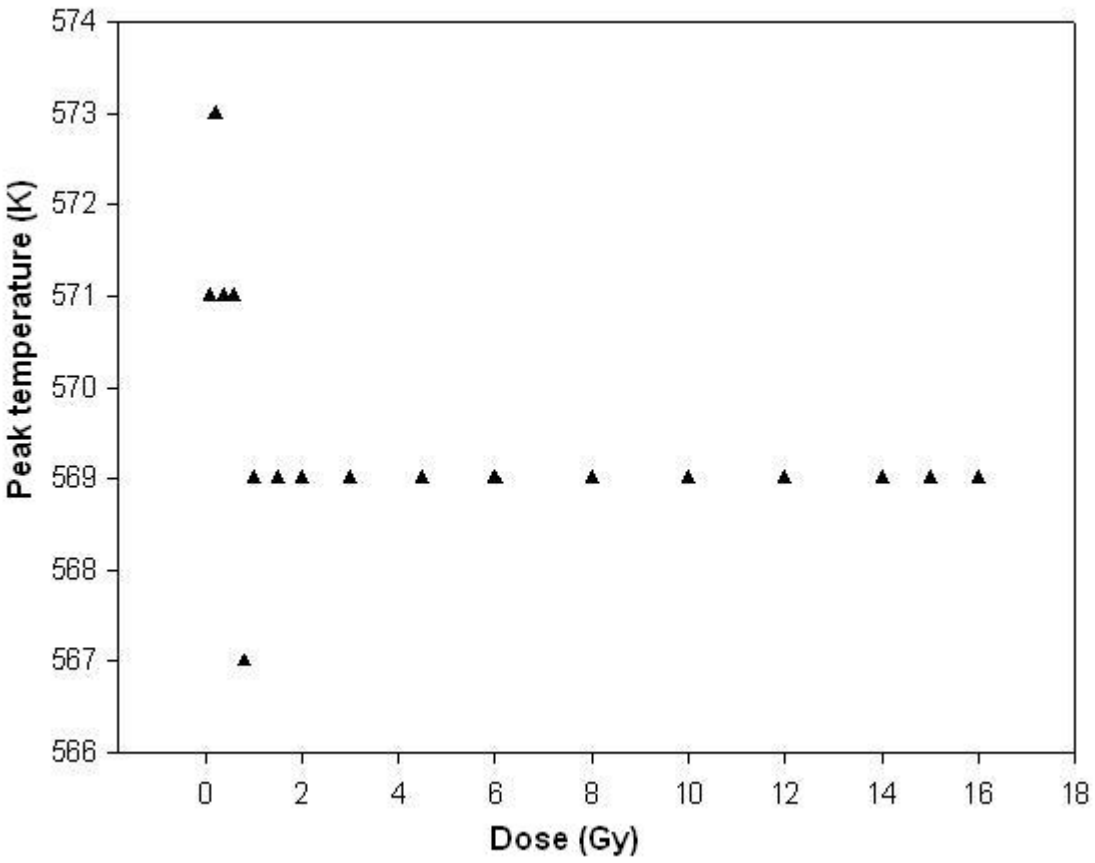

Figure 6.16: Peak position plotted againts dose for peak III in the range of 0.1 - 16 Gy. The heating rate used was 0.5 K/s.

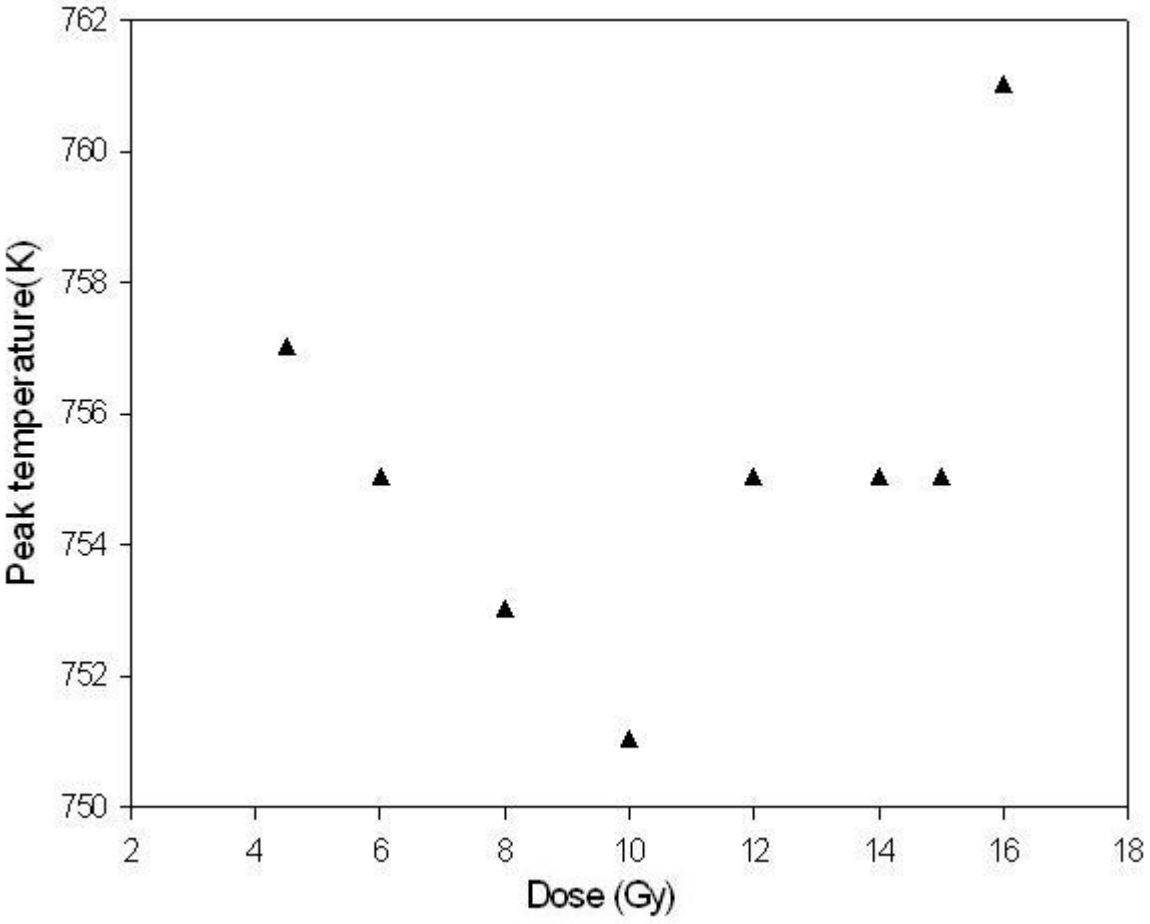

Figure 6.17: Peak position plotted againts dose for peak V in the range of 0.1 - 16 Gy. The heating rate used was 0.5 K/s.

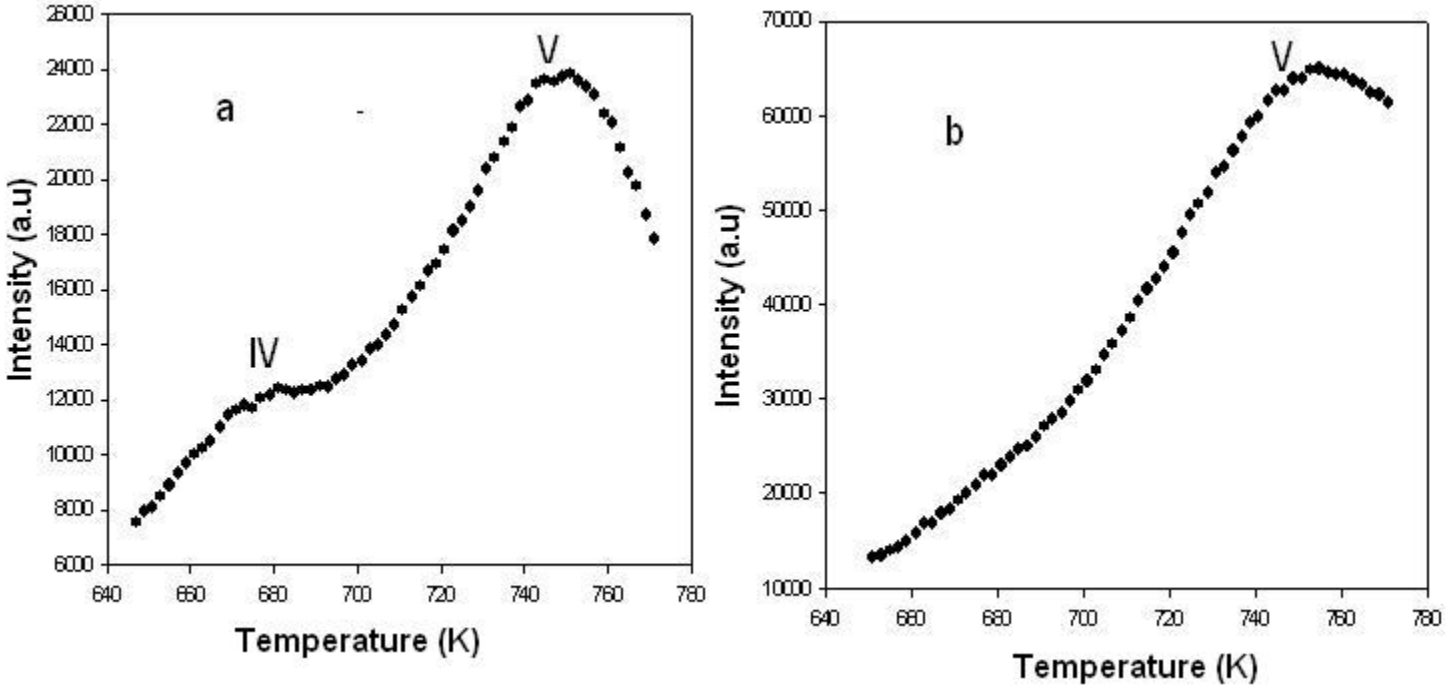

Figure 6.18: (a) Peaks IV and V at a dose of 12.0 Gy showing some overlapping. (b) Peaks IV and V at 16.0 Gy show total overlapping to the extent that they appear as a single peak. TL was recorded at a heating rate of 0.5 K/s.

6.2 Time-resolved optically stimulated luminescence

6.2.1 Dependence of luminescence lifetimes on measurement temperature

The aim of this experiment was to investigate the dependence of luminescence lifetimes i.e. the time delay between sample stimulation and emission of light in α-Al_2O_3:C using time-resolved optical stimulation technique. Samples of α-Al_2O_3:C were annealed at 900°C for 15 minutes and quickly cooled in air, then irradiated to 1.0 Gy. Time-resolved luminescence measurements were done from 30°C to 200°C in steps of 10°C without intermediate annealing or irradiation. The TR-OSL signal after the light pulse was fitted using a simple exponential and a scaling term C in accordance with the theoretical considerations of TR-OSL, in particular, equation 3.56. The exponential function that was used for fitting is of the form:

$$I_{OSL}(t) = A\exp(-\frac{t}{\tau}) + C, \tag{6.2}$$

where A is a scaling factor, τ is the luminescence lifetime and C is a scaling term that seemed to vary with measurement temperature i.e. C became negligible at high measurement temperatures. Thus, C can be interpreted as a term representing optically stimulated phosphorescence. A plot of natural log of intensity versus time as shown in figure 6.19 shows a straight line for a considerable part of the graph, a justification that the decay component of the TR-OSL spectrum can be approximated by a single exponential and a scaling term C. Equation 6.2 has also been used by other researchers for fitting TR-OSL decay curves in α-Al_2O_3:C e.g. Pagonis et al [25], Akselrod et al [36].

Sample 1 showed the presence of lower temperature peak (peak I) in the TL glow curve whereas sample 2 did not show the presence of peak I in the TL glow curve (see Figure 6.20). Measurements of the temperature dependence of luminescence lifetimes were carried out on samples 1 and 2. Figure 6.21a shows the plot of luminescence lifetimes against measurement temperature for both sample 1 and sample 2.

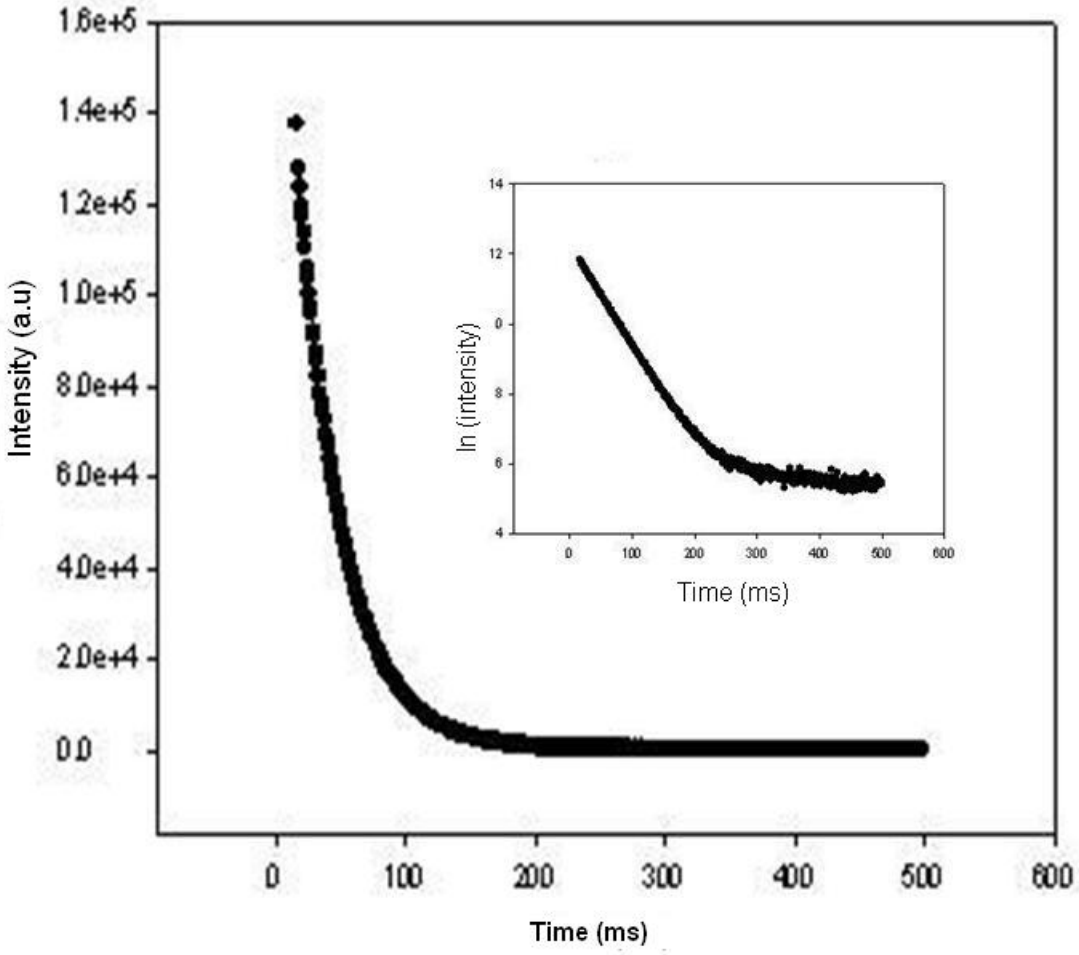

Figure 6.19: The TR-OSL signal obtained when the stimulation pulse is off. In the inset, the TR-OSL signal intensity has been plotted in natural log scale. The sample was irradiated to 1.0 Gy beta dose at ambient temperature.

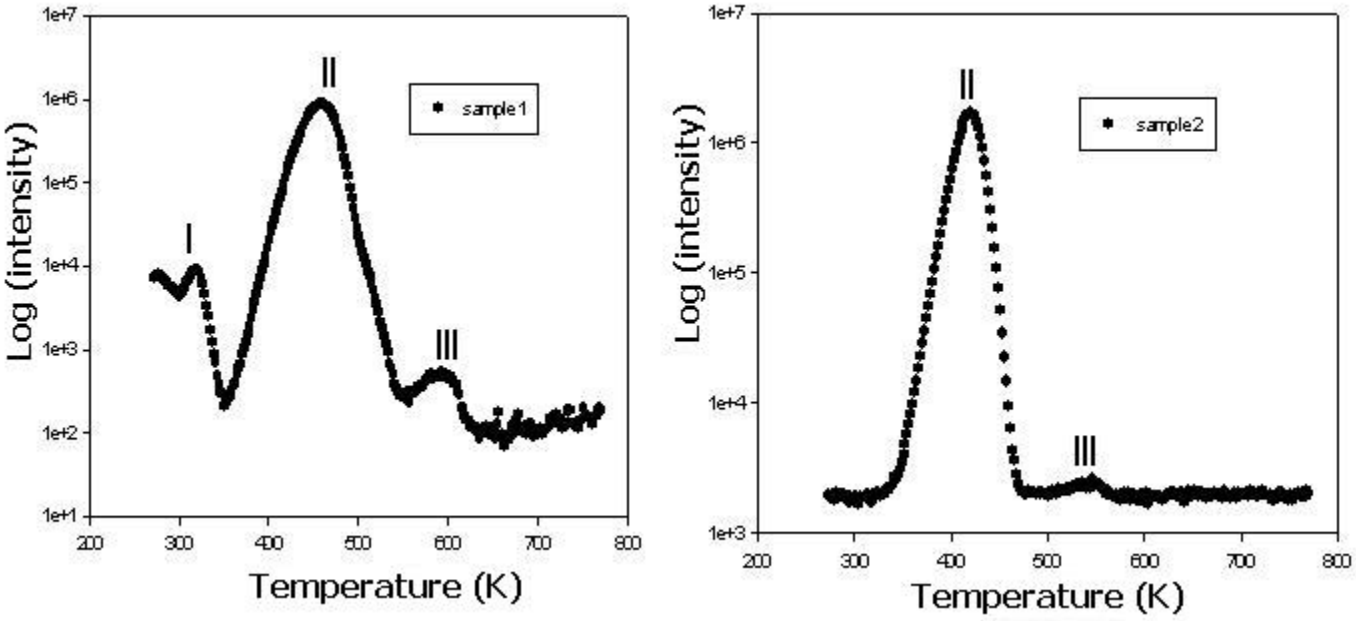

Figure 6.20: TL glow curves for sample 1 that shows peak I and sample 2 that does not show peak I. Both samples were irradiated to 1.0 Gy of beta dose and a TL measurement was taken at a heating rate of 0.1 K/s.

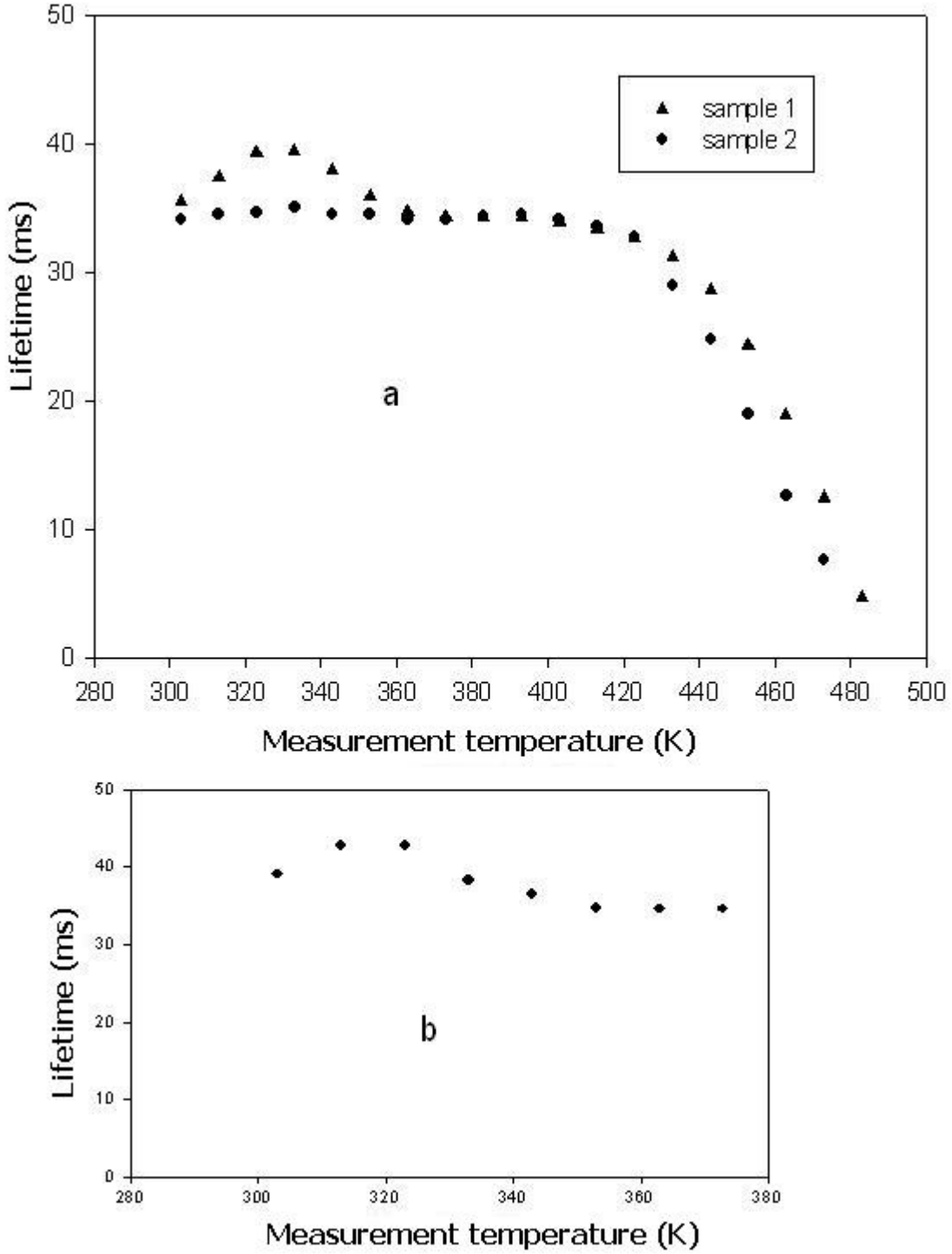

Figure 6.21: Luminescence lifetimes plotted against measurement temperature for sample 1 (triangles) and sample 2 (solid circles) starting from 30°C to 200°C (a) and for sample 1 starting from 100°C to 30°C (b). TR-OSL measurements were taken at a pulse width of 18.0 ms after irradiating the samples to 1.0 Gy of beta dose.

As shown in figure 6.21a, the lifetimes for sample 1 go through a peak in the temperature ranges of 30°C - 80°C (303 - 353 K) unlike lifetimes for sample 2. Coincidentally, this is the temperature range for the peak I in the TL glow curve. Since shallow traps are responsible for the presence of peak I in the TL glow curve, it can be concluded therefore that shallow traps are responsible for the presence of the peak shown in the lifetimes against measurement temperature plot (Figure 6.21) for sample 1. It appears that significant retrapping of charge carriers during readout stage occurs at the shallow traps which in turn tends to delay recombination subsequently elongating the luminescence lifetimes in sample 1. During optical stimulation, electrons evicted from optically sensitive deeper traps seem to be recaptured at the shallow traps before recombining at the luminescence centers. At higher temperatures i.e. 80°C (353 K) and above, the lower temperature traps are apparently empty and any charge retrapped there is quickly stimulated back into the conduction band resulting into usual average lifetimes of luminescence in the sample i.e. 35 ± 1 ms. Above 140°C (400 K), the lifetimes start decreasing continuously such that at about 200°C (470 K) it is only about 7 ms. This decrease can be explained as being due to an increase in the probability of non-radiative recombination. This is discussed later.

That the peak is possibly due to retrapping at the shallow traps is further demonstrated by its reproducibility when the measurements are taken from 200°C decreasing to 30°C. Figure 6.21b is the plot of lifetime of luminescence obtained from sample 1 against measurement temperature starting from 100°C (373 K) down to 30°C (303 K) in steps of 10°C without intermediate irradiation and annealing as before, using the same dose as in the previous investigations. As it can be seen from Figure 6.21b, the peak as shown in Figure 6.21a is reproduced. As previously argued, at temperatures above 80°C, the shallow traps are apparently empty, and any charge retrapped at the shallow traps is immediately evicted back to the conduction band, hence shallow traps show no effect on the luminescence lifetimes at such temperatures ranges. The degree of retrapping begins to become significant as the temperature of measurement approaches the temperature ranges where the shallow traps are thermally activated (i.e. produce peak I in TL) resulting once again, into elongation of luminescence lifetimes. The effect of shallow traps on luminescence lifetimes observed in this work i.e. elongation of lifetimes at low temperatures, was also observed by Akselrod et al [36] in Al_2O_3:C using pulsed xenon arc lamp in time-resolved photoluminescence measurements and they also attributed the effect to charge retrapping at shallow traps. Pagonis et al [25] also showed the effect of measurement temperature on luminescence lifetimes in this material using computer simulations.

6.2.2 Thermal Quenching

Thermal quenching is the phenomenon associated with the reduction in luminescence intensity with increasing measurement temperature due to increased probability of non-radiative transitions at high temperatures. In the standard Mott−Seitz model based on the configurational coordinate diagram (Figure 6.22) [33], an excited state of a luminescence centre can decay via radiative transitions, or non-radiative transitions. In this model, thermal quenching is a result of decrease in the luminescence efficiency with increasing measurement temperature due to reduction in quantum efficiency of luminescence centers [33] i.e. the probability of non-radiative transitions increases with increasing measurement temperature. When the phonon-assisted radiative transitions are negligible, the luminescence lifetime (i.e. the delay between stimulation and emission of light) decreases as a function of temperature with the following dependence on the measurement temperature [36]:

$$\tau = \frac{\tau_0}{1 + D\exp[\frac{-W}{kT}]} \tag{6.3}$$

where τ_0 is the mean radiative lifetime, W (eV) is the activation energy for thermal quenching and D is a constant associated with thermal quenching, k (eV/K) is Boltzmann's constant and T is absolute temperature. By measuring τ as a function of measurement temperature and fitting the experimental curve with equation 6.3 ,the parameters W and D can be evaluated. Similarly, the radiative luminescence intensity gets reduced according to:

$$I = \frac{I_0}{1 + D\exp[-\frac{W}{kT}} \tag{6.4}$$

where I_0 is the unquenched luminescence intensity obtained at low temperatures [17]. In Figure 6.22, R_0 is the equilibrium position of the recombination center in its ground state while R_0' is the equilibrium position of the recombination center in its excited state. The symbol *abs* represents absorption; *em* represents emission; horizontal lines are phonon vibrational states and ΔE is the activation energy for thermal quenching. Thermal quenching occurs when an electron in the excited state absorbs a phonon of energy equal to ΔE which results into crossing of potential curves of the ground state, g, and excited state, e, and the subsequent non-radiative electron decay to ground state with emission of phonons.

This work was aimed at evaluating the parameters of thermal quenching i.e. W and D. For this particular purpose, sample 2 (without peak I) was used. The sample was annealed at 900°C for 15 minutes and quickly cooled in air, then irradiated to 1.0 Gy. Time-resolved measurements using blue LEDs pulsed at a pulse width of 18.0 ms, were done from 30°C to 200°C in steps of

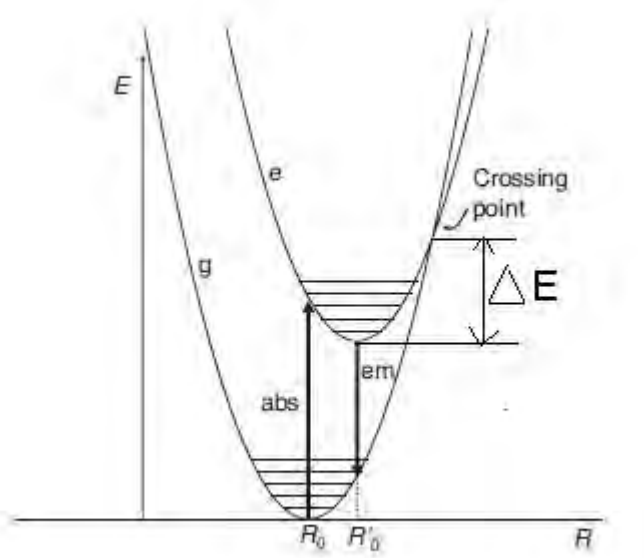

Figure 6.22: Configurational coordinate diagram showing potential energy curves of the ground state g and excited state e of the luminescence center. R_0 is the equilibrium position of the recombination center in ground state and R'_0 is the equilibrium position of the recombination center in excited state. *abs* represents absorption, *em* represents emission and horizontal lines are phonon vibrational states. Drawing taken from Yukihara and McKeever [12] and modified to include ΔE.

10°C without intermediate annealing or irradiation. The data obtained from the measurements was analysed for luminescence lifetimes using equation 6.2. Figure 6.23 shows the plot of luminescence lifetimes against measurement temperature for sample 2 which was fitted with equation 6.3 in order to extract thermal quenching parameters. The values of parameters of thermal quenching obtained from the fitting are $W = 1.045 \pm 0.002$ eV; $D = 2.1 \times 10^{11}$. The Debye frequency, $\nu = \frac{D}{\tau_0} = 6.0 \times 10^{12}$ s^{-1}. The value of W obtained is a remarkable result considering that it is very precise and agrees very well with the value of activation energy of thermal quenching for the material that was established by Akselrod et al of 1.08 ± 0.03 eV . Table 6.7 compares the value of the activation energy obtained in this work and those obtained previously by other researches experimenting with the same material. The value of Debye frequency calculated from D and the average lifetime, agrees quite well with theory i.e ν lies between 10^{12} and 10^{14} (see section 2.1.1.2). It is evident from table 6.7 that the value of the activation energy of thermal quenching obtained in this work using TR-OSL method agrees very well with and is as accurate and precise as those obtained using other methods as listed.

Using the data obtained from section 6.2.1 i.e. dependence of luminescence lifetimes on mea-

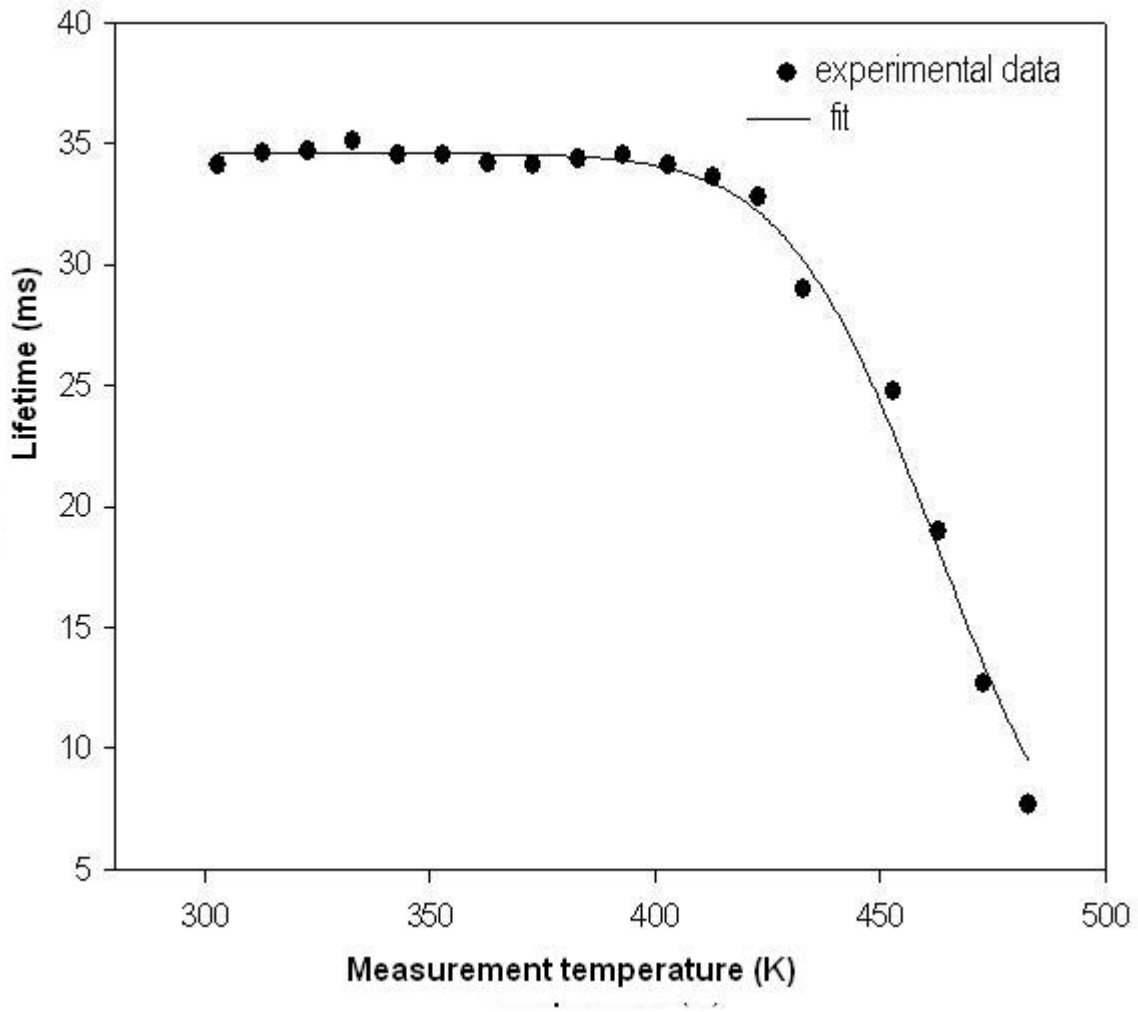

Figure 6.23: Luminescence lifetime plotted against measurement temperature and fitted with equation of thermal quenching , equation 6.3. The sample was irridiated to 1.0 Gy of beta dose, and time-resolved measurements were taken at a pulse width of 18.0 ms using 470 nm blue LEDs. From the fit, the activation energy of thermal quenching, W=1.045±0.002 eV; D =2.1×10^{11}; τ_0=35.0±1.0 ms; R^2=0.99.

surement temperature, we went further to evaluate lifetimes from the signal obtained when the stimulating pulse is on (the rising part of the TR-OSL spectrum), so that we could make comparisons with the lifetimes evaluated from the signal obtained when the stimulating pulse is off (the decay part). The rising part of the TR-OSL signal, was fitted with a saturating exponential as discussed in kinetic analysis of TR-OSL (equation 3.55) plus a scaling term :

$$I(t) = A(1 - e^{-\frac{t}{\tau}}) + B \tag{6.5}$$

where A is the scaling factor, τ (ms) is the luminescence lifetime at a particular measurement

Table 6.7: A comparison of values of the activation energy W (eV) of thermal quenching obtained in this work with those by other researchers. In the table, dose is in Gy, HR is heating rate in K/s , $TR-PL$ represents time-resolved photoluminescence, $STR-PL$ is the simulated TR-PL, *stim.source* represents stimulating source and *pw* is pulse width.

Reference	method	stim. source	HR	dose	pw	W
Current work	TR-OSL	blue LEDs		0.1	18 ms	1.045 ± 0.002
Akserlod et al [36]	TR-PL	xenon arc lamp			20μs/10 ns	1.08 ± 0.03
Pagonis et al [25]	STR-PL	UV-light			0.2 s	1.0
Larsen [37]	TL	heat	various	3.3		1.01
Kitis [35]	TL	heat	various			1.08

temperature, and B is a scaling term that is dimensionless. Figure 6.24 is the corresponding plot of luminescence lifetimes against measurement temperatures for sample 1 (with TL peak I) and sample 2 (without TL peak I).

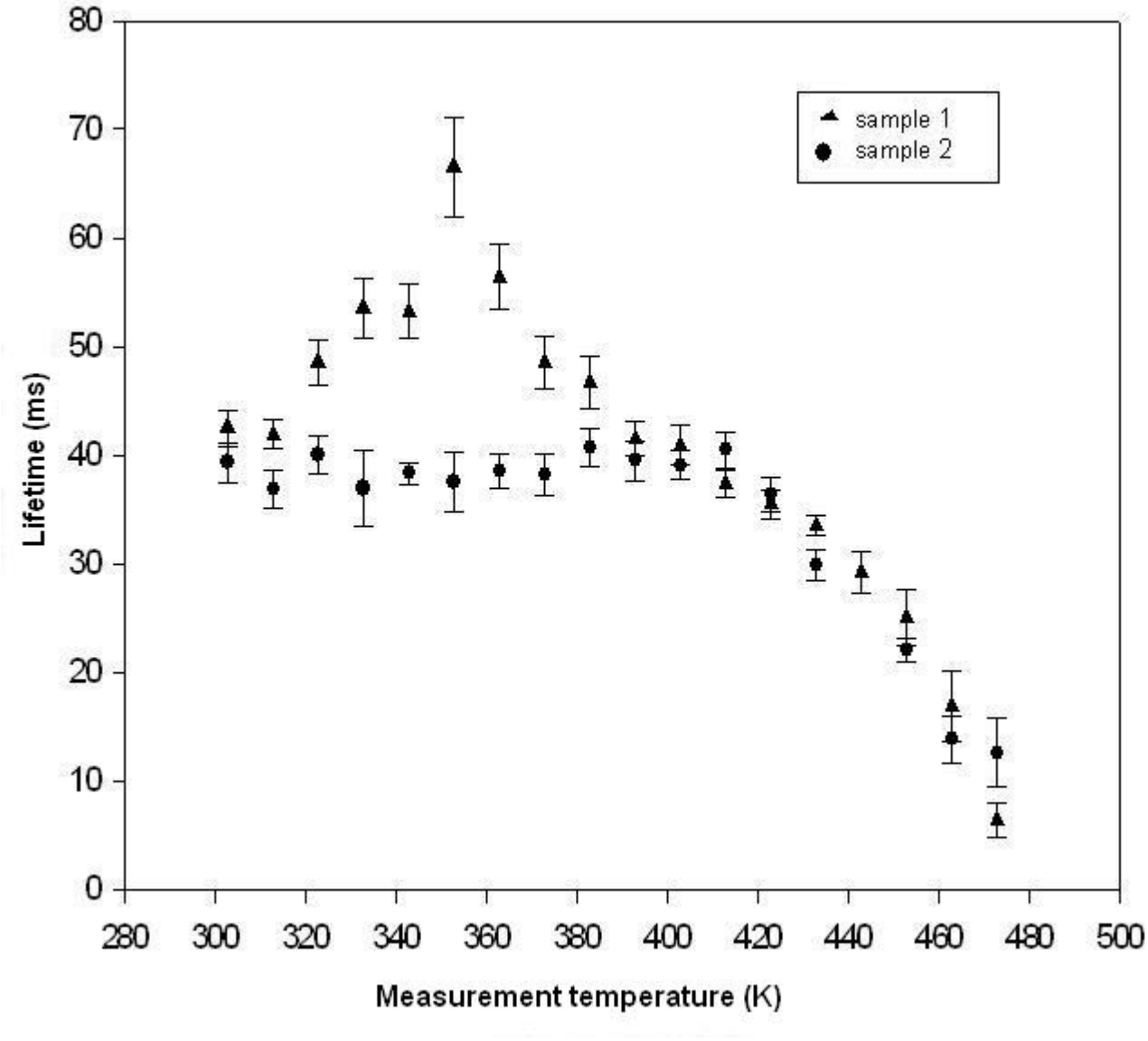

Figure 6.24: Luminescence lifetimes plotted against measurement temperature for sample 1 (triangle) and sample 2 (solid circles). Luminescence lifetimes were obtained from the rising signal of the TR-OSL spectrum by fitting with a saturating exponential i.e. equation 6.5. TR-OSL measurements were taken at a pulse width of 18.0 ms.

As shown in Figure 6.24, the shapes of the graphs are similar to those obtained from decay component of the TR-OSL spectrum with a peak in lifetimes reproduced in sample 1. Sample 2 does not show a peak as expected. The replication of the peak in sample 1, and no peak in sample 2 for the rising part of the TR-OSL spectrum is evidence enough that the underlying physical processes of luminescence are the same both during the stimulation pulse and after the stimulation pulse [21], and that the same traps and recombination centres may be involved. The graph for sample 2, was

fitted with the equation of thermal quenching, equation 6.3, in order to evaluate thermal quenching parameters W and D (see Figure 6.25). The values of thermal quenching parameters obtained from the fit are W =1.094±0.004 eV; D=1.2×10^{12}. To a very good extent, these values for thermal quenching parameters are in close agreement with those obtained by the fit in Figure 6.23. The activation energy of thermal quenching, W corresponds to transition P_F in the luminescence model as shown in Figure 4.1. If an excited F-center in ^3P state absorbs thermal energy equal to W, it will return to the ground state, ^1S, non-radiatively through path P_F resulting into reduction of the luminescence yield.

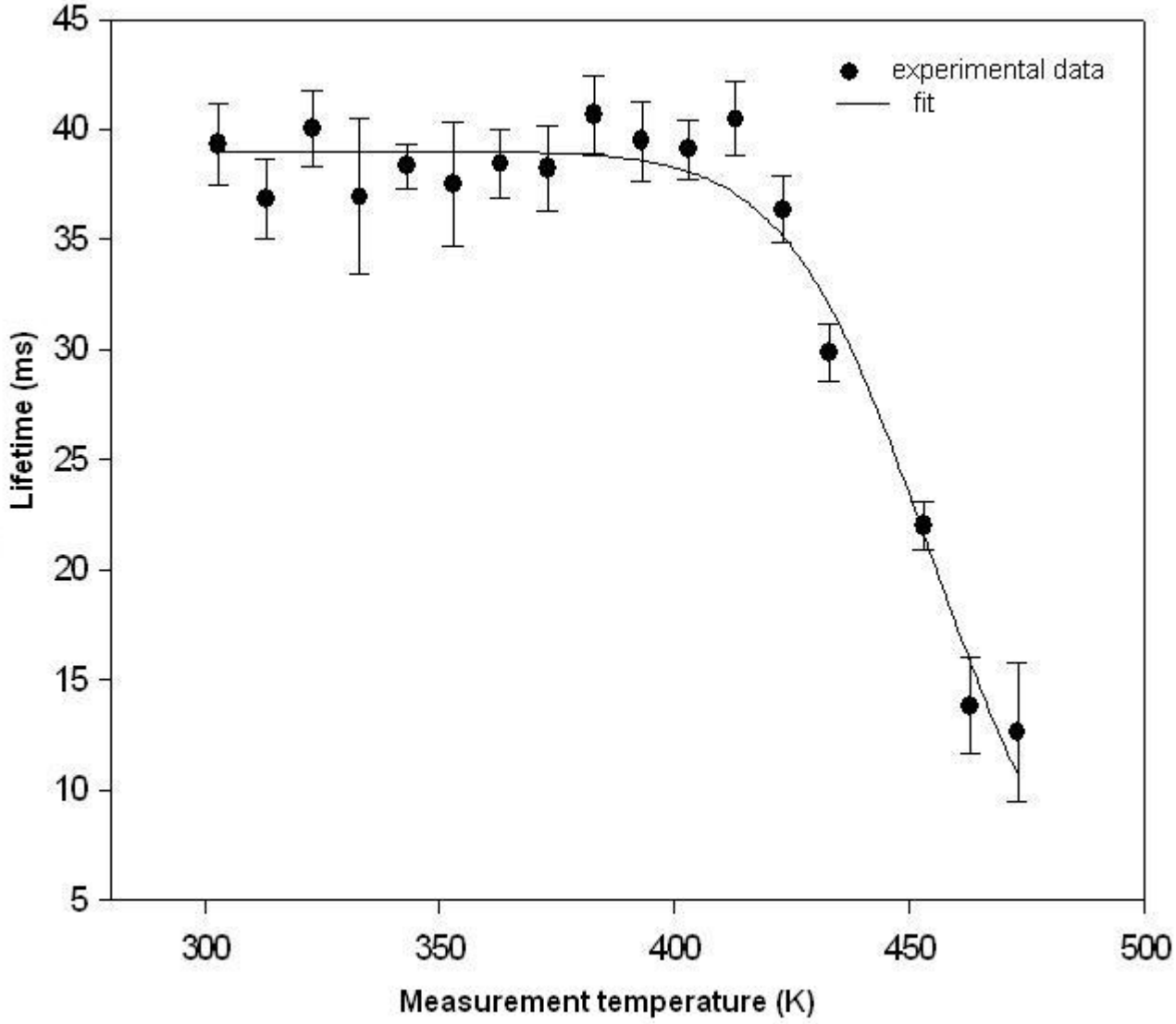

Figure 6.25: Luminescence lifetime for sample 2 plotted against measurement temperature and fitted with the equation of thermal quenching. As evaluated from the fit, the activation energy of thermal quenching, W=1.094±0.004 eV; C=1.2×10^{12}; τ_0=40.0±3.0 ms; R^2=0.97.

6.2.3 Influence of measurement temperature on maximum luminescence intensity

The aim of this investigation was to see how the maximum intensity of time-resolved optically stimulated luminescence depends on measurement temperature. The maximum OSL intensities were extracted from the experimental data used in the previous investigations, the dependence of

luminescence lifetime on measurement temperature (section 4.2.1), for both sample 1 (with TL peak I) and sample 2 (without TL peak I). The maximum OSL intensities obtained for samples 1 and 2 were plotted against measurement temperatures and Figure 6.26 shows the resulting plots.

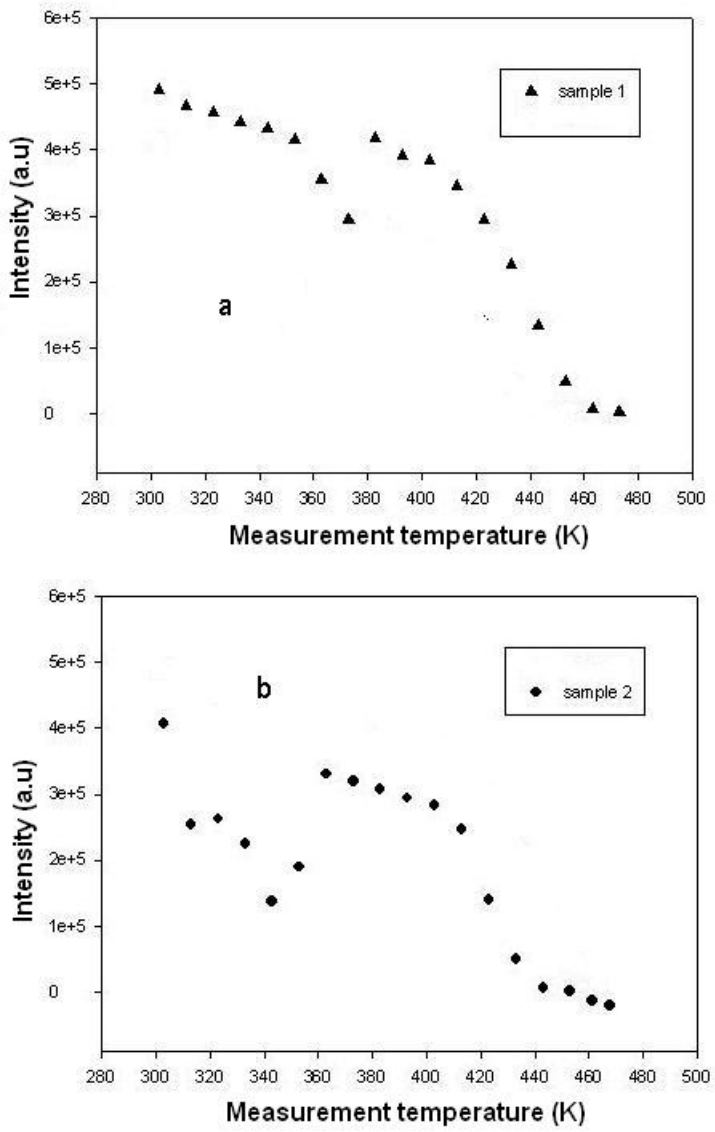

Figure 6.26: Maximum OSL intensity plotted against measurement temperature for sample 1 (a) and sample 2 (b). Both samples were irradiated to 1.0 Gy and TR-OSL taken at pulse width of 18.0 ms using blue LEDs.

The maximum OSL intensity of sample 1 decreases slowly at the temperature ranges in which peak I appears in the TL glow curve, then increases to a higher intensity around 87°C to 100°C (360-373 K) and decreases continuously thereafter. The maximum OSL intensity of sample 2 on the other hand, initially decays rapidly at low measurement temperatures and then increases around 77°C to

87°C (350 -360 K) and decreases continuously thereafter. Both samples show the same behaviour above 77°C (350 K), but different behaviour in the temperature range between 30°C to 77°C . This difference in behaviour could be attributed to the presence of shallow traps in sample 1. Sample 2 exhibits the expected behaviour i.e. that maximum intensity must decay almost exponentially with repeated measurements without intermediate irradiation, because charge concentration in the traps is also decaying almost exponentially. In contrast, the maximum OSL intensity of sample 1 decreases almost linearly at low measurement temperatures. The gradual decrease in maximum intensity may be attributed to significant retrapping of charges at shallow traps from the deeper traps as explained in section 4.2.1. The increase in maximum OSL intensity that happens at around 80°C in both samples could be a result of a thermally assisted OSL signal from the dosimetric trap being superimposed on the TR-OSL signal owing to the fact that the TL main peak (peak II) starts appearing at around the same temperatures (80°C and above) in which the increase occurs. The eventual decrease in maximum OSL intensity at higher temperatures is due to thermal quenching effects present in both samples.

6.2.4 Effect of measurement temperature on the dynamic throughput

The dynamic throughput for TR-OSL is defined as the ratio of the integrated OSL signal after the stimulating pulse, L_2 to the total OSL signal, L_T, where $L_T = L_1 + L_2$ and L_1 is the integrated signal during the stimulating pulse [24] (see section 3.4.6.1). This definition of dynamic throughput applies to both L_1/L_T or L_2/L_T. In this investigation, the focus was on the behaviour of the dynamic throughput with respect to the temperature at which the TR-OSL measurement was being made. The data used in this investigation is the experimental data obtained during investigations of dependence of luminescence lifetimes on measurement temperature (section 4.2.1). L_T was obtained by computing the integral area under the whole TR-OSL spectrum, whereas L_2 was obtained by computing the integral area under the signal after the stimulating pulse. The dynamic throughput was calculated from the values of L_T and L_2 using equation 3.65 and the results were plotted against the measurement temperatures as shown in figure 6.27.

It can be seen in figure 6.27 that the dynamic throughput for both samples is almost constant (about 75 %) at low measurement temperatures from 30°C to 140°C. Beyond the measurement temperature of 140°C (413 K), the dynamic throughput increases rapidly to about 90 % and then starts decaying beyond 170°C. Above 130°C, L_2 increases enormously as compared to L_1 such that $L_2/L_T \rightarrow 1$. This shows that at moderately high temperatures between (140°C - 180°C) more

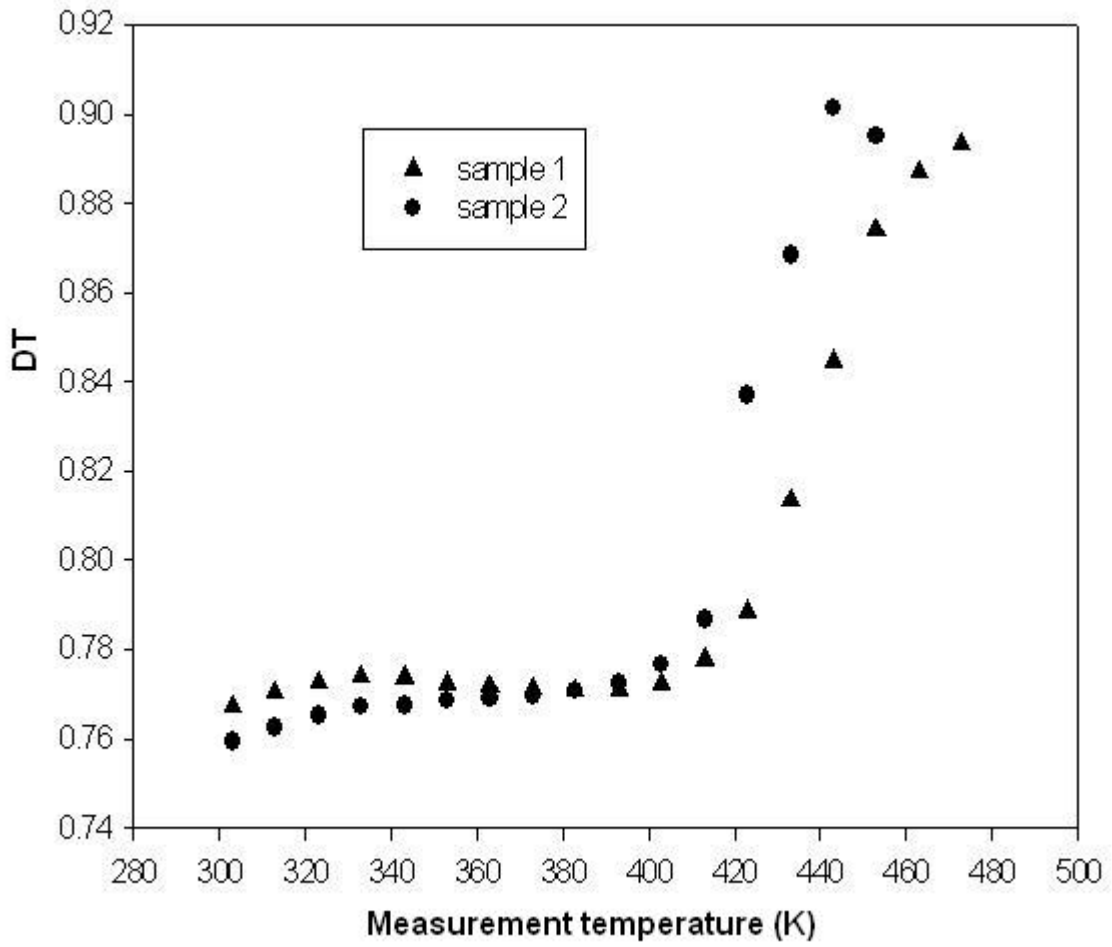

Figure 6.27: Dynamic throughput (L_2/L_T) plotted against measurement temperature for sample 1 (triangle) and sample 2 (solid circle). Both samples were irradiated to 1.0 Gy of beta dose and TR-OSL measurements were taken at a pulse width of 18.0 ms using 470 nm blue LEDs for stimulation. L_T is the total luminescence signal and L_2 is the luminescence signal after the pulse.

recombinations occur when the stimulating pulse is off than when the stimulating pulse is on. The reduction in dynamic throughput beyond 180°C, could be attributed to significant reduction in luminescence yield at higher temperatures due to thermal quenching effects.

The plot of dynamic throughput against measurement temperature as shown in Figure 6.27 can be used as qualitative evidence of thermal quenching in the sample besides the plot of lifetime against measurement temperature when using TR-OSL technique in the sense that the dynamic throughput, DT, is almost constant at lower temperatures, and then grows rapidly towards 1 at temperature ranges where thermal quenching effects manifest themselves. The value of DT starts dropping before

reaching 1 at even higher temperatures.

6.2.5 Dynamic throughput against pulse width

In this experiment, the aim was to investigate how changing pulse width during TR-OSL measurements affects the dynamic throughput. This investigation was performed to provide us with some insight into the recombination processes during and after the excitation pulse and how changing the duration of illumination i.e. pulse width, affects such recombination processes. For the purpose of this investigation, measurements were done at ambient temperatures using the following pulse widths: 6.0 , 9.0, 14.0, 18.0, and 30.0 ms. The sample was annealed at 900°C, cooled quickly in air to room temperature, irradiated to 1.0 Gy of beta dose and then a TR-OSL measurement taken on the sample. This procedure was repeated for all measurements at the selected pulse widths. The dynamic throughput, DT, was calculated from the integrated signal after the pulse L_2 and the integrated total signal, L_T, using equation 3.65 and plotted against pulse width as shown in Figure 6.28. It is clear from inspection of Figure 6.28 that the dynamic throughput decays with increasing pulse width for a constant stimulation energy. The decay of dynamic throughput with increasing pulse width of stimulation signal suggests that the ratio of radiative recombinations after the pulse to those during the pulse, decreases with increasing pulse widths. Increasing the pulse width implies an increase in total illumination time. Consequently the number of stimulated charges from the traps into conduction band also increases. And it seems that longer stimulation time i.e. large pulse width, ensures that more recombinations of the stimulated charges occur during stimulation i.e. when the pulse is on. As a consequence, L_1 increases more than L_2 with increasing pulse width. Therefore, $L_T = L_1 + L_2$, grows quicker than L_2 resulting into the dynamic throughput decay. This behaviour of dynamic throughput is similar to that reported by Chithambo [24] for quartz, hence can be approximated by the following equation:

$$f(t_w) = \frac{\tau_0}{t_w}\left(1 - \exp(-t_w/\tau_0)\right) \tag{6.6}$$

where t_w is the pulse width and τ_0 is the mean luminescence lifetime at room temperature. Fitting the plot in Figure 6.28 with equation 6.6 gives the mean luminescence lifetime for α-Al_2O_3 :C of 35.6±1.4 ms which agrees very well with the value of the mean lifetime for the material reported in previous sections. It must be pointed out that the results of this investigation auger well with the theory of OSL as well as the results of similar investigations on the sample that were carried out by McKeever et al. [17] who used a pulsed laser for a stimulation source while varying the pulse width

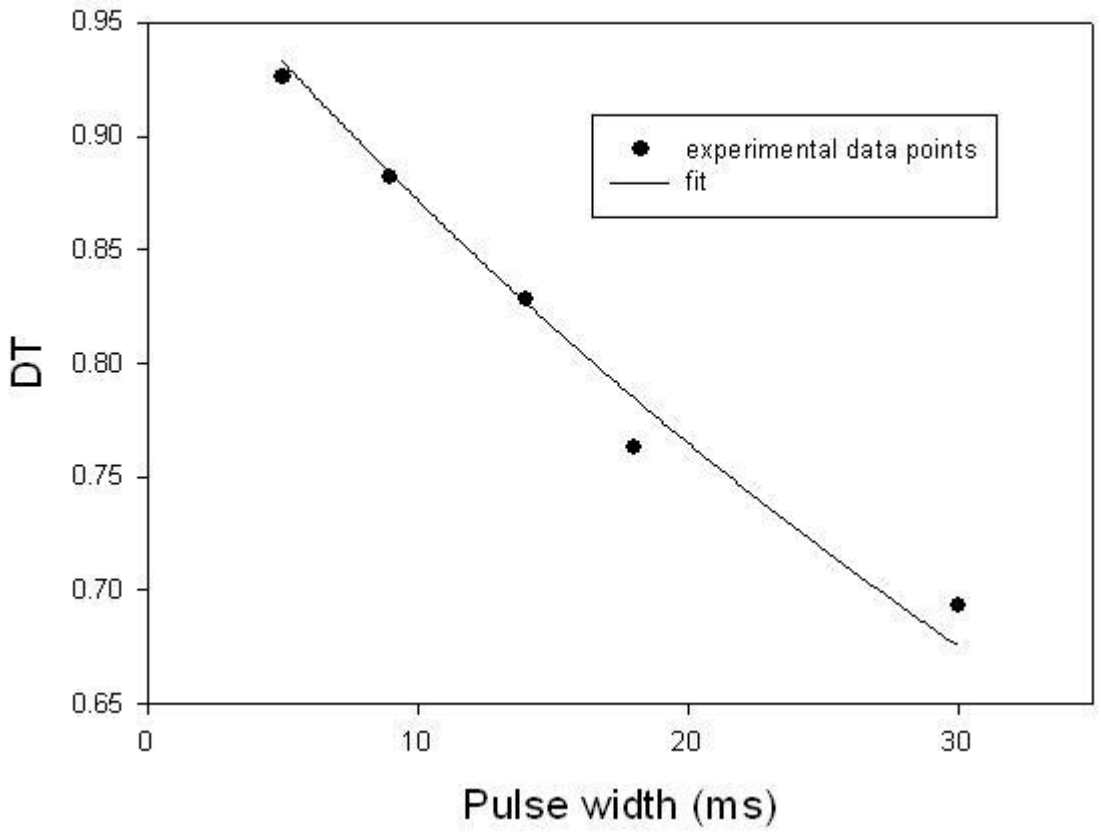

Figure 6.28: Dynamic throughput plotted against pulse width and fitted with equation 6.6 for a sample irradiated to 1.0 Gy and TR-OSL measurements made at ambient temperature. The mean lifetime for α-Al_2O_3 :C obtained from the fit is 35.6±1.4 ms.

at constant pulse energy.

6.2.6 Fading characteristics

The term fading in this investigation refers to the reduction in TR-OSL signal intensity due to sample storage after irradiation. The sample was given a dose only once, and then stored in a suitable place for a defined period of time before taking the TR-OSL measurements. The aim of this experiment, was therefore to investigate how the OSL signal of a previously irradiated sample varies with storage time.

For fading investigations, 10 samples were annealed, rapidly cooled in air, and then irradiated to 1.0 Gy. After the initial measurements, samples were annealed again to remove any residual dose from the previous measurement, rapidly cooled in air, irradiated again to 0.1 Gy and then stored in

the dark at ambient temperature. The dark conditions ensure that bleaching of the sample, which would affect the investigations, does not take place. TR-OSL measurements were then performed on the samples after 2 , 5, 10, 15, and 20 days without any more irradiation. No other treatment was given to the samples in between measurements. Maximum intensities were extracted from the data for corresponding days and recorded as shown it Table 6.7. Errors in maximum intensities were approximated using Poisson statistics i.e.

$$error = \sqrt{n} \tag{6.7}$$

where n is the number of actual events observed. In this particular case n was taken to be equal to maximum intensity observed. Figure 6.29 is the corresponding plot of the maximum intensities against the readout days. (Note: Only two samples were used in the plot, but the behaviour was similar in the rest of the samples.) It has to be pointed out that the plots of integrated signal during the pulse L_1, and the integrated signal after the pulse, L_2, against readout days both produced similar graphs.

Table 6.8: Readout days and corresponding OSL intensities. I_{M1} ≡intensity of sample 1, I_{M10} ≡intensity of sample 1 at day 0. Same definition applies for sample 2 i.e. I_{M2} and I_{M20} .

No. of Days	I_{M1} (a.u)	I_{M1}/I_{M10}	I_{M2} (a.u)	I_{M2}/I_{M20}
0	94093	1.00	233676	1.00
2	55589	0.59	227130	0.97
5	167891	1.78	137655	0.59
10	70492	0.75	199857	0.86
15	101709	1.08	44071	0.19
20	77147	0.82	74305	0.32

As shown in Figure 6.29, the maximum intensities of both samples oscillate with number of readout days. Figure 6.29 shows that the intensity of sample A decreases on day 2 after irradiation without prior readout, followed by alternating increase and decrease on days 5, 10,15 and 20. A similar pattern of variation of intensity with readout days is displayed by sample B. As already pointed out, both samples show a decrease on day 2 even without any prior readout after irradiation. This decrease in intensity on day 2 is evidence of fading of the OSL signal with storage time. The fading of the OSL signal shown on day 2 could be attributed to emptying of unstable shallow traps

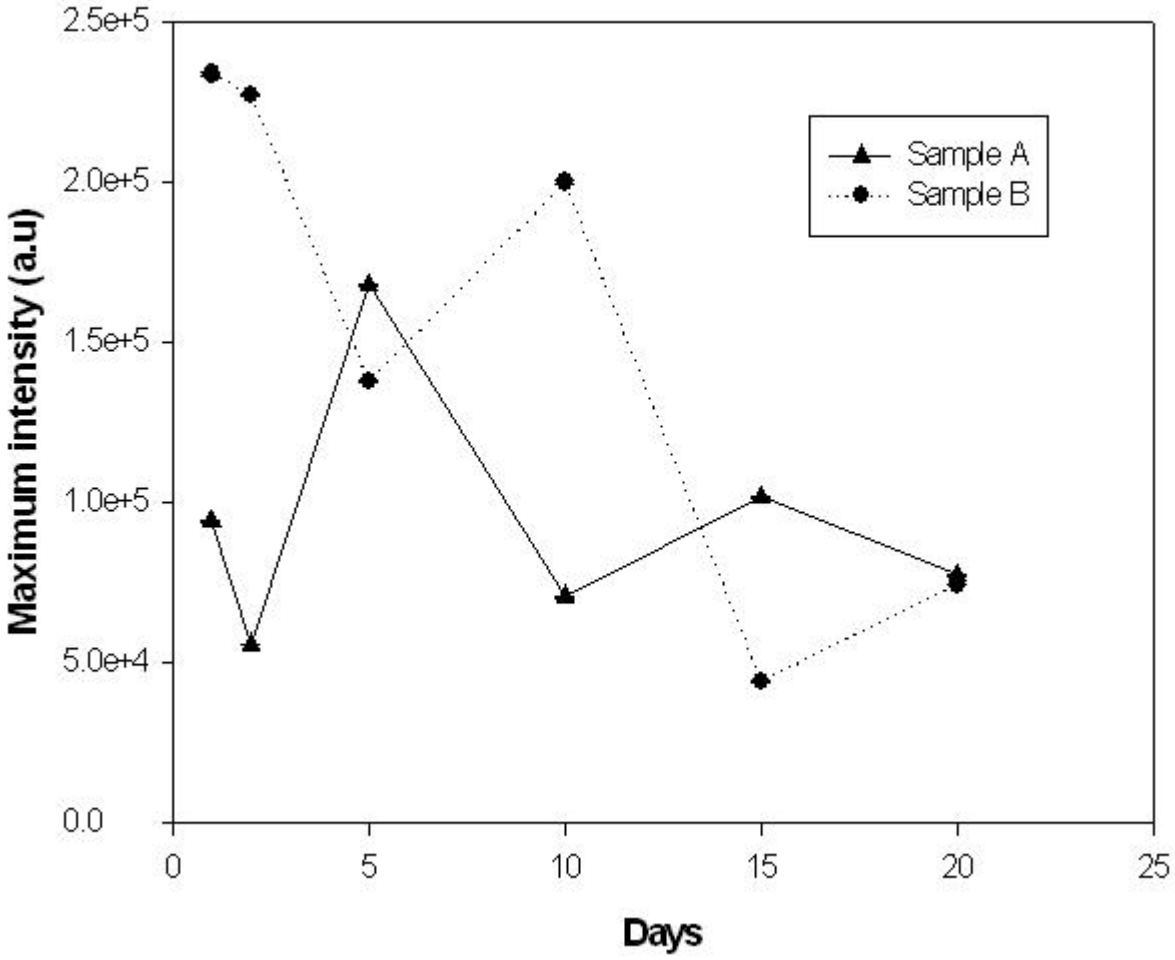

Figure 6.29: Maximum luminescence intensities plotted against storage days for sample A (triangles) and sample B (solid circles) in fading investiagations. Samples were irradiated to 1.0 Gy of beta dose. TR-OSL measurements done at a pulse width of 18.0 ms using blue LEDs at ambient temperatures.

at ambient temperatures. It is also worth to note from Figure 6.29 that there is a significant degree of signal growth for both samples several days after irradiation regardless of the previous readouts, for example, on day 5 for sample A and on day 10 for Sample B. This growth in OSL intensity happening after some previous readout would be taken as a sign of signal recuperation i.e. charges trapped in traps that do not contribute directly to OSL signal migrate to OSL traps resulting into an increase in the concentration of charges in the OSL traps hence a boost in the OSL signal. It is difficult from the results shown in Figure 6.29 to decide whether α-Al_2O_3:C suffers significantly from fading considering that the intensities keep on increasing and decreasing alternatively until day 20

of readout. We suggest that the fading investigations can be adequately done for longer periods of sample storage.

Chapter 7

Conclusions

According to this study α-Al_2O_3:C has a thermoluminescence glow curve that shows apparently five peaks at 37°C, 160°C, 300°C, 410°C and 480°C at a heating rate of 0.03 K/s when irradiated to more than 6.0 Gy of beta dose with the peak at 160°C being the main peak used for dosimetry. The presence of five peaks in the TL glow curve signifies the presence of at least five species of traps (defects) located at different levels in the forbidden gap. Whether these traps are of the same kind, requires further research on the sample.

From kinetic analysis carried out on the main peak, it can be concluded that the main peak follows general order behaviour, with the kinetic order b ranging between 1.2 - 1.3. This difficulty in pinpointing the actual kinetic order of the main peak may strongly suggests that it is a complex peak consisting of closely overlapping peaks. The activation energy of the dosimetric trap can be estimated to be in the range of 1.3 to 1.4 eV, which also signifies the complexity of the peak.

For the TL measurements carried out at different heating rates, at the same dose, it has been shown that the peak heights of the main peak (peak II), peak III and peak V, decrease with increasing heating rate, while peak I shows an increase in peak height with increasing heating rate followed by a decrease at higher heating rates. The decrease in peak height for the main peak (II) is due to thermal quenching. The cause of the decrease of peak height with increasing heating rate for peaks III and V is not yet known and requires further investigations. Likewise, the cause of the increase in peak height for peak I with heating rate followed by a decrease, also requires further investigations. We have also seen that with increasing heating rate, the peak positions of all the peaks, shift towards higher temperatures, because of the direct mathematical relationship that exists between the heating rate and the peak position. In addition, the heating rate affects the shape of the peaks in such a way that the peaks become broader with increasing heating rate as shown by

increasing FWHM with increasing heating rate.

The dose response of the main peak is linear from 0.1 Gy up to around 10 Gy then goes sublinear. The peak position of the main peak seems to shift towards low temperatures at low doses (0.1 Gy - 10 Gy), then towards high temperatures thereafter. Peak I shows a sublinear dose response at doses ranging from 0.1 Gy to 10 Gy and then seems to saturate at doses above 10 Gy. The peak position of peak I seems to be stable with dose. As opposed to peak I, the dose response for peak III grows from linear from 0.1 Gy to 10 Gy to supralinear at high doses. The peak position of peak III is almost stable beyond 1 Gy of beta irradiation. Peak V shows supralinear growth with increasing dose, and the peak position of peak V, moves towards low temperatures at low doses (0.1 - 10 Gy) then towards high temperatures at doses above 10 Gy, replicating the behaviour of the main peak.

TR-OSL was measured at various measurement temperatures in the range of 30°C to 200°C using 470 nm blue LEDs and show evidence of thermal quenching in α-Al_2O_3:C at measurement temperatures above 140°C. The activation energy of thermal quenching has been calculated to be 1.045 $\pm$0.002 eV, which is significantly precise and is consistent with the model of α-Al_2O_3:C proposed by Pagonis et al [25] which has been used to explain the results in this study. The study also demonstrated the influence of shallow traps on luminescence lifetimes at low temperatures. The study has shown that at temperature ranges between room temperature and 80°C, shallow traps tend to elongate luminescence lifetimes due to retrapping of charges during the readout stage. Furthermore, it has been demonstrated that both the rising part and decay part of the TR-OSL spectrum can be used for the evaluation of luminescence lifetimes. The mean luminescence lifetime calculated from the signal during the pulse is 40.0$\pm$3.0 ms whereas the mean luminescence lifetime obtained from the signal after the pulse is 35.0$\pm$1.0 ms. A plot of dynamic throughput against measurement, has been proposed as one graphical method of showing the evidence of thermal quenching in the material when using TR-OSL technique of luminescence measurement. The dynamic throughput is expected to be constant at low temperatures and grows rapidly towards 1 in the temperature range where thermal quenching manifests itself in the material.

A choice of a proper pulse width in TR-OSL measurements is very important because it has been shown in our study that increasing the pulse width of the stimulating signal reduces the dynamic throughput i.e. it reduces the signal after the pulse.

The OSL signal in α-Al_2O_3:C has proved to fade with storage time. But at the same time it has been shown that the OSL signal is capable of recuperation after fading. It should be pointed out though, that the storage times used in the study were not long enough, hence further studies on

sample fading with long storage times are essential.

Areas requiring further studies

Further studies are required to investigate the types of defects that are responsible for both thermoluminescence and optically stimulated luminescence in α-Al_2O_3:C. The effect of deep electron traps on both TL and OSL also requires further studies. Further studies are also required to identify which traps are responsible for OSL in α-Al_2O_3:C. It is also necessary to investigate thermal quenching of deep electron traps.

References

[1] D.R. Mirsha, M.S. Kulkarin, N.S. Rawat, D.R. Mishra, B.C. Bhatt, A. Singh, and S.K. Gupta. Luminescence properties of α-Al_2O_3:C crystal with intense low temperature tl peak. *Radiat. Meas.*, 42:170–176, 2007.

[2] K.P. Muthe, M.S. Kulkarni, N.S. Rawat, D.R. Mishra, B.C. Bhatt, A. Singh, and S.K. Gupta. Melt processing of alumina in graphite ambient for dosimetric applications. *J. Lumin.*, 128:445–450, 2008.

[3] S.W.S. McKeever, M. Moscovitch, and P.D. Townsend. *Thermoluminescence dosimetry of materials: properties and uses*. Nuclear Technology Publishing, Ashford, Kent TN23 1YW, England, 1995.

[4] M.S. Akserlod, V.S. Kortov, and E.A. Gorelova. Preparation and properties of α-Al_2O_3:C. *Radiat. Prot. Dos.*, 47:159–164, 1993.

[5] K.P. Muthe, S.K. Gupta, and J.V. Yakhmi. Development of α-Al_2O_3:C phosphor for personal dosimetry using optically stimulated luminescence technique. *DR Homi BHABHA Centenary year*, 308:2–8, 2009.

[6] A.K. Yuri, F.Z.and Eugene, A.E. Robert, and E.E. Donald. Periodic models of quantum chemical simulations of f centres in crystalline metal international. *J. of Q.Chem.*, 107:2956–2985, 2007.

[7] G. Kitis, G.J. Papadopoulos, S. Charalambous, and J.W.N. Tuyn. The influence of heating rate on the response and trapping parameters of α-Al_2O_3:C. *Radiat. Prot. Dos.*, 55:183–190, 1994.

[8] V.S. Kortov, I. Milman, V.I. Kirpa, and J. Lesz. Some features of α-Al_2O_3 dosimetric thermoluminescence crystals. *Radiat. Prot. Dosim.*, 55:279–283, 1994.

[9] V. Kortov and I. Milman. Some new data on thermoluminescence properties of dosimetric α-Al_2O_3:C crystals. *Radiat. Prot. Dos.*, 65:179–184, 1996.

[10] S.W.S. McKeever. *Thermoluminescence of solids*. Cambridge University Press, 1985.

[11] C. Furreta. *The Handbook of Thermoluminescence*. World Scientific Publishing Co. Pte. Ltd, Singapore, 2003.

[12] E.G. Yukihara and S.W.S. McKeever. *Optically stimulated luminescence fundamentals and applications*. John Wiley and Sons, Ltd, 2011.

[13] V. Pagonis, G. Kitis, and C. Furreta. *Numerical and Practical Exercises in Thermoluminescence*. Springer, 2006.

[14] Y. Kirsh. Kinetic analysis of thermoluminescence. *Phy. stat. sol.*, 129:15, 1992.

[15] R. Chen and V. Pagonis. *Thermally and Optically stimulated luminescence*. John Wiley and Sons Ltd, 2011.

[16] Chen R. Glow curves with general order kinetics. *J. Electrochem. Soc.*, 116:1254–1257, 1969.

[17] L. Bøtter-Jensen, S.W.S. McKeever, and A.G. Wintle. *Optically Stimulated Luminescence Dosimetry*. Elsevier, Amsterdam, 2003.

[18] R.M. Bailey, B.W. Smith, and E.J. Rhodes. Partial bleaching and the decay from characteristics of quartz OSL. *Radiat. Meas.*, 27:123–136, 1997.

[19] M.L. Chithambo and R.B. Galloway. On the slow component of luminescence stimulated from quartz by pulsed blue light-emitting diodes. *Nuclear Instrum. Methods B*, 183:358–368, 2001.

[20] E. Bulur, L. Bøtter-Jensen, and A.S. Murry. Optically stimulated luminescence from quartz measured using the linear modulation technique. *Radiat. Meas.*, 32:407–411, 2000.

[21] M.L. Chithambo. The analysis of time-resolved optically stimulated luminescence: II. computer simulations and experimental results. *J. Phys. D: Appl. Phys.*, 40:1880–1889, 2007.

[22] V. Pagonis, J. Lawless, R. Chen, and M.L. Chithambo. Analytical expressions for time-resolved optically stimulated luminescence experiments in quartz. *Journal of luminescence*, 131:1827–1835, 2011.

[23] V. Pagonis, S.M Mian, M.L. Chithambo, and C. Barnold. Experimental and modelling study of pulsed optically stimulated luminescence in quartz, marble and beta irradiated salt. *J. Phys. D. Appl. Phys.*, 42:1–12, 2009.

[24] M.L. Chithambo. The analysis of time-resolved optically stimulated luminescence: I. theoretical considerations. *J. Phys. D: Appl. Phys.*, 40:1874–1879, 2007.

[25] V. Pagonis, R. Chen, J.W. Maddrey, and B. Sapp. Simulations of time-resolved photoluminescence experiments in α- Al_2O_3:C. *J. Lumin.*, 131:1086–1094, 2011.

[26] S.V. Nikiforov, I.I. Milman, and V.S. Kortov. Thermal and optical ionization of f-centers in the luminescence mechanism of anion-defective corundum crystals. *Radiat. Meas.*, 33:547–551, 2001.

[27] M.L. Chithambo and R.B. Galloway. A pulsed light-emitting-diode system for stimulation of luminescence. *Meas. Sci. Technol.*, 11:418, 2000.

[28] M.L. Chithambo. A time-correlated photon counting system for measurement of pulsed optically stimulated luminescence. *J. Lumin.*, 131:92–98, 2011.

[29] Risø DTU. *Guide to the Risø TL/OSL Reader*. 2010.

[30] M.L. Chithambo. Concerning secondary peaks in α-Al_2O_3:C. *South African J. Sci.*, 100:524–527, 2004.

[31] M.S. Kulkarni, D.R. Mishra, K.P. Muthe, A. Singh, M. Roy, S.K. Gupta, and S. Kannan. An alternative method of preparation of dosimetric grade α- Al_2O_3:C by vacuum-assisted post growth thermal impurification technique. *Radiat. Meas.*, 39:277–282, 2005.

[32] E. Bulur and H.Y. Gøksu. Phototransferred thermoluminescence from α-Al_2O_3:C using blue light emitting diodes. *Radiat. Meas.*, 30:203–206, 1999.

[33] E.G. Yukihara, V.H. Whitley, J.C. Polf, D.M. Klein, S.W.S. McKeever, A.E. Akserlod, and M.S. Akserlod. The effects of deep trap population on the thermoluminescence of al_2o_3:C. *Radiat. Meas.*, 37:627–638, 2003.

[34] D. Lo, J.L. Lawless, and R. Chen. Superlinear dose dependence of high temperature thermoluminescence peaks in α-Al_2O_3:C. *Radiat. Prot. Dos.*, 119:71–74, 2006.

[35] G. Kitis. Confirmation of the influence of thermal quenching on the initial rise method in α-Al_2O_3:C. *phys. stat. sol.*, 191:621–627, 2002.

[36] M.S. Akserlod, N.A. Larsen, V. Whitley, and S.W.S. McKeever. Thermal quenching of F-centre luminescence in Al_2O_3:C. *J. Lumin.*, 131:1086–1094, 1998.

[37] N.A. Larsen. *Dosimetry based on thermally and optically stimulated luminescence, PhD Dissertation.* Niels Bohr Inst., Univ. of Copenhagen, 1997.